Fluid Dynamics of Packed Columns

Principles of the Fluid Dynamic Design of Columns for Gas/Liquid and Liquid/Liquid Systems

Bearbeitet von
Jerzy Mackowiak, Claudia Hall

1. Auflage 2012. Taschenbuch. xxi, 355 S. Paperback
ISBN 978 3 642 26206 7
Format (B x L): 15,5 x 23,5 cm
Gewicht: 581 g

Two-Phase Flow and Operating Range 2

2.1 Hydraulic Processes in Packed Columns

The accurate design of packed columns requires a knowledge of the hydraulic characteristics of the respective packing element throughout the entire operating range. The gas velocity at the flooding point $u_{V,Fl}$ is a particularly important parameter in this context, as it is required for the calculation of the maximum loading capacity at a given specific liquid load u_L. The higher the loading capacity of the column in the case of countercurrent flow of the phases, i.e. the higher the gas velocity at the flooding point u_V, the smaller the required cross-section and diameter of the column.

When designing a packed column, it is also important to calculate the pressure drop of the irrigated packing $\Delta p/H$ per 1 m packed bed height and the respective liquid hold-up h_L. In recent years, these have become important technical-economic parameters. They allow the assessment of packed columns in terms of their suitability for the rectification of temperature-sensitive mixtures and for all gas/liquid systems, i.e. for absorption, desorption, cooling and preheating of gas as well as for absorption using slow chemical reactions, where the residence time of the liquid must be known.

If there is only gas flowing through the packing, i.e. $u_L = 0$, a pressure drop occurs in the column Δp_0, Fig. 2-1, and increasingly so, as the gas capacity F_V rises. The pressure drop also depends on the dimension and shape of the packing and is directly proportional to the packing height H. If the packing is irrigated by the downward countercurrent flow of the liquid, i.e. $u_L > 0$, there are mostly films and runlets forming on the individual packing elements, assuming these are small and non-perforated. In the case of highly perforated packing elements of any size, the so-called lattice work packings, which are used more and more frequently, there are not only films and runlets, but also a large number of droplets and sprays, which increases with the size of the packing. On the basis of today's knowledge, this applies to any type of packing of any shape and material, i.e. plastic, ceramic and metal, in particular in the case of very small and moderate liquid loads. In two-phase flow, once the gas has reached a certain velocity, the formation of additional droplets can occur through separation from films. The total liquid hold-up h_L of such droplets, runlets and films reduces the free cross-section available for the gas flow.

J. Maćkowiak, *Fluid Dynamics of Packed Columns*,
Chemische Technik/Verfahrenstechnik, DOI 10.1007/b98397_2,

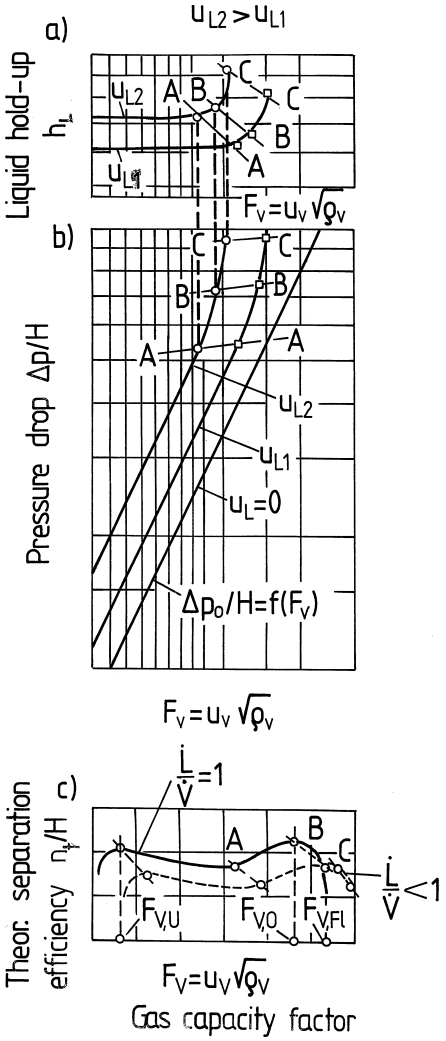

Figure 2-1. Dependencies (**a**) $h_L = f(F_V)$, (**b**) $\Delta p/H = f(F_V)$, (**c**) $n_t/H = f(F_V)$ as examples of qualitative illustration of activities in packed columns

The effective void fraction of the packing (ε-h_L) decreases, which results in an increase in pressure drop $\Delta p/H$, based on the accepted law of resistance acc. to Darcy and Weisbach. As the specific liquid load u_L increases and the gas velocity u_V remains constant, the liquid hold-up h_L and the pressure drop of the irrigated packing $\Delta p/H$ also increase (see Fig. 2-1a,b).

Figure 2-1b shows a qualitative, double-logarithmic representation of the dependency of the pressure drop per 1 m packing height for irrigated random or structured packings $\Delta p/H$ on the gas capacity factor F_V, whereas Figs. 2-2a and 2-2b is a quantitative representation, applicable to randomly filled 25 mm metal Białecki rings, with the

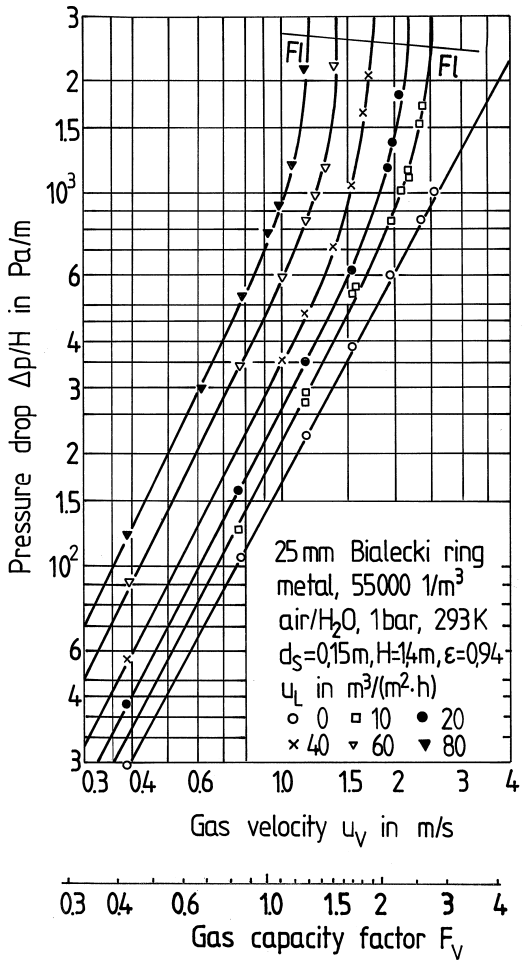

Figure 2-2a. Hydraulic characteristics of random 25 mm metal Białecki rings, valid for the system air/water under normal conditions. Pressure drop $\Delta p/H$ as a function of the gas velocity u_V or gas capacity factor F_V, u_L with the specific liquid load u_L as a parameter

specific liquid load u_L as the parameter. The occurrence of different flow ranges within the operating range is very distinctive and is marked by the limit lines $\overline{AA}$, $\overline{BB}$ and $\overline{CC}$, as shown in Fig. 2-1. Figure 2-1a is a qualitative representation of the correlation between the total liquid hold-up h_L and the gas capacity factor F_V for empty columns, whereas Fig. 2-2b shows the correlation for randomly filled, 25 mm Białecki rings of metal. The diagrams are similar for other random or structured packings, analogous to Figs. 2-2a and 2-2b. The combined representation of the correlation between the pressure drop $\Delta p/H$ and liquid hold-up h_L and the vapour capacity factor F_V highlights the characteristic relationship between the parameters shown here.

Up to the first limit line $\overline{AA}$, the so-called loading line, the pressure drop curves $\Delta p/H$ of irrigated packings at small and/or moderate liquid loads $u_{L,1}$ and $u_{L,2}$ run parallel

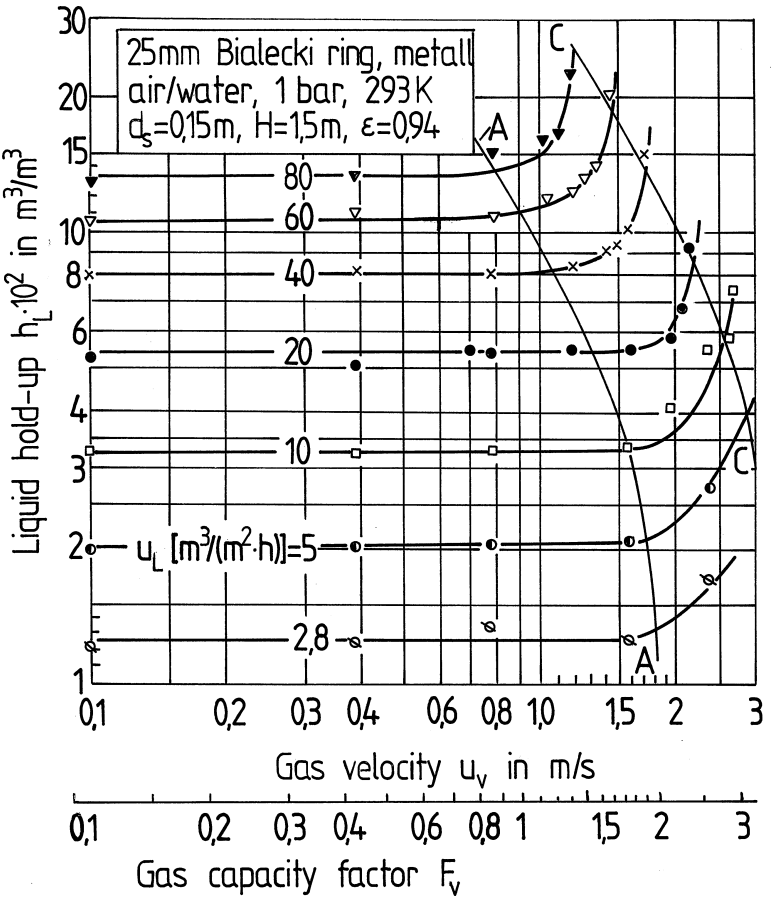

Figure 2-2b. Hydraulic characteristics of random 25 mm metal Białecki rings, valid for the system air/water under normal conditions. Liquid hold-up h_L as a function of the gas velocity u_V or gas capacity factor F_V, u_L with the specific liquid load u_L as a parameter

with the pressure drop curve $\Delta p_0/H$ of dry packings with $u_L = 0$, based on experimental research on modern types of packings. The loading line is at approx. 65% of the flood load factor $F_{V,FL}$ pertaining to the flooding line $\overline{CC}$. In this operating range, the liquid flow has practically no influence on the gas flow. Hence, the liquid hold-up h_L does not depend on the gas capacity factor F_V and/or the gas velocity u_V, but it increases with the liquid load u_L.

A further increase in the gas velocity u_V above the loading line $\overline{AA}$ results in an increase in the liquid hold-up h_L, Fig. 2-2b, and in the pressure drop, Fig. 2-2a. In this operating range, the shearing forces of the gas prevent the liquid from flowing off.

The pressure drop curves in the range between the loading line $\overline{AA}$ and the upper loading line $\overline{BB}$ rise steadily from 1.95 to 2.95 [2, 3, 12], Fig. 2-2a. At the same time, the

liquid hold-up h_L increases, leading to an increase in the effective mass transfer area, see Fig. 2-2b. Packed columns are usually operated at gas velocities u_V between 30 and 80% of the gas velocity at the flooding point $u_{V,Fl}$.

The term "packed columns" refers to columns with randomly filled packings, with stacked or structured packings and tube columns filled aligned with packing elements.

2.2 Flooding Point

2.2.1 Flooding Mechanisms

Depending on the liquid load, the type and size of the packing and the physical properties, there are two different flooding mechanisms which can occur in packed columns:

(a) flooding at high phase flow ratios

$$\lambda_0 = \left(\frac{u_L}{u_V}\right)_{Fl} \tag{2-1}$$

where columns with large-surface packing elements are being filled with liquid with phase inversion

(b) flooding at small phase flow ratios λ_0, due to droplet entrainment in the gas phase

In packed columns, the liquid flows in counter-current to the gas, in the form of films and runlets. This applies in particular to small, non-perforated packing elements with low void fraction, e.g. $\varepsilon = 0.4{-}0.6\ m^3\ m^{-3}$. The void space of the packing elements contains dead space, which is filled with more and more liquid as the liquid load u_L increases. Flooding occurs when the entire column is filled with liquid. In the case of high specific liquid loads u_L and very low gas velocities u_V, i.e. at very high phase flow ratios at the flooding point λ_0, the so-called phase inversion occurs through the formation of bubbles, whereby the gas phase is dispersed and the liquid now forms the continuous phase.

The flooding mechanism is characterised by a steep increase in the pressure drop curve $\Delta p/H = f(F_V)$ as the gas capacity factor F_V increases, line $u_{L,3}$ in Fig. 2-1b.

The last 30 years have seen a new development in the packings design, as more and more metal and plastic packings with an open structure are being produced – the so-called lattice packings. Today, the use of perforated packing elements with dimensions of $d \geq 0.050$ m is common practice for industrial applications. The void fraction of these metal and plastic packing elements with $d \geq 0.025$ m is in the range of $\varepsilon = 0.92{-}0.98\ m^3\ m^{-3}$. They do not contain any dead space that can be filled with liquid. The operating range of modern "lattice packings" is therefore greater than that of full-surface packing

elements, which means that the influence of the gas on the liquid flow is different, compared to the first type of packing.

In the case of highly perforated packing elements, or lattice packings, the formation of droplets occurs as a result of liquid dripping from the individual packing elements or from films and runlets, and can be entrained by the upward gas flow. This process is shown in Fig. 2-3, acc. to Bornhütter and Mersmann [66, 87]. The amount of droplets in the total hold-up ranges between 5 and 42%, depending on the type and size of the packing. As a rule, the number of droplets in the packing increases, the higher the liquid load u_L and the larger the size of the packing elements. Low phase flow ratios at the flooding point λ_0 are characteristic of columns operated in the vacuum and normal pressure range. This mechanism of droplet formation has been verified by specific studies carried out by Bornhütter and Mersmann [66, 87].

As a result, smaller as well as larger perforated packing elements are characterised by a different flooding mechanism, as droplets occur in liquid-fluidised beds, compared to

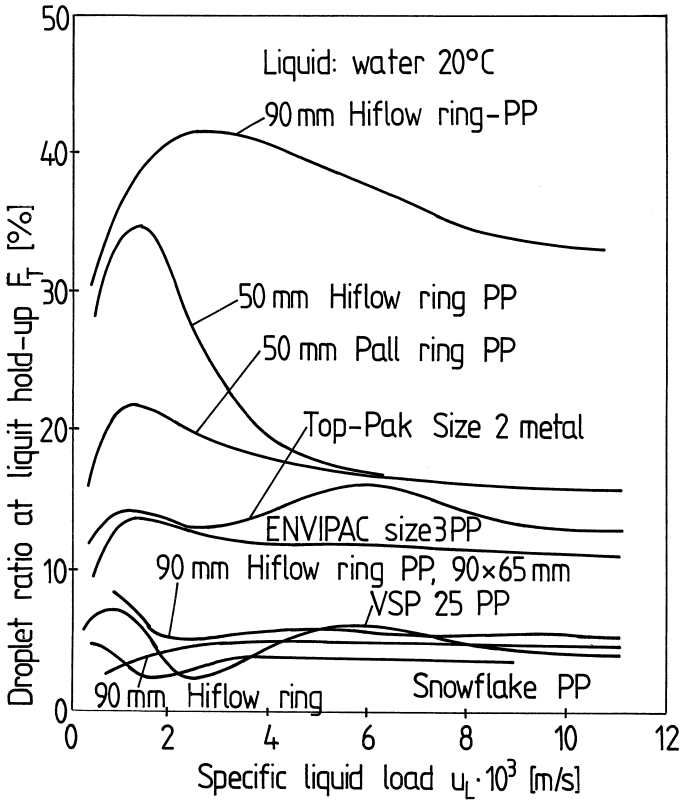

Figure 2-3. Droplet hold-up for various packings during water irrigation acc. to Bornhütter/Mersmann [66, 87]

classic, non-perforated packings, where flooding is caused by droplets being entrained upwards, in particular in the case of smaller phase flow ratios at the flooding point λ_0. The latter is characterised by a constant increase in pressure drop $\Delta p/H$, as the gas capacity factor F_V rises, Fig. 2-1b, lines $u_{L,1}$ and $u_{L,2}$.

Accurate gas velocities at the flooding point can only be obtained by means of pressure drop curves, as shown in Fig. 2-1b. The visual determination of the flooding point, on the other hand, can cause large errors.

2.2.2 Droplet Formation in Packed Columns

Droplet Formation

Droplet formation at lattice packing elements can occur without the influence of gas, as a result of the following: dripping from the sharp-edged packing elements, break-up of sprays and threads (runlets) at a certain distance from the individual packing element and through contact with the ledges of the packing elements. In the case of higher gas velocities, droplet formation can occur through transfer of the gas kinetic energy to runlets and films [66, 87].

The following considerations initially refer to the second case only and are based on the physical notion that a large number of droplets are sheared from the films and runlets of the liquid and entrained by the upward gas flow. As a result, the proportion of droplets to the total hold-up is even higher than shown in Fig. 2-2b. By shearing off droplets from the runlets, the gas transfers an impulse onto the droplets. The shear force of the gas K_R

$$K_R = C_0' \cdot \frac{\pi \cdot d_T^2}{4} \cdot \frac{\rho_V}{2} u_V^2 \tag{2-2}$$

is partly converted during droplet formation as a result of the surface tension σ_L. (C_0' is the so-called shear factor [58]). The surface force K_0 is given as:

$$K_0 = \pi \cdot d_T \cdot \sigma_L. \tag{2-3}$$

While in suspension, the displaced droplet has to overcome the gravitational force minus the lifting force.

$$K_g = \frac{\pi \cdot d_T^3}{6} \cdot (\rho_L - \rho_V) \cdot g = \frac{\pi \cdot d_T^3}{6} \cdot \rho_L \cdot g \quad \text{for } \rho_L >> \rho_V. \tag{2-4}$$

The balance of forces

$$K_R = K_0 + K_g \tag{2-5}$$

leads to the following correlation (2-6), acc. to Covelli, Mülli [58], based on the solution of Eq. (2-5) for a minimal effective gas velocity, at which it is just possible to separate droplets from runlets:

$$\bar{u}_{V,crit} = \left[\frac{16 \cdot 9\sigma_L \cdot \Delta\rho \cdot g}{3C_0'^2 \cdot \rho_V^2}\right]^{1/4} = 1.55 \cdot \frac{1}{\sqrt{C_0'}} \cdot \left(\frac{\sigma_L \cdot \Delta\rho \cdot g}{\rho_V^2}\right)^{1/4}. \tag{2-6}$$

For $C_0' = 1$, the formula (2-6) is identical to the one developed by Mersmann [38] and Levich [57] for droplets falling in gases and liquids.

This permissible velocity $\bar{u}_{V,crit}$ can be used to determine a critical droplet diameter $d_{T,crit}$, based on Eq. (2-5):

$$d_{T,crit} = \frac{6}{16} \cdot \frac{C_0' \cdot \rho_V \cdot \bar{u}_{V,crit}^2}{(\rho_L - \rho_V) \cdot g} = 2 \cdot \left[\frac{3\sigma_L}{2 \cdot g(\rho_L - \rho_V)}\right]^{1/2} \Rightarrow$$

$$d_{T,crit} = 2.44 \cdot \left[\frac{\sigma_L}{\Delta\rho \cdot g}\right]^{1/2} \tag{2-7}$$

Larger droplets with diameters greater than $d_{T,crit}$ break down into smaller droplets. Covelli, Mülli [58] presented the following theory for the shear factor C_0' in Eq. (2-2):

$$C_0' = 6.53 \cdot \sqrt{\frac{\sigma_L \cdot g \cdot (\rho_L - \rho_V)}{\rho_V^2 \cdot u_V^4}} \cdot \left(1 + 245.4 \cdot \mathrm{Re}_T^{-0.842}\right) \tag{2-8}$$

It was developed on the basis of data, taken at a heated tube for the test system water/steam at 1 bar, and applies to Reynolds numbers of droplets Re_T, acc. to Eq. (2-9), in the range of $Re_T = 300$ to $Re_T = 8000$:

$$Re_T = \frac{\bar{u}_V \cdot d_T}{\upsilon_V} \tag{2-9}$$

Based on Eq. (2-9), it is possible, for a given gas velocity $\bar{u}_V$, to calculate the shear factor C_0', acc. to Eq. (2-8), followed by the critical effective gas velocity $\bar{u}_{V,crit}$, acc. to Eq. (2-6), if the Reynolds number Re_T is known.

If the following is true:

$$\bar{u}_V \geq \bar{u}_{V,crit} \tag{2-10}$$

then droplet formation occurs in the packing by shearing from films and runlets. In the case of high gas velocities, the shear factor C_0' is expected to be minimal, acc. to Eq. (2-8). These conditions are most likely to trigger droplet formation.

The formation of droplets is usually described by means of the so-called critical Weber number We_{crit}:

$$\frac{\bar{u}_{V,crit} \cdot d_T \cdot \rho_V \cdot C_0'}{\sigma_L} = \frac{F_{V,crit}^2 \cdot d_T \cdot C_0'}{\varepsilon^2 \cdot \sigma_L} = We_{crit} \cdot C_0' / \varepsilon_2 = const. \Rightarrow$$

$$We_{crit} \cong \frac{12 \cdot \varepsilon^2}{C_0'} \tag{2-11}$$

which is based on the ratio of the shear force K_R, acc. to Eq. (2-2), to the surface force K_0, Eq. (2-3). Equation (2-11), developed by Wallis and quoted by Stichlmair [55], applies to low-viscosity mixtures ($\eta_L \approx 1$ mPas).

If the critical Weber number is not reached, there is no droplet formation from runlets and films. This is expected to be the case for high liquid loads, for random packings with low void fraction as well as for systems with extremely low surface tension σ_L, i.e. for pressure rectification.

Droplet Entrainment

The droplets forming in the packing can only be entrained if the gas velocity is sufficiently high. The gas velocity can be ascertained from the balance of forces acting on a suspended droplet. The thrust force of the gas K_ψ must be equated to the gravitational force K_g minus the lifting force K_A. The following correlation applies:

$$K_\psi = K_g - K_A \Rightarrow$$

$$\psi_{Fl} \cdot \frac{\bar{u}_V^2 \cdot \rho_V}{2} \cdot \frac{d_T^2}{4} = \frac{\pi \cdot d_T^3}{6} \cdot (\rho_L - \rho_V) \cdot g \tag{2-12}$$

Solving Eq. (2-12) for $\bar{u}_V$ gives Eq. (2-13)

$$\bar{u}_V = \sqrt{\frac{4}{3} \cdot \frac{d_T \cdot g}{\psi_{Fl}}} \cdot \sqrt{\frac{\rho_L - \rho_V}{\rho_V}} \tag{2-13}$$

Estimating the Lower Limit, Which Allows Droplet Formation from Films and Runlets in Packed Columns

It is possible to give an approximate estimation of the lowest effective gas velocity $u_{V,Fl,min}$ for the test system air/water at 20 °C and 1 bar, which allows droplet entrainment from the packing. This is based on the assumption that the packing elements are sufficiently large to allow the substitution of the same resistance coefficient $\psi_{Fl} \cong \psi_R$ into Eq. (2-13) that applies to a droplet swarm in an empty column. It can be calculated using Chao's formula (2-14), quoted by Soo [59]:

$$\psi_R = \frac{32}{Re_T} \left[1 + 2 \cdot \frac{\eta_L}{\eta_V} - 0.314 \cdot \frac{1 + 4 \cdot (\eta_L / \eta_V)}{\sqrt{Re_T}} \right] \tag{2-14}$$

For the test system air/water, the droplets in packed columns reach an average diameter of $d_T \cong 0.003$ m. u_V is now substituted for the value $u_V \cong 1.5\ ms^{-1}$. The objective is to find out whether, given the above gas velocity, it is still possible for droplets of this size to be entrained from the packing. Equation (2-9) gives the value $Re_T = 268.95$ and Eq. (2-14) leads to a resistance coefficient ψ_R of 12.68, which is then used to calculate the gas velocity u_V, acc. to Eq. (2-13), as $1.5\ ms^{-1}$. The example shows that, at a gas velocity of $1.5\ ms^{-1}$ or higher, it is still possible for droplets to be entrained in columns containing larger packing elements of, e.g., $d \geq 0.050$ m. Given a packing size of $d \cong 0.090$ m and $u_V \approx 1.5\ ms^{-1}$, the liquid load at the flooding point is in excess of $100\ m^3m^{-2}\ h^{-1}$ [27, 28]. The maximum operating range for larger, perforated packing elements with $d \geq 0.050$ m, at which droplet formation and entrainment can occur, is relatively wide. However, it decreases with the size of the packing elements. It is difficult to provide a more accurate estimation of the lower limit of the model's validity, which assumes that flooding occurs through droplet entrainment by the upward gas flow. This is due to the fact that no numerical values are currently available for the resistance coefficient in connection with droplet fall in the packing.

In addition, it is not yet possible to estimate the proportion of droplets formed through dripping from the packing edges and those formed through shearing. The lower value of the gas velocity in the air/water system is estimated to be $u_V \geq 1{-}1.5\ ms^{-1}$. In the case of F_V factors, it is in the region of 1.1–1.65 or considerably lower.

Based on Eq. (2-13), it is possible to calculate the gas velocity u_V that allows the suspension of droplets with a diameter of d_T. If this value is lower than the gas velocity $u_{V,Fl}$, it is no longer possible for droplets with d_T to be entrained by the upward gas flow. In such cases, it is recommended to describe the flooding mechanism in packed columns using the *film gas thrust shear force model* or *film model* developed by Mersmann [2, 3], see Sect. 2.2.3.

Bornhütter (1991) [66, 87] carried out experiments to analyse the formation of droplets in a column with a diameter of 1 m containing modern packing elements, such as Hiflow ring, Pall ring, VSP ring, Envipac, Snowflake, with diameters ranging between 25 and 90 mm and using liquids with viscosities between 1 and 27 mPas. He found that the proportion of droplets to the hold-up ranged between 5 and 45%, see Fig. 2-3. What all types of packings had in common was the fact that the proportion of droplets remained largely constant as the specific liquid load increased, whereas the proportion increased if the loads were reduced, falling below $u_L = 0.003\ ms^{-1}$.

Based on the theoretical considerations illustrated above and the experimental data found in literature [66], it can be assumed that, due to the constant occurrence of droplets in the packing, the flooding point mechanism in packed columns is defined by the entrainment of droplets.

2.2.3 Literature Overview – Status of Knowledge

The analysis of most representative correlations for evaluation of flooding gas velocity in packed column was provided by Kister [88], Piche [73], Kuźniewska-Lach [74], Grabbert [92] et al.

The methods described in the relevant literature for determining the gas velocity at the flooding point $u_{V,Fl}$ can be divided into two groups. The first group includes graphic correlations developed by Sherwood, Shipley and Holloway [4], Lobo, Leva [6], Billet [5], Eckert, Kafarov, Planowski [1, 50], Kirschbaum [19], Strigle [31] etc., who assume droplet formation at the flooding point. Table 2-1 shows the individual developmental stages of the most important correlations developed by this group (no. 1–7). The second group of methods assumes film flow in the packing, see correlations 8–14 in Table 2-1 [1, 4, 5, 6, 8, 9, 37–89, 94].

The first group of flooding point correlations is based on the assumption that, in accordance with visual observations, droplets are formed in the void spaces of the packing elements, which then fall down into the packing elements situated below, see Sect. 2.2.1.

At the flooding point, the balance of forces acting on a suspended droplet leads to correlation (2-12), which is then transposed to give the following equation for the flood load factor $F^*_{V,Fl}$:

$$F^*_{V,Fl} = \frac{F_{V,Fl}}{\sqrt{\rho_L - \rho_V}} = \sqrt{\frac{4}{3} \cdot \frac{d_T \cdot g}{\psi_0}} \qquad \left[\mathrm{ms}^{-1}\right]. \tag{2-15}$$

The term $\sqrt{(4/3) \cdot d_T \cdot g \cdot \psi_0^{-1}}$ in Eq. (2-15) is summed up to the so-called flood load factor $F^*_{V,Fl}$, which can only be determined experimentally for packed columns. Here, the quotient, Eq. (2-15), is given by dividing the gas capacity factors $F_{V,Fl}$, known from experiments, by the root of the density difference $(\rho_L - \rho_V)$ and applied to the operating conditions at the flooding point using the term $(L/V)_{Fl} \cdot \sqrt{\rho_V/\rho_L}$ (2-16).

$$F^*_{V,Fl} = f(X_{Fl}) \quad \text{with } X_{Fl} = \left(\frac{L}{V}\right)_{Fl} \cdot \sqrt{\frac{\rho_V}{\rho_L}} \tag{2-16}$$

The term X_{Fl} in Eq. (2-16), known as the flow parameter, is the root of the ratio of the kinetic energy of the liquid $E_{K,L}$ to the kinetic energy of the gas $E_{K,V}$. This type of capacity diagram, based on Eq. (2-16), was adopted by Böden [1, 4, 8, 55] and is still used today [40–48], mostly for the air/water system.

Figure 2-4a shows a typical capacity diagram for 15 mm metal Pall rings, based on Eq. (2-16). Figures 2-4b and 2-4c show further examples of capacity diagrams for various random and structured packings, which were developed on the basis of recent experiments. The figures clearly show to what extent the flooding point is influenced by the size, type and material of the packing. These variables were initially described by introducing the quotient a/ε [1] (Eq. (2-17)) and later by using the packing factor $F_P = a/\varepsilon^3$ of the dry packing [4], see Eq. (2-18).

$$\frac{u^2_{V,Fl}}{2 \cdot g} \cdot \frac{a}{\varepsilon} \cdot \frac{\rho_V}{\rho_L} = f\left[\left(\frac{L}{V}\right)_{Fl} \cdot \sqrt{\frac{\rho_V}{\rho_L}}\right] \tag{2-17}$$

The above correlation (2-17) was developed by Walker et al. [1] as early as 1937, on the basis of experiments using the test system air/water. Spirals and ceramic Lessing rings

Table 2-1. List of correlations for predicting the flooding point; A* ≡ valid for air/liquid systems, R* ≡ valid for destillation systems

No.	Author	Correlation	Remarks	Lit.
1	**Sherwood, Shipley and Holloway** (1938)	$u_{V,Fl}^2 \cdot \frac{\rho_V}{\rho_L \cdot g} \cdot \frac{a}{\varepsilon^3} \cdot \left(\frac{\eta_L}{\eta_{L,W}}\right)^{0.2} = f\left(\frac{L}{V} \cdot \sqrt{\frac{\rho_V}{\rho_L}}\right)_{Fl}$	A*, for ceramic Raschig rings	[4]
2	**Kirschbaum** (1969)	$u_{V,Fl} \cdot \sqrt{\frac{\rho_V}{\rho_L}} = \sqrt{\text{const.} \cdot d_T} \approx \text{const.}$	R*, for ceramic Raschig rings	[19]
3	**Lobo et al.** (1945)	$u_{V,Fl}^2 \cdot \frac{\rho_V}{\rho_L \cdot g} \cdot F_P \cdot \left(\frac{\eta_L}{\eta_{L,W}}\right)^{0.2} = f\left(\frac{L}{V} \cdot \sqrt{\frac{\rho_V}{\rho_L}}\right)_{Fl}$	A*	[6]
4	**Eckert** (1963 and 1970)	$u_{V,Fl}^2 \cdot \frac{\rho_V}{\rho_L \cdot g} \cdot (F_P)_{exp} \cdot \frac{\rho_W}{\rho_L} \cdot \left(\frac{\eta_L}{\eta_{L,W}}\right)^{0.2} = f\left(\frac{L}{V} \cdot \sqrt{\frac{\rho_V}{\rho_L}}\right)_{Fl}$	A*, $F_P = f\left(\frac{L}{V} \cdot \sqrt{\frac{\rho_V}{\rho_L}}\right)$; $\delta\left(u_{V,Fl}\right) \leq \pm 50\%$ *for R**	[9, 8]
5	**Billet** (1968 and 1979)	$\frac{u_{V,FL}}{3.14} \cdot \sqrt{(F_P)_{exp} \cdot \frac{\rho_V}{\rho_L} \cdot \frac{\rho_W}{\rho_L} \cdot \eta_L^{0.12}} = f\left(\frac{L}{V} \cdot \sqrt{\frac{\rho_V}{\rho_L}}\right)_{Fl}$	R*, $\delta\left(u_{V,Fl}\right) \leq \pm 15\%$, for metal Raschig and Pall rings	[5]
6	**Billet -Maćkowiak** (1985)	$F_{V,Fl}^* = \left(u_{V,Fl} \cdot \sqrt{\frac{\rho_V}{\rho_L - \rho_V}}\right)_{N=const.} = f\left(\frac{L}{V} \cdot \sqrt{\frac{\rho_V}{\rho_L}}\right)_{Fl}$	A* and R*, $\delta\left(u_{V,Fl}\right) \leq \pm 10\%$	[40–48]
7	**Planowski – Kafarow** (1972)	$\log\left(u_{V,Fl}^2 \cdot \frac{\rho_V}{\rho_L \cdot g} \frac{a}{\varepsilon^3} \cdot \eta_L^{0.16}\right) = C - 1.75 \cdot \left(\frac{L}{V} \cdot \sqrt{\frac{\rho_V}{\rho_L}}\right)^{1/4}$	A*: $C = +0.022$ R*: $C = -0.125$	[11, 50]
8	**Mersmann** (1965) **Vogt** (1985)	$\frac{\Delta p_0}{\rho_L \cdot g \cdot H} = f\left[\left(\frac{\eta_L}{\rho_L \cdot g^2}\right)^{1/3} \cdot \frac{u_L}{\varepsilon} \cdot \frac{1-\varepsilon}{\varepsilon \cdot d_P}\right] = f(B_L)$	$B_L \sim \delta_L / d_h$ A*, $\delta\left(u_{V,Fl}\right) \leq \pm 20\%$	[2, 3, 34]
9	**Reichelt** (1973)	$\frac{\Delta p_0}{\rho_L \cdot g \cdot H} = f\left[\left(\frac{\eta_L}{\rho_L \cdot g^2}\right)^{1/3} \cdot \frac{u_L}{\varepsilon} \cdot \frac{1-\varepsilon}{\varepsilon \cdot d_P \cdot K} \cdot \left(\frac{\nu_V}{\nu_L}\right)^{0.1}\right]$	A*, $\delta\left(u_{V,Fl}\right) \leq \pm 20 - 50\%$ acc. to [37], valid for $d_S/d = 1.6 - 1.7$	[12]
		$\frac{\Delta p_0}{\rho_L \cdot g \cdot H} = \left[50 \cdot \left(B_L^+\right)^{0.16} + 2.5 \cdot 10^6 \cdot \left(B_L^+\right)^{1.9}\right]^{-1}$		

Table 2-1. (continued)

No.	Author	Correlation	Remarks	Lit.
10	**Schumacher** (1976)	B_L^* = dimensionless liquid load, C = gas flow parameter $B_L^* = \frac{1}{x_P} \cdot \sqrt{\frac{u_L^2}{d \cdot g} \cdot \left(\frac{x_P \cdot \nu_L}{d \cdot u_L}\right)^{0.1}}$; $C = \frac{1}{x_P} \cdot \sqrt{\frac{u_V^2}{d \cdot g} \cdot \frac{\rho_V}{\rho_L} \cdot \frac{\psi_V}{\psi_{Luft}}}$	A^* and R^* $x_P = f(d)$ x_P = packing parameter, $C = f(B_L^*)$	[10]
11	**Blaß and Kurz** (1976)	$Re_{V,Fl} =$ $k_0 \cdot \left(\frac{\eta_L}{\eta_V}\right)^{0.85} \cdot \left[\frac{d_h}{\left(\frac{3 \cdot \nu_L^2}{g}\right)^{1/3}} - 1\right]^{m_1} \cdot Re_{L,Fl}^{m_2}$	A^*, k_0, m_1, m_2 = const. $\delta(u_{V,Fl}) \leq \pm 50\%$	[37]
12	**Kister/Gill** (1992)	GRDC- graphical correlation, extended flood load factor $F_{V,Fl}^* = f(X_{Fl})$	flow parameter $X_{Fl} = \left(\frac{L}{V}\right)_{Fl} \cdot \sqrt{\frac{\rho_V}{\rho_L}}$	[88]
13	**Bornhüter/ Mersmann** (1992)	graphical correlation $\frac{\Delta p_0}{\rho_L \cdot g \cdot h} \cdot P = f(B_L)$ $\quad P \equiv$ $\frac{\varepsilon - h_{L,Fl}}{a \cdot d_T} \cdot (1 - h_{L,Fl})^{2.5}$	extended for lattice packings 25—90 mm	[66, 87]
14	**Billet, Schultes** (1995)	$u_{V,Fl} = \sqrt{\frac{2g}{\xi_{Fl}}} \cdot \frac{(\varepsilon - h_{L,Fl})^{1.5}}{\varepsilon^{0.5}} \cdot \sqrt{\frac{h_{L,Fl}}{a}} \cdot \sqrt{\frac{\rho_L}{\rho_V}}$ with $h_{L,Fl} = 0.3741\varepsilon \cdot \left(\frac{\eta_L}{\rho_L} \cdot \frac{\rho_w}{\eta_w}\right)^{0.05}_{\eta_L > 10^{-4}}$ and $h_{L,Fl} = f\left(\frac{\eta_L}{\rho_L}\right), \varepsilon/3 \leq h_{L,Fl} \leq \varepsilon$	ξ_{Fl} = resistance coefficient $= f\left(C_{Fl} \cdot \left(\frac{L}{V} \cdot \sqrt{\frac{\rho_L}{\rho_V}} \cdot \left(\frac{\eta_L}{\eta_V}\right)^{0.2}\right)^{2 \cdot n_{Fl}}\right) n_{Fl} =$ $f(X_{Fl})$ C_{Fl} = packing specific constant for $u_L <$ 80 $m^3(m^2\ h)^{-1}$, valid for 44 packing types	[89]
15	**Grabbert, Bonitz (1995)**	$u_{V,Fl} = u_{V,Fl,\,film} \cdot \gamma_{film} + u_{V,Fl,SBD} \cdot \gamma_{SBD}$ with $\gamma_{film} = \left(1 + 7.486 \cdot 10^{-3} \cdot \frac{\varepsilon}{\lambda_{0,Fl}}\right)^{-1}$	Compilation of two models: $u_{V,Fl,\,film}$ acc. to film model by Mersmann (1965) $u_{V,Fl,\,SBD}$ acc. to SBD model by Maćkowiak (1991)	[92]

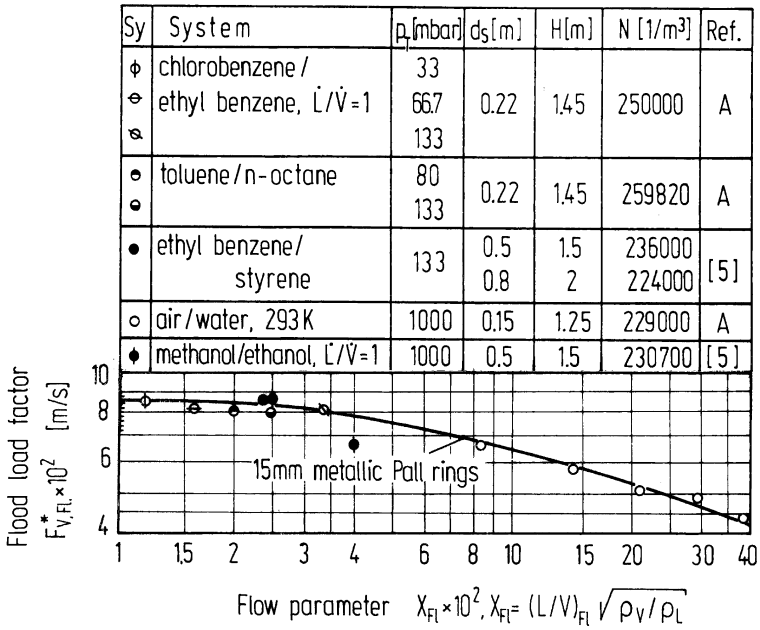

Figure 2-4a. Capacity diagram $F^*_{V,Fl} = f(X_{Fl})$ for random 15 mm metal Pall rings

were among the types of packings used. Sherwood, Shipley and Holloway [4] further modified the model developed by Walker et al. [1] by introducing the empirical factor $(\eta_L/\eta_{L,W})^{0.2}$ and the effective gas velocity $u_{V,eff.} = u_V/\varepsilon$ into Eq. (2-17). The numerical factor 1/2 in Eq. (2-17) was dropped. The result is as follows:

$$\frac{u^2_{V,Fl} \cdot \rho_V}{g \cdot \rho_L} \cdot \frac{a}{\varepsilon^3} \cdot \left[\frac{\eta_L}{\eta_{L,W}}\right]^{1/5} = f\left[\left(\frac{L}{V}\right)_{Fl} \cdot \sqrt{\frac{\rho_V}{\rho_L}}\right] \tag{2-18}$$

This type of presentation of flooding point data is still used by packing manufacturers today, albeit with minor modifications [31, 88]. There have been a number of attempts over the years to improve the accuracy of the correlation expressed in Eq. (2-18). Lobo et al. [6], Eckert [9] introduced the quotient $(\rho_{L,W}/\rho_L)$ into the left-hand side of Eq. (2-18) and proposed to replace the packing factors $F_P = a/\varepsilon^3$ of the dry packing with experimentally determined variables $F_{p,exp}$, in order to show the flooding point for all types of packings in a single load curve. The numerical values for the experimentally derived packing factors $F_{P,exp}$, using the test system air/water, were listed the study [9] in relation to various operating ranges. In Eckert's correlation, the packing factor $F_{P,exp}$ is not a packing constant, due to the fact that it is also load-dependent.

Billet [5] found new numerical values for the packing factors $F_{P,exp}$, based on comprehensive rectification investigations for 15—50 mm metal Pall and Raschig rings. They are considerably higher for given packing sizes than those derived by Eckert [9] from experiments using the air/water system. The following numerical values are given as an

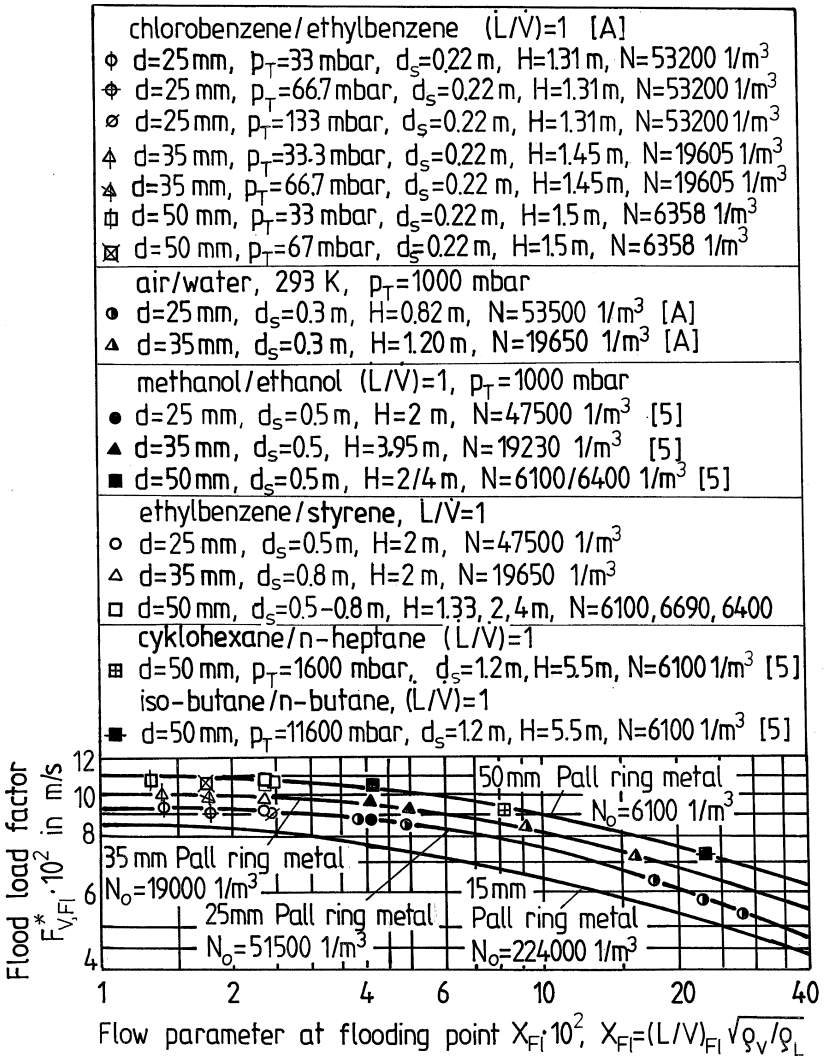

Figure 2-4b. Capacity diagram $F^*_{V,Fl} = f(X_{Fl})$ for random 15–50 mm metal Pall rings. The experimental values are based on the standard packing density N_0

example for 50 mm metal Pall rings (s = 1 mm):

$$F_{p,Billet}[5] = 107\ m^{-1} \qquad F_{p,Eckert}[9] = 65.6\ m^{-1}$$

and for 25 mm metal Pall rings:

$$F_{p,Billet}[5] = 202\ m^{-1} \qquad F_{p,Eckert}[9] = 157.4\ m^{-1}$$

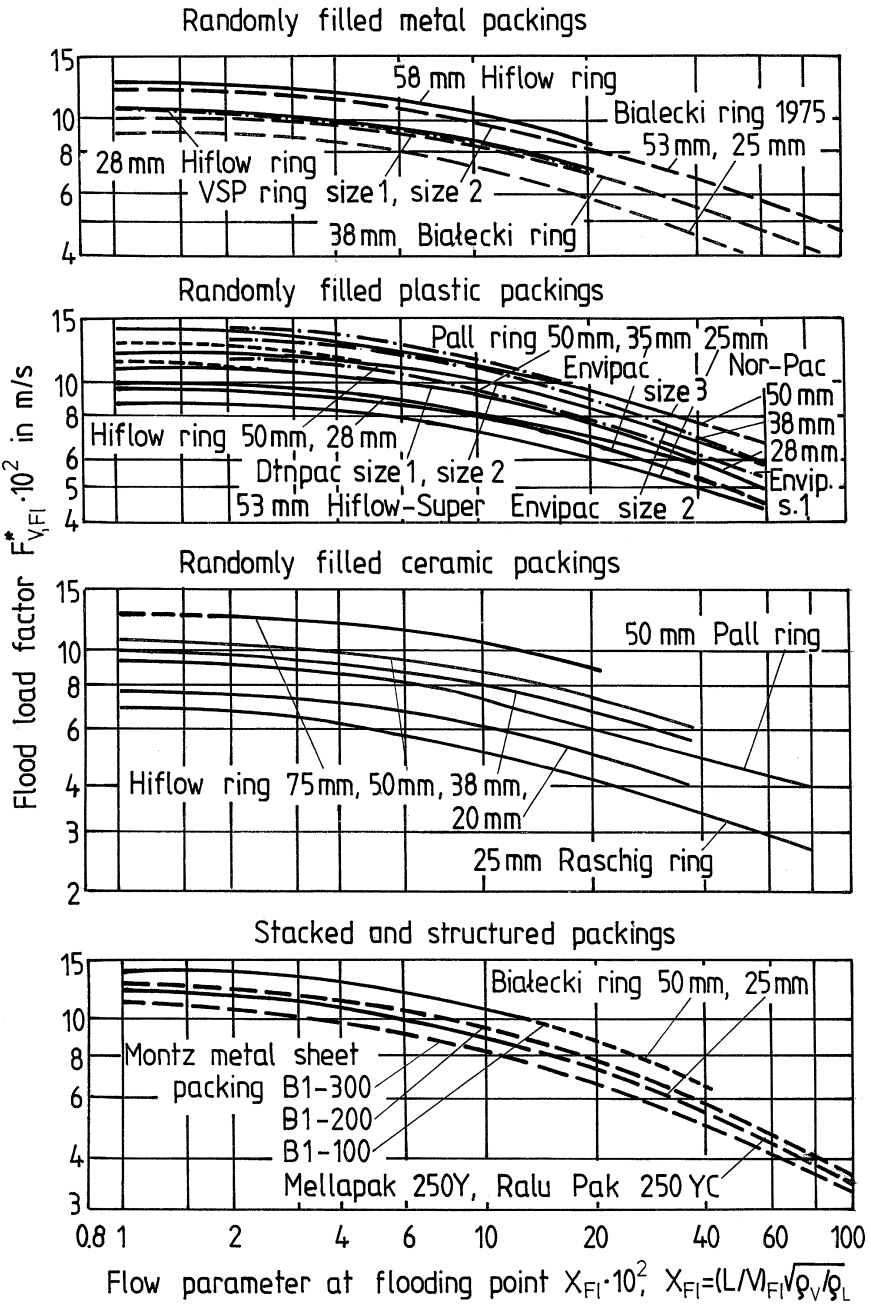

Figure 2-4c. Capacity diagram $F^*_{V,Fl} = f(X_{Fl})$ for various packing shapes. The experimental values are based on the standard packing density N_0. Experimental data – see figures in annex to Chap. 2

The empirical flooding point correlation developed by Billet [15] applies to metal Raschig and Pall rings and reflects the experimental data for the vapour/liquid systems much more accurately, $\delta(u_{V,Fl}) = \pm 15{-}20\%$, than Eckert's correlation [9] does.

Depending on the packing size, acc. to Eq. (2-4), Table 2-1, the use of packing factors $F_{p,exp}$, based on Eckert [9] correlation, results in a deviation of approx. +29.1% when determining the vapour velocity $u_{V,Fl}$.

Bolles and Fair [8] compared data found in literature, in particular experimentally derived data provided by Billet [15], with the values calculated using Eckert's correlation [9]. The comparison also showed that the values for the vapour velocity $u_{V,Fl}$, which were calculated using Eckert's correlation, were 50% higher than the numerical values which were experimentally derived, particularly for systems in the vacuum range and for larger-diameter packing elements. Consequently, the correlation valid for air/water is not applicable to vapour/liquid systems.

Planovski and Kafarov [50], quoted by Weiß et al. [11], also differentiate between flooding in distillation columns and in absorption columns. This manifests itself quantitatively in the different numerical values for the constant C_i(see Table 2-1).

The other group of methods (no. 8–11 in Table 2-1), which apply to classic packing elements with smaller sizes of up to 0.025 m, are based on the so-called *film model* [3, 60] developed by Mersmann (1965). Here, the packing is assumed to be a bundle of flow channels with equal diameters d_h. Both phases pass evenly through each flow channel, which results in the formation of a downward flowing liquid film with a thickness of δ_L. The capacity diagram shows the correlation between the dimensionless pressure drop $\Delta p_0/(\rho_L \cdot g \cdot H)$ at the flooding point (proportional to $(F_{V,Fl})^2$) and the dimensionless film thickness δ_L/d_h, Fig. 2-5a. This film thickness δ_L determines the maximum capacity of the column. A rise in the liquid loads u_L leads to an increase in the film thickness δ_L, which, in turn, leads to a reduction of the free channel cross sections. This manifests itself in the increasing pressure drop $\Delta p/H$ of the gas, see Fig. 2-1b.

The measure used by Mersmann for the film thickness is the dimensionless liquid load B_L, which is based on the known proportionality $B_L \sim (\delta_L/d_h)^2$ [2, 3]. Further modifications by Reichelt [12], Gieseler [35], Vogt [49], Kleinhückenkotten [51], Bornhütter [66, 87], Bylica, Jaroszyński [81], Grabbert, Bonitz [92] et al. [20, 30, 78] have extended the range of validity of Mersmann's correlation [2, 3, 34], see Table 2-1. The correlation developed by Billet and Schultes [89] is also based on the film model.

Conclusions Paragraph 2.2.3 – Literature Overview

When the first correlations for determining the flooding point were developed, see Table 2-1, the only types of packing available were classic, ceramic packing elements such as Raschig rings, Lessing rings, Intalox and Berl saddles as well as spheres, with preferred diameters of up to 35 mm. It was only in the late 1960s that metal packings [5] became increasingly popular and the first plastic packings came on the market. The flooding point model developed by Mersmann (1965) [2, 3] therefore assumed a film flow in the packing. It is based on the assumption that the thrust force of the gas acts on the surface of the trickle film moving downwards in the packing. This is why the model is called *film gas thrust shear force model or film model* [60].

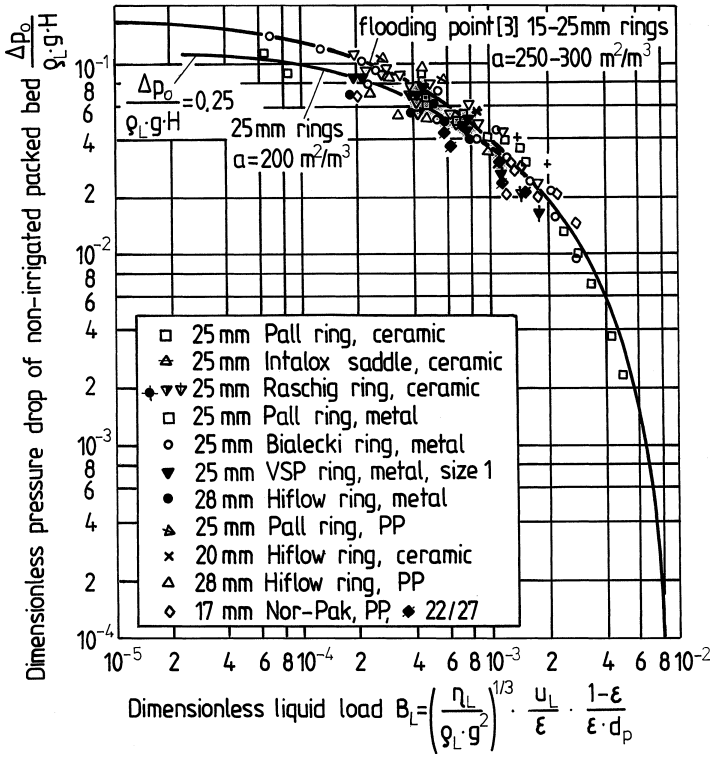

Figure 2-5a. Flooding line, dependent on the dimensionless liquid load acc. to Mersmann [3] with experimental data for various packings and test systems [20, 30, 44, 45, 46]

When, at a given liquid load u_L, certain gas velocities u_V are exceeded, the trickle film builds up in the void spaces of the packing elements, which are then gradually filled with liquid until flooding occurs. The film model is therefore a good method of describing the flooding point mechanism for operations with little droplet formation, i.e. for large-surface packing elements with low void fraction and *very high liquid loads*, e.g. for pressure rectification and pressure absorption.

This has also been confirmed by experimental data presented in this book. Figures 2-5a, 2-5b, 2-5c and 2-5d show the flooding point diagram developed by Mersmann. The diagram indicates that the experimental values for 25 mm Raschig rings, 25 mm metal Pall, Białecki and Hiflow rings, VSP rings etc., only deviate marginally from the flooding line plotted by Mersmann [2, 3]. This is based on a dimensionless dry pressure drop $\Delta p_0/\rho_L \cdot g \cdot H$ of 0.25. In the case of a low dimensionless liquid load B_L and increasing packing sizes, however, the deviation from the basic line plotted by Mersmann increases, see Figs. 2-5b, 2-5c and 2-5d. The position of the test points on the diagram reveals the following trend: A column filled with packing elements with a geometric surface of a $\approx$150 m^2 $m^{-3}$is flooded at a dimensionless dry pressure drop of $\Delta p_0/\rho_L \cdot g \cdot H$

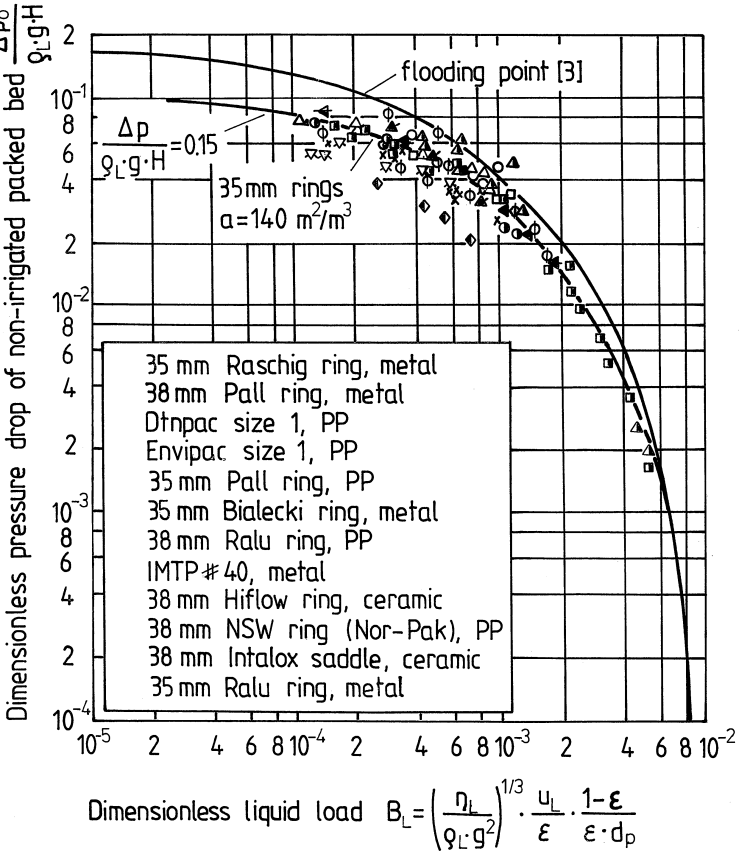

Figure 2-5b. Flooding line, dependent on the dimensionless liquid load acc. to Mersmann [3] with experimental data for various packings and test systems

≈ 0.15. If the surfaces are even larger, i.e. a $\cong 100$ m^2 m^{-3} and a $\cong 80$ m^2 m^{-3}, flooding is triggered in the case of dimensionless dry pressure drops of $\Delta p_0/\rho_L \cdot g \cdot H = 0.1$ and 0.05, respectively. As the dimensionless liquid load B_L increases, the individual surface-related flood lines move closer to the basic line given by Mersmann. This indicates that Mersmann's *film model* [3] can be used to describe the flooding point mechanism even in the case of larger packing elements, if the dimensionless liquid loads B_L are extremely high. Under such operating conditions, there is little droplet formation, and the energy of the gas is not sufficient to keep the droplets suspended.

This clearly shows that the validity range of the *film model* covers operations running at very low gas velocities and using liquids with high surface tension. This applies, in particular, to large-surface, smooth and easily irrigatable packing materials, such as ceramic. In order to describe the fluid dynamics outside this validity range, it would be better to

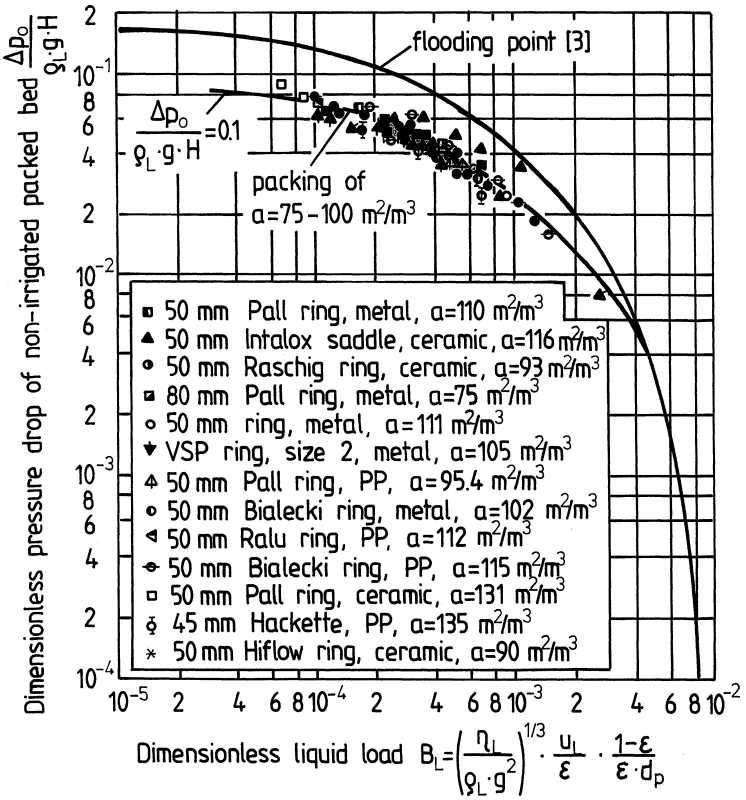

Figure 2-5c. Flooding line, dependent on the dimensionless liquid load acc. to Mersmann [3] with experimental data for various packings and test systems

develop a new model applicable to random, perforated packings with dimensions of $d \geq 0.015$ m as well as to structured packings, which takes into account a considerable droplet entrainment by the gas flow.

2.2.4
New Model of Suspended Bed of Droplets (SBD) for Determining Gas Velocity $u_{V,FI}$ at Flooding Point

One of the basic processes in technology occurs when a bed of particles is passed through by another phase. Examples of this process are: fixed bed flow, fluidised bed flow, pneumatic transport etc., all of which are qualitatively similar, as the flow occurs around single particles in the presence of surrounding particles. The basic processes mentioned above also include the flooding of packed columns under certain operating conditions, i.e. in

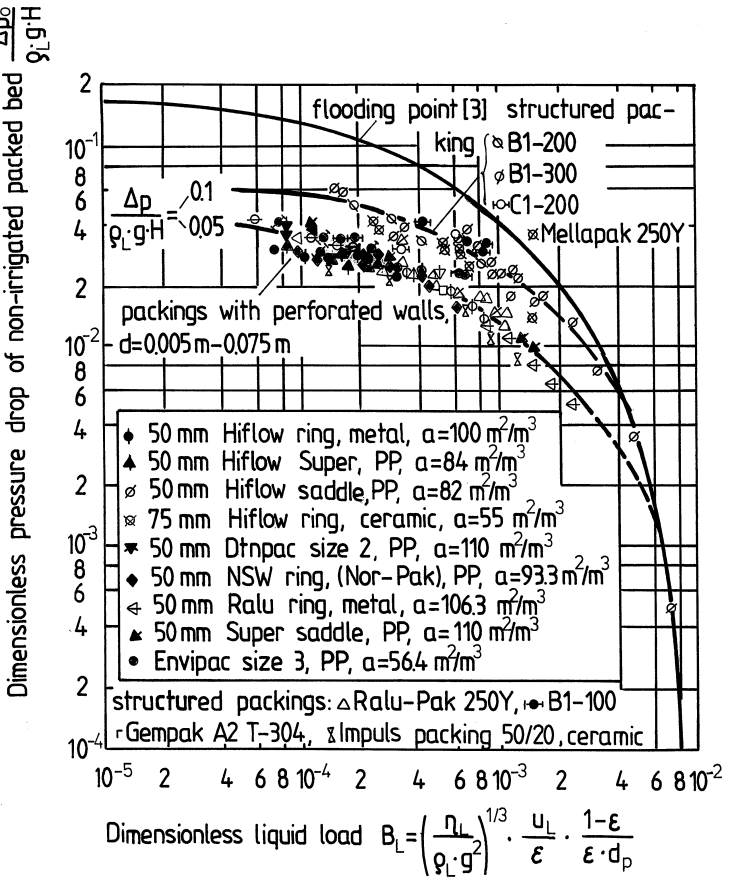

Figure 2-5d. Flooding line, dependent on the dimensionless liquid load acc. to Mersmann [3] with experimental data for various packings and test systems

the case of gas flowing through the suspended bed of droplets. This model is therefore known as the *suspended bed of droplets model*, see Fig. 2-6. First evaluated in 1986, it was presented at the GVC-VDI symposium in Strasburg (F) and published in the first German edition (1991) of this book.

Figure 2-6 shows a diagram of the terms which are useful for deriving the formula to calculate the flooding point. u_0 is used to express the superficial velocity of the gas which enables the suspension of a droplet with a diameter of d_T. $u_{V,Fl}$ describes the superficial velocity of the gas which enables the suspension of a droplet swarm. If the amount of droplets $h^0_{L,Fl}$ in the gas increases, flooding occurs at lower gas velocities $u_{V,Fl}$ in the column. The liquid hold-up $h^0_{L,Fl}$ is therefore the most important factor which influences the ratio of both gas velocities $u_{V,Fl}/u_0$. Figure 2-7 shows an example of the experimental flooding point data, acc. to Fig. 2-2a, using the function $u_{V,Fl} = f_1(1\text{-}h^0_{L,Fl})$. This confirms

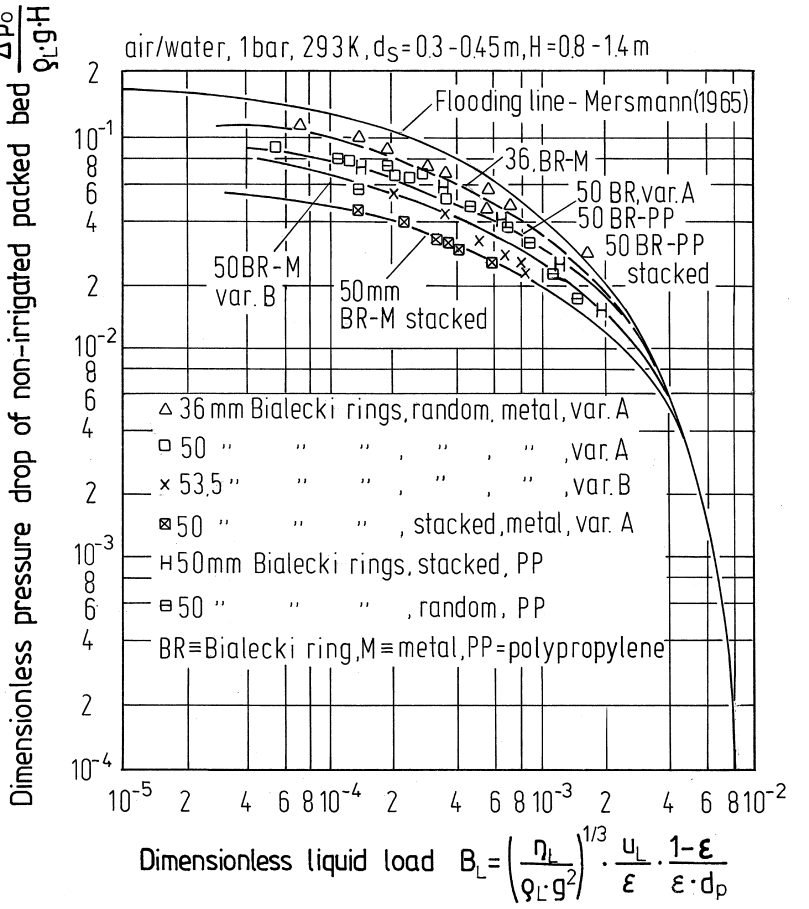

Figure 2-5e. Flooding line, dependent on the dimensionless liquid load acc. to Mersmann [3] with experimental data for random and stacked Białecki rings

the applicability of the following model:

$$\frac{u_{V,Fl}}{u_0} = \left(1 - h^0_{L,Fl}\right)^n \tag{2-19}$$

where $h^0_{L,Fl}$ is the liquid hold-up $h^0_{L,Fl}$ of the free packing volume at the flooding point, acc. to Eq. (2-19a),

$$h^0_{L,Fl} = \frac{V_{L,Fl}}{V_S \cdot \varepsilon} = \frac{h_{L,Fl}}{\varepsilon} \quad \left[m^3 m^{-3}\right] \tag{2-20}$$

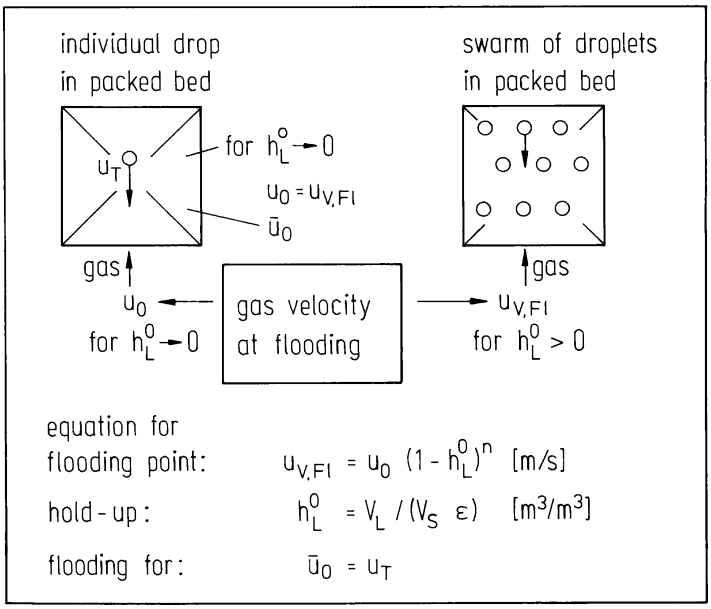

Figure 2-6. Model of suspended bed of droplets (SBD) for describing the flooding point in packed columns for gas (or vapour)/liquid systems

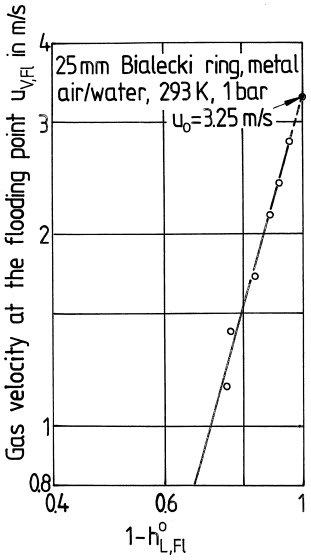

Figure 2-7. Dependence $u_{V,Fl} = f(1-h_{L,Fl}^0)$ for random metal Białecki rings. Experimental data see Fig. 2-3

Based on this model, flooding occurs when the effective gas velocity in the packing $\bar{u}_0$ has reached the value of the effective droplet velocity u_T in the packing, i.e.:

$$h^0_{L,Fl} \to 0 \quad \Rightarrow \quad \bar{u}_0 = u_T \tag{2-21}$$

An analogous condition applies to droplet swarms.

Acc. to Eqs. (2-19) and (2-21), a droplet swarm falls more slowly than a single droplet. This is due to the increased relative velocity of both phases under the influence of a modified lifting force [55], which changes as a result of the mean density change of the two-phase mixture, similarly to the sedimentation and/or fluidisation process.

The function $f_1\left(1 - h^0_{L,Fl}\right)$ describes the contraction effect, which occurs as the gas flows through the droplet swarm. The application of Eq. (2-19) for calculating the gas velocity at the flooding point $u_{V,Fl}$ requires the knowledge of the velocity u_0, the exponent n as well as the liquid hold-up at the flooding point $h^0_{L,Fl}$, which is dependent on the phase flow ratio λ_0 at the flooding point [13, 17, 18, 38], in analogy to liquid/liquid systems. Section 2.2.4.4 takes a closer look at the derivation of the equation for calculating the liquid hold-up $h^0_{L,Fl}$ for gas/liquid systems in packed columns. Tables 2-2a and 2-2b contains a list of mixtures and their properties at different top pressures p_T up to 100 bar, based on the author's own experimental flooding point data as well as on literature data.

2.2.4.1
Effective Falling Velocity of a Single Droplet in the Packing u_T

The effective falling velocity u_T of droplets in the packing is determined on the basis of Eq. (2-12). Analogy to Eq. (2-13), the balance of forces acting on a droplet leads to the following formula (2-22):

$$u_T = \sqrt{\frac{4}{3}} \cdot \sqrt{\frac{d_T \cdot g}{\psi_0}} \cdot \sqrt{\frac{\rho_L - \rho_V}{\rho_V}} \tag{2-22}$$

where ψ_0 is the resistance coefficient of a single droplet falling through the packing.

The term

$$\sqrt{\frac{4}{3}} \cdot \sqrt{\frac{d_T \cdot g}{\psi_0}} \equiv \bar{u}_T \quad \Rightarrow \quad \bar{u}_T = u_T \cdot \sqrt{\frac{\rho_V}{\rho_L - \rho_V}} \tag{2-23}$$

represents the reduced falling velocity of a single droplet $\bar{u}_T$ in the packing.

Figures 2-4a, 2-4b and 2-4c as well as the analysis of the models described in paragraph 2.2.3 provide important information on the parameters which influence the effective droplet velocity u_T. In the case of decreasing flow parameters $X_{Fl} < 10^{-2}$, the flood load factor $F^*_{V,Fl}$ remains virtually constant and is proportional to the reduced droplet

Table 2-2a. Physical properties of the test systems under vacuum and in the normal pressure range

No.	System	p_T [mbar]	ρ_V [kg/m^3]	ρ_L [kg/m^3]	$\eta_L \cdot 10^3$ [kg/(m.s)]	$\eta_V \cdot 10^6$ [kg/(m.s)]	$\sigma_L \cdot 10^3$ [N/m]	Literature
1	**air/ water**	1000	1.180	998.2	1.0	18.2	72.5	[A] et al.
2	**ethylbenzene / styrene**	133.0	0.486	826.0	0.38	7.57	23.0	[5]
	$y_T \approx 0.8$ mol/mol	66.7	0.256	837.0	0.44		25.0	
3	**methanol / ethanol**	1000	1.250	742.0	0.355	11.2	17.7	
	$y_T \approx 0.8$ mol/mol							
4	**cyclohexane / n-heptane**	344	1.140	727.0	0.505	7.06	20.6	
	$y_T \approx 0.8$ mol/mol							
5	**1,2-propylene glycol/ ethylene glycol**	13	0.032	1018.0	4.0	9.5	35.0	
6	**chlorbenzene / ethylbenzene**	33.0	0.142	954.0	0.58	7.53	30.0	[A] et al.
	$y_T \approx 0.65-0.8$ mol/mol	66.7	0.270	992.0	0.50	7.90	27.3	
		66.7	0.268	941.0	0.43	7.68	25.0	
		133.0	0.517	974.0	0.38	8.27	23.2	
		266.0	0.963	911.0	0.32	9.76	22.4	
		532.0	1.863	957.8	0.27		19.5	
		1000.0	3.334	995.0				
7	**toluene / n-octane**	133	0.473	792.0	0.39	7.23	23.0	
	$y_T \approx 0.85$ mol/mol	80	0.300	829.9	0.42	6.83	24.7	
8	**ethanol / water**	1000	1.210	786.0	0.495	10.5	25.0	
	$y_T \approx 0.65$ mol/mol							
9	**iso-octane / toluene**	133	0.545	713.3	0.40	6.71	22.5	[8, 16, 25]
		1000	3.460	660.9	0.23	8.00	14.4	
		400	1.170	831.0	0.37	8.3	23.0	[7, 26]
10	**benzene / toluene**	1000	2.740	803.0	0.28	9.0	20.0	
11	**trans-decaline / cis-decaline**	13	0.066	850.0	1.27	7.0	26.3	[5]

Table 2-2a. (continued)

No.	System	p_T [mbar]	ρ_V [kg/m^3]	ρ_L [kg/m^3]	$\eta_L \cdot 10^3$ [kg/(m.s)]	$\eta_V \cdot 10^6$ [kg/(m.s)]	$\sigma_L \cdot 10^3$ [N/m]	Literature
12	**p-xylene / m-xylene**	66.7	0.250	830.0	0.42	7.28	24.2	[A] et al.
13	**benzene / ethylene chloride**	1000	3.0	816.0	0.45	8.9	20.0	[5, 19]
14	**ethylene chloride / toluene**	20	0.088	1127.0	1.11	10.9	36.0	
		1000	3.300	1158.0	0.40		24.0	
15$^+$	**methanol / water**	466	0.54	778.0	0.41	11.81	21.7	[A]
	$y_T \approx 0.9$ mol/mol	1000	1.10	760.0	0.33	11.60	19.8	
16	**water vapour / water**	1000	0.598	958.3	0.282	15.0	58.8	[19]
17	**air / ethylene glycol** 305 K	1000	1.160	1110.0	18.50	18.2	48.0	[5, 36, 37]
18	**air / engine oil** 305 K	1000	1.160	850.0	90.0	18.2	25.6	[5]
19	**air / propylene carbonate** 293 K	1000	1.160	1259.0	2.70	18.2	44.5	[39]
20	**air / silicone oil**	1000	1.160	932.0	9.60	18.2	21.3	[36, 37]
21	**air / 98% sulphuric acid** 293 K	1000	1.160	1830.0	29.0	18.2	80.0	[29]
22	**air / 4% NaOH** 293 K	1000	1.160	1040.0	1.50	18.2	27.0	[A]
23$^+$	**1,2-dichloroethane / toluene** $y_T \approx 0.7$ mol/mol	1000	3.260	1020.0	0.36	0.45	22.0	
31	**benzene / n-heptane**	1000	2.84	765.9	0.296	8.55	19.5	[A]
32	**ethanol / benzene**	1000	2.55	787.7	0.375	8.95	21.7	[A]

A ≡ Author

$^+$ ≡ there is no flooding point data for these systems in the flooding point database; only pressure drop data $\Delta p/H$ is available

Table 2-2b. Physical properties of test systems for higher pressures

No.	System	p_T [bar]	ρ_V [kg/m^3]	ρ_L [kg/m^3]	$\eta_L \cdot 10^3$ [kg/(m.s)]	$\eta_V \cdot 10^6$ [kg/(m.s)]	$\sigma_L \cdot 10^3$ [N/m]	Literature
24	**air / propylene carbonate**	5	5.92	1204	2.69	18.2	43.7	[39]
		10	11.61				42.2	
		15	17.40				41.4	
25	**cyclohexane / n-heptane**	1.69	4.74	682.9	0.285		15.7	[5]
26	**iso-butane / n-butane**	11.6	32.2	477	0.083		6.15	[5]
27	**methanol / nitrogen (N_2)**	5	6.7	830	1.32	15.6	26.3	[75]
		10	12.5	813	0.87	16.8	23.8	
		15	20.9	833	1.27	15.9	25.4	
		20	26.6	826	1.10	16.5	24.4	
		30	41.6	834	1.32	16.0	24.5	
		40	53.8	826	1.11	16.7	23.0	
		65	86.5	822	1.03	17.4	21.5	
		80	110.4	826	0.93	18.2	20.7	
		90	127.0	833	1.27	17.9	20.7	
		100	128.8	816	0.91	18.8	18.6	
28	**ethane diol / nitrogen (N_2)**	20	23/25	1111/1128	19.1	18.6	49.7	[75]
29	**water / nitrogen (N_2)**	12.8	15.2	1000	1.30	17.5	73.8	
		20	24.0		1.27	17.7		
30	**methane / ethane**	30	51/63	393	0.08	9.0	1.8/2.5	[72]

velocity u_T, which for $h^0_{L,Fl} \rightarrow 0$ tends to the value $F^*_{V,Fl}$, i.e. $u_T \rightarrow F^*_{V,Fl}$. This applies to a given mixture and packing size.

In addition, Figs. 2-4a, 2-4b and 2-4c indicate that the reduced droplet velocity u_T increases with the packing size d. The material of the packing elements also has an influence on the parameter u_T. It follows from this that the resistance coefficient ψ_0 in Eq. (2-22) is a function of the size and the surface properties of the packing. The first influencing factor can be expressed dimensionless by the quotient $f_2(d_h/d_T)$. The second factor is linked to the resistance coefficient ψ of the dry packing. These two effects are reflected in the general correlation (2-24):

$$u_T = C_1 \cdot \sqrt{\frac{d_T \cdot \Delta\rho \cdot g}{\rho_V}} \cdot f_2\left(\frac{d_h}{d_T}\right) \cdot f_3(\psi) \tag{2-24}$$

where C_1 is a dimensionless constant. Sections 2.2.4.5 and 2.2.4.6 take a closer look at the derivation of the functions $f_2\left(d_h/d_T\right)$ and $f_3(\psi)$.

2.2.4.2
Droplet Size and Range of Droplet Movement

Figure 2-8 [15] shows that, in the case of droplet Reynolds numbers $Re_T > 400$, the resistance coefficient ψ_0 increases with the Reynolds number Re_T, contrary to expectations. Acc. to the research of numerous authors, such as Mersmann [33, 38], Reinhart [63] and Kovalenko [64], this is applicable in the range of $Re_T > 400$ only to large, deformed droplets in excess of 1 mm, falling in liquids and gases, and for $\eta_V/\eta_L \rightarrow 0$ and $\rho_V/\rho_L \ll 1$. Mersmann [2, 38, 60] found that such types of droplets are stable in the following range:

$$\frac{d_T^2 \cdot \Delta\rho \cdot g}{\sigma} < 9 \tag{2-25}$$

To calculate the droplet Reynolds number in the packing, it is necessary to ascertain the droplet velocity u_T as well as the droplet size d_T and the kinematic viscosity of the surrounding phase ν_V.

There are equations available to calculate the size of deformed droplets generated in liquid/liquid systems in packed columns. These equations can be found in the work of Mersmann [38] as well as Maćkowiak and Billet [17, 18].

For simplification purposes, the fluid dynamics model described here is based on a mean droplet diameter of:

$$d_T = C_T\sqrt{\frac{\sigma_L}{(\rho_L - \rho_V)g}} \qquad where\ C_T = 1 \qquad [17, 18] \tag{2-26}$$

Based on this, it is possible to estimate the Reynolds numbers Re_T, acc. to Eq. (2-9), with $u_V = u_T$ [17, 18, 38].

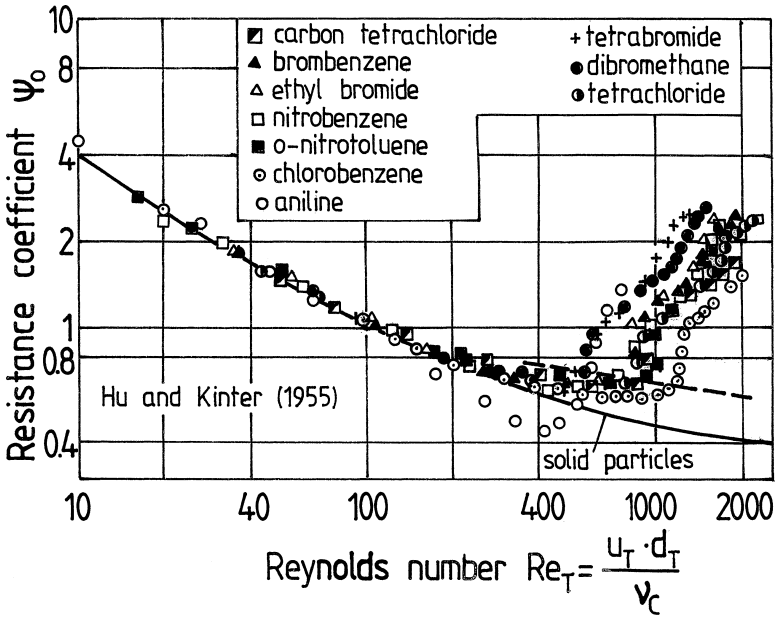

Figure 2-8. Dependence of the resistance coefficient of individual droplets ψ_0 on the Reynolds number Re_T acc. to Hu and Kinter [15]. ν_C = kinematic viscosity of the surrounding liquid. $\nu_C = \nu_V$. applies to droplet fall in gases

$$Re_T = \frac{u_T \cdot d_T}{\nu_V} \tag{2-9}$$

For the maximum stable droplet size, $C_T = 2.44$ is substituted into Eq. (2-26) [38, 57].

Bornhütter [66] has published new experimental data on the prediction of droplet size in gas/liquid systems with relation to dripping processes as well as the breakdown of sprays and threads, using water, ethylene glycol and methanol. The evaluation of the experiments shows that the droplet diameter, acc. to Eq. (2-26), is independent of the specific liquid load and of the size and type of the packing. It does, however, depend on the wetting properties and the physical properties of the liquid. In the case of ceramic, the droplets are larger than for other materials, such as PP, PTFE and stainless steel. In terms of the adhesion work $(1 + cos\,\theta) \cdot 10^3 = 80 - 120$, the constant C_T is approx. 1 ± 0.15.

Based on Eq. (2-26), with $C_T = 1$, the droplet sizes for the systems listed in Table 2-2 are approx. $1.5 \cdot 10^{-3}$ to $2.7 \cdot 10^{-3}$ m. The corresponding Reynolds numbers, acc. to Eq. (2-9), are in the range of $400 < Re_T < 1400$. Based on Fig. 2-8, this is the range in which the resistance coefficient ψ_0 increases as the Reynolds number Re_T increases, see Fig. 2-6.

Systems with very low surface tensions σ_L are characterised by smaller Reynolds numbers Re_T in the transition and/or laminar range, and the resistance coefficient ψ_0 in Fig. 2-8 decreases as the Reynolds number increases.

As a result, C_1 in Eq. (2-24) can no longer be defined as a constant. In this range, the correlations for the effective droplet velocity u_T are different from those expressed in Eq. (2-24). However, this range is less significant for practical applications.

2.2.4.3 Analogy Between the Falling Process of Particles in Fluidised Beds and the Droplet Fall in Random Packings

The analogy between the flooding process in packed columns and in fluidised beds was discussed at the beginning of Sect. 2.2.4. The diagram in Fig. 2-9, which was developed by Zenz [61], modified by Wunder and quoted, amongst others, by Mersmann [2] and Stichlmair [55], is used for determining the falling velocity of particles in the systems mentioned above. The superficial velocity is plotted on the ordinate axis of this diagram,

$$u_0 \cdot \sqrt[3]{\frac{\rho_V^2}{\Delta\rho \cdot g \cdot \eta_V}}$$

whereas the dimensionless particle diameter d_T^*, acc. to Eq. (2-27)

$$d_T^* = Ar^{1/3} \tag{2-27}$$

is plotted on the abscissa axis. Ar stands for the Archimedes number, described as:

$$Ar = \frac{d_T^3 \cdot \rho_V}{\eta_V^2} \cdot \Delta\rho \cdot g. \tag{2-28}$$

Based on Eq. (2-27), the dimensionless particle diameters d_T^* for the systems listed in Table 2-2 range between 40 and 170. Acc. to Fig. 2-9, the dimensionless superficial velocity in this range is approximately dependent on the root of the dimensionless particle diameter d_T^*. The following correlation applies:

$$u_0 \cdot \sqrt[3]{\frac{\rho_V^2}{\Delta\rho \cdot g \cdot \eta_V}} = A_i \cdot d_T^{*1/2}. \tag{2-29}$$

where A_i is the packing constant.

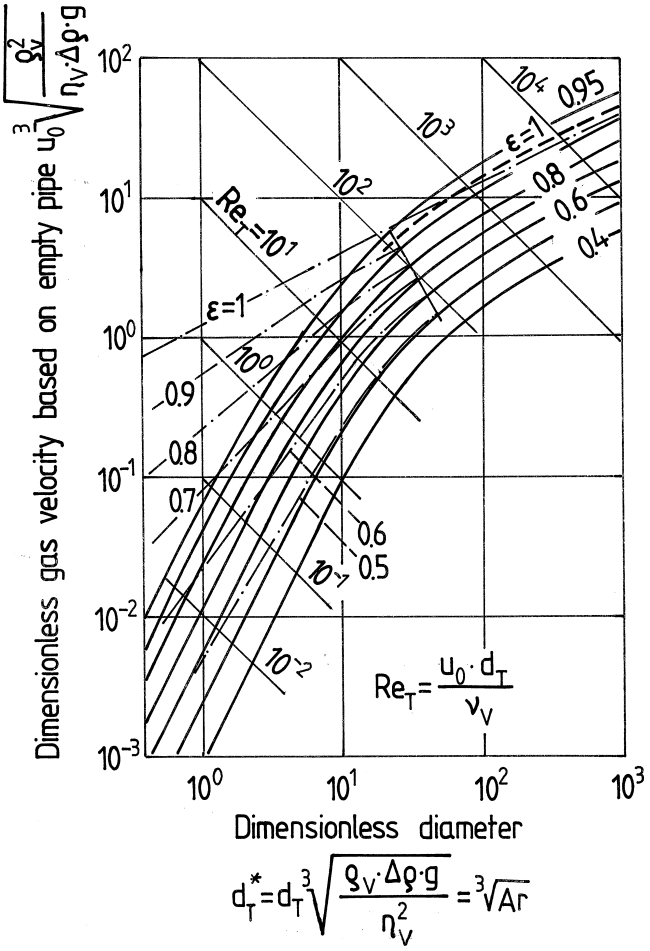

Figure 2-9. Diagram for determining the velocity, at which particles are kept in suspension [55]. _____ homogenous two-phase bed (particulate fluidisation); -.-.-.-.- inhomogenous two-phase bed (aggregative fluidisation)

By substituting Eqs. (2-27) and (2-28) into Eq. (2-29), it possible to find the correlation (2-30) for the superficial velocity u_0, in which droplets are suspended in a certain type of packing.

$$u_0 = A_i \cdot \sqrt[3]{\frac{\Delta\rho \cdot \eta_V \cdot g}{\rho_V^2}} \cdot (\sqrt[3]{Ar})^{1/2} = A_i \cdot \sqrt{\frac{\Delta\rho \cdot d_T \cdot g}{\rho_V}} \qquad \begin{array}{l} A_i = \text{packing} \\ \quad\ \text{constant} \end{array} \tag{2-30}$$

This functional correlation is comparable with Eq. (2-22).

It follows from this that both velocities — u_0 acc. to Eq. (2-30) and u_T acc. to Eq. (2-22) – are dependent on the same term:

$$u_0, u_T \approx \sqrt{\frac{d_T \cdot \Delta\rho \cdot g}{\rho_V}} \quad \text{for } d_T^* \in (40 - 170) \tag{2-31}$$

Deriving the formula, (2-27) to (2-31), showed the analogy between the model of *suspended bed of droplets* and the well-known model of fluidised beds, Fig. 2-9, in the range of $d_T^* \geq 40$.

2.2.4.4 Determining Liquid Hold-Up $h^0_{L,Fl}$ at Flooding Point

The free cross section available for gas flow changes in the presence of several droplets (droplet swarm). Droplet swarms move more slowly than individual droplets, which is due to the different lifting forces. The contraction effect is given by the function $f_1\left(h^0_{L,Fl}\right) = \left(1 - h^0_{L,Fl}\right)^n$, see Eq. (2-19).

Acc. to the SBD model described above, flooding is triggered for $h^0_{L,Fl} \to 0$, when the effective gas velocity $\bar{u}_0$ has reached the effective falling velocity of a droplet u_T, see Eq. (2-21).

It is possible, for a given packing element, to calculate the gas velocity u_0 of an empty column as well as the exponent n, using Eq. (2-19), provided there is sufficient experimental data available on the liquid hold-up $h^0_{L,Fl}$ and the corresponding gas velocities at the flooding point $u_{V,Fl}$. The variables u_0 and n for Eq. (2-19) were determined using the data for 25 mm Białecki rings shown in Figs. 2-2a and 2-2b. The results are listed in Table 2-3, see Fig. 2-7. The variables $u_0$and n were determined using the experimentally derived gas velocities $u_{V,Fl}$ at the flooding point, the corresponding specific liquid loads u_L and the respective liquid hold-ups $h^0_{L,Fl}$ as well as the properties ρ_V, ρ_L and σ_L of the test system air/water under ambient conditions. The calculation was performed using the optimisation method, based on the simplex method:

$$u_0 \cong 3.25\ ms^{-1} \pm 3\% \quad \text{and } n = 3.5 = const. \tag{2-32}$$

Table 2-3. Flooding point data acc. to Figs. 2-2a and 2-2b, valid for 25 mm random Białecki rings made of metal. Sytstem: air/water,1 bar, 293 K, $d_S = 0.15$ m, H = 1.4 m, $\varepsilon = 0.94\ m^3\ m^{-3}$, $a = 238\ m^2\ m^{-3}$, $Re_L \geq 2$

TP	$u_{V,Fl}$	$u_L \cdot 10^3$	$h_{L,Fl} \cdot 10^2$	$\lambda_0 \cdot 10^3$	$h^0_{L,Fl} \cdot 10^2$	$\frac{u_{V,Fl}}{(1-h^0_{L,Fl})^{3.5}}$	u_0
–	ms^{-1}	ms^{-1}	$m^3\ m^{-3}$	[–]	$m^3\ m^{-3}$	ms^{-1}	ms^{-1}
1	2.80	1.39	4.26	0.496	4.84	3.330	3.331
2	2.45	2.78	6.38	1.135	7.20	3.183	3.184
3	2.15	5.55	9.79	2.58	10.60	3.186	3.187
4	1.75	11.1	16.0	6.53	16.2	3.164	3.249
5	1.40	16.7	21.3	11.93	21.2	3.225	3.227
6	1.15	22.2	23.4	19.3	26.0	3.302	3.305

The simplex method is used to minimise the mean square error in the calculation of the gas velocity at the flooding point $u_{V,Fl}$, acc. to the formula:

$$\bar{\delta}(u_{V,Fl}) = \frac{1}{n_i}\sqrt{\sum_{i=1}^{n_i}\left[\frac{u_{V,Fl,exp} - u_{V,Fl,calc}}{u_{V,Fl,exp}}\right]_i^2} \tag{2-33}$$

where n_i is the number of test points. $\bar{\delta}\left(u_{V,Fl}\right)$ is the mean error in the determination of the gas velocity at the flooding point.

The constant numerical value of the exponent n = 3.5 also applies to other packing elements, for which the experimental flooding point data $u_{V,Fl}$ and u_L as well as the liquid loads $h^0_{L,Fl}$ are available, e.g. [3, 12, 22, 36, 37].

The validity verification of the method based on Eq. (2-19), for any type of system is only possible if the specific liquid hold-up $h^0_{L,Fl}$ at the flooding point is known or can be calculated. There is no such correlation available in literature for gas/liquid systems. However, the velocities $u_{V,Fl}$ and u_L at the flooding point can generally be ascertained from experiment data. In order to evaluate Eq. (2-19), it is therefore necessary to derive a correlation for determining the liquid hold-up $h^0_{L,Fl}$, which is valid for all systems.

Deriving the Correlation for Determining the Liquid Hold-Up at the Flooding Point $h^0_{L,Fl}$

Based on the two layer model for counter-current processes [13, 14, 38], the relative velocity u_R is given by the sum of the effective gas velocity of both phases $u_{V,eff}$ and $u_{L,eff}$

$$u_R = u_{V,eff} + u_{L,eff} = \frac{u_L}{\varepsilon \cdot h_L^0} + \frac{u_V}{\varepsilon \cdot \left(1 - h_L^0\right)} = f_1\left(1 - h_L^0\right). \tag{2-34}$$

The mean relative velocity u_R is usually referred to as 'slip velocity'. It is dependent on the gas content $(1–h^0_L)$ and the falling velocity of a droplet in an infinitely extended continuous phase. The falling velocity of a droplet, acc. to Eq. (2-31), only takes into account the physical properties of the system and the droplet size, whereas the gas content $(1–h^0_L)$ also includes the mutual interaction of the individual droplets. There are numerous formulas for calculating the function $f_1(1–h^0_L)$ in Eq. (2-34) for bubble columns, fluidised beds, liquid/liquid extractors, and for fluidisation and sedimentation [14, 38, 52]. These can be found in literature. However, there are no such methods available for systems, in which gas, as a continuous phase, flows through the packing counter-current to the downward moving liquid phase.

Figure 2-10 shows the slip velocity u_R plotted against the liquid hold-up h^0_L for randomly filled Białecki rings. The parameter here is the liquid load u_L.

A set of curves is generated by different liquid loads $u_{L,i}$, which can be expressed near the flooding point by the following equation:

$$u_{R,i} = P_i \cdot \left(1 - h_L^0\right)^m \tag{2-35}$$

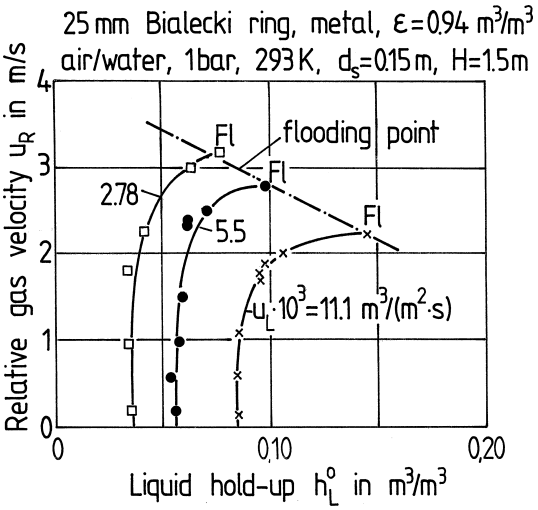

Figure 2-10. Experimentally derived relative velocity u_R as a function of the liquid hold-up h_L^0, valid for random 25 mm metal Białecki rings, based on data shown in Fig. 2-2b

in analogy to the known models developed, e.g., by Mersmann [38]. Figure 2-10 indicates that the characteristic gas velocity P_i is a function of the specific liquid load, i.e. $f(u_L)$, which means $P_i$is only constant for a specific liquid load $u_{L,i}$, and the curve $u_R = f(h_L^0)$ tends to zero near the flooding point. The two layer model is therefore suitable for determining the liquid hold-up at the flooding point $h_{L,Fl}^0$. However, it does not lead to a general method for determining the gas velocity at the flooding point. This is why the method for calculating the gas velocity $u_{V,Fl}$ was derived using Eq. (2-19).

Combining Eqs. (2-34) and (2-35) gives the following equation:

$$\frac{u_L}{\varepsilon \cdot h_L^0} + \frac{u_V}{\varepsilon(1 - h_L^0)} = P_i(1 - h_L^0)^m \tag{2-36}$$

Figure 2-11 shows a diagram of the correlation between the liquid hold-up h_L^0 and the gas velocity u_V. The correlation for $h_{L,Fl}^0$ was derived, based on the following assumptions: $\left(\partial u_V / \partial h_L^0\right) = 0$ at the flooding point for $u_L = \text{const}$.

In the operating range above 65% of the flooding point, the differentiation of the transposed Eq. (2-36)

$$u_V = \varepsilon \cdot \left[P_i \cdot \left(1 - h_L^0\right)^{m+1} - u_L \cdot \left(h_L^0 - 1\right)^{-1}\right] \tag{2-37}$$

for $\left(\partial u_V / \partial h_L^0\right) = 0$ and for selected specific liquid loads $u_{L,i} = \text{const}$.

$$\left[\frac{\partial u_V}{\partial h_L^0}\right]_{uL,i=const} = (P_i \cdot \varepsilon) \cdot (m+1) \cdot \left(1 - h_L^0\right)^m \cdot (-1) - u_L \cdot \left(-\frac{1}{\left(h_L^0\right)^2}\right) = 0 \tag{2-38}$$

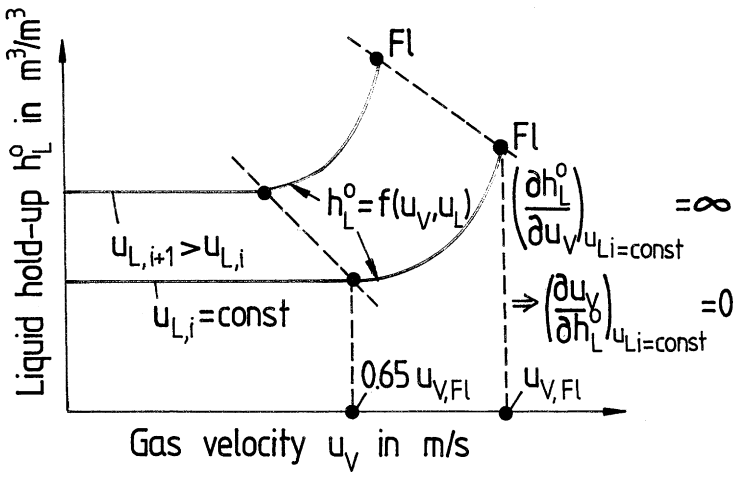

Figure 2-11. Schematic representation of the dependence of h_L^0 on the gas velocity u_V in packed columns

leads to the following solution:

$$(1 - h_L^0)_{Fl}^m = \frac{u_{L,Fl}}{(P_i \cdot \varepsilon) \cdot \left(h_{L,Fl}^0\right)^2 \cdot (m+1)} \tag{2-39}$$

Substituting Eqs. (2-1) and (2-39) into Eq. (2-36) gives the relationship between the phase flow ratio and the liquid hold-up $h_{L,Fl}^0$ at the flooding point:

$$\lambda_0 = \frac{(h_{L,Fl}^0)^2(m+1)}{[1 - h_{L,Fl}^0][1 - h_{L,Fl}^0(m+1)]} \tag{2-40}$$

The differentiation of Eq. (2-36) leads to the same Eq. (2-40), under the following conditions:

for $u_V = \text{const.}$ $\rightarrow$ $(\partial u_V / \partial h_L^0) = 0$ and
for $u_L/u_V = \text{const.}$ $\rightarrow$ $(\partial u_V / \partial h_L^0) = 0$

For reasons of brevity, the analogous derivation process, based on Eqs. (2-36) and (2-40), is not discussed here.

The derived Eq. (2-40) shows that the liquid hold-up at the flooding point $h_{L,Fl}^0$ is only dependent on the phase flow ration λ_0 at the flooding point and on the parameter m. The exponent m can be determined from experiments with known value pairs $\lambda_0 = (u_L/u_V)_{Fl}$, acc. to Eq. (2-1), and $h_{L,Fl}^0$ by transposing Eq. (2-30), using the following formula:

$$m = \left[h_{L,Fl}^0 \left(\frac{h_{L,Fl}^0}{\lambda_0 \cdot (1 - h_{L,Fl}^0)} + 1 \right) \right]^{-1} - 1 \tag{2-41}$$

Evaluation of Experimental Results for the Range of Low and Moderate Phase Flow Ratios λ_0 at Flooding Point

The experimental data available for the evaluation of Eq. (2-41) gives a constant numerical value for the exponent m, based on $\lambda_0 \leq 0.025$ and on the Reynolds numbers of the liquid $Re_L = u_L/a \cdot \nu_L \geq 2$, Eq. (2-42)

$$m \approx -0.8 \pm 12\ \% \tag{2-42}$$

The numerical value of the parameter *m* was determined for various systems, namely air/water, ethanol/water, steam/water [7], air/silicone oil [36, 37], using various random and structured packings made of different materials. In the range of low and moderate λ_0 numbers below $\lambda_0 < 0.025$, the parameter m is not dependent on the phase flow ratio λ_0 at the flooding point, see Fig. 2-12a.

For $h^0_{L,Fl} \leq 0.3$, the Archimedes number was found to have no impact. The same applies to fluidised beds [2, 55, 38]. Figure 2-12b is based on experimental data taken by Pliss, Ender [67] and Bornhütter [66] at an industrial pilot plant at the Technical University of Munich, using modern 50−90 mm lattice packings produced by Envipac (size 3), Hiflow rings, VSP rings and 50 mm Pall rings made of metal and plastic, with $d_S = 1$ m and a packing height of approx. 3.5 m, as well as experimental data for structured packings (Mellapak 250Y, 250X and 500Y), taken at an industrial pilot plant, operated by Sulzer, with $d_S = 1$ m and H = 3.7 m [67–69], plus additional data [79, 71]. The diagram

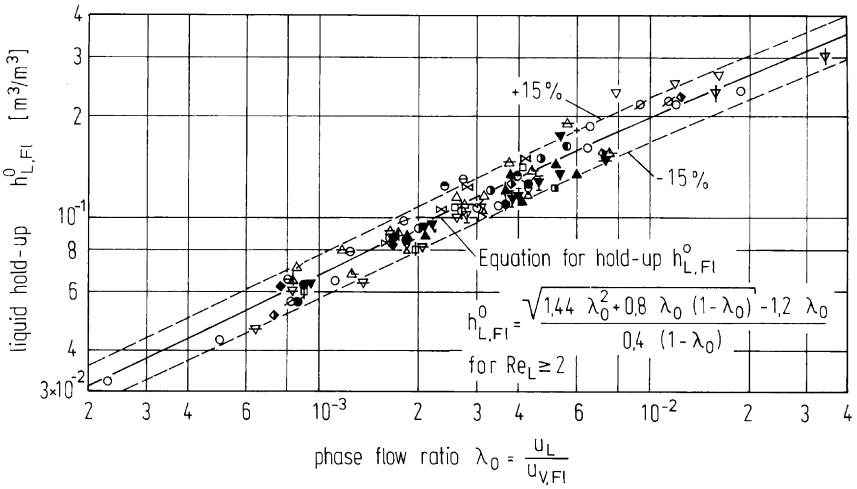

Figure 2-12a. Dependence of the liquid hold-up at the flooding point $h^0_{L,Fl}$ on the phase flow ratio λ_0, valid for various systems and packings made of metal, ceramic and plastic for $Re_L \geq 2$ – experimental data taken by the author in comparison to calculated values based on Eq. (2-47)

Table Relating to Fig. 2-12 a Experimental hold-up data at the flooding point $h^0_{L,Fl}$

TP	d·10³ [m]	Packing	Material	System	ε [m³/m³]	d_S [m]	H [m]	Lit.
○	25	**Białecki rings** random	metal	air/water 1bar, 293 K	0.94	0.154	1.5	[43]
▽	15	**Raschig rings** random	ceramic		0.676	0.226	0.63	[22]
▼	25	**Raschig rings** random	glass		0.82	0.15	1.0	[36,37]
▽	25			air/silicone oil 1 bar, 293 K				
▽	25		ceramic	C_2H_5OH/H_2O	0.667	0.3	2.0	[7]
▼				H_2O/H_2O				
+	20	**Hiflow ring** random		air/water 1 bar, 293 K	0.762	0.3	1.2	[A]
⊕	75				0.865	0.45	2.0	
●	28	**Hiflow ring** random	metal		0.962	0.3	1.46	
●	58				0.97	0.45	2.0	
□	25	**Pall ring** random			0.95	0.3	1.46	
◨	35				0.95	0.3	1.46	
◧	58				0.97	0.45	2.0	
▷	32 (Gr.1)	**VSPring** random			0.976	0.30/0.45	1.46/2.0	
▶	50 (Gr.2)				0.98	0.45	2.0	
▲	30 (Gr.1A)	**Envipac** random	plastic (PP)		0.932	0.3	1.96	
△	35	**Intalox saddle** random	plastic		0.90	0.3	1.36	
▲	50	**Hiflow ring** random			0.94	0.45	2.0	
◫		**Pall ring**			0.926			
◬	25	**Intalox saddle** random	ceramic		0.73	0.30	0.9	
◬	38				0.757		1.4	
◆	50	**NSW ring**	plastic		0.950	0.45	2.0	
◬		**Ralu ring**			0.940			
◆	25	**NSW ring, Typ C** random			0.92	0.15	1.3	[40]
⌀	25	**Białecki ring stacked**	metal		0.928	0.15	1.5	[A]
◐	–	**Montz packing B1-300**	sheet metal		0.972	0.3	1.4	
◑	–	**Montz packing B1-200**			0.978			
◍	–	**Montz packing C1-200**	plastic		0.954			
⊖	–	**Mellapak 250Y**	sheet metal		0.96	0.22	1.25	
⋈	70 (Gr.2)	**Dtnpac**	plastic		0.938	0.3	1.4	
⧖	45 (Gr.1)				0.92	0.45	2.0	

shows the hold-up at the flooding point $h^0_{L,Fl}$ as a function of the phase flow ratio at the flooding point λ_0 in the range up to $\lambda_0 \to 1$.

The parameter m, calculated by means of the simplex method, can be described by the new model for phase flow ratios ranging from $\lambda_0 = 0.001$ to 1.0:

$$m = -0.82 + \frac{\lambda_0}{\lambda_0 + 0.5} \tag{2-43}$$

This changes to $m \approx -0.80$ in Eq. (2-42) for lower phase flow ratios λ_0 in the range shown in Fig. 2-12a. Equation (2-43) leads to a correlation for $m = (\lambda_0)$, which covers practically all areas of application of packed columns for gas/liquid systems, ranging from vacuum rectification to pressure rectification and pressure absorption.

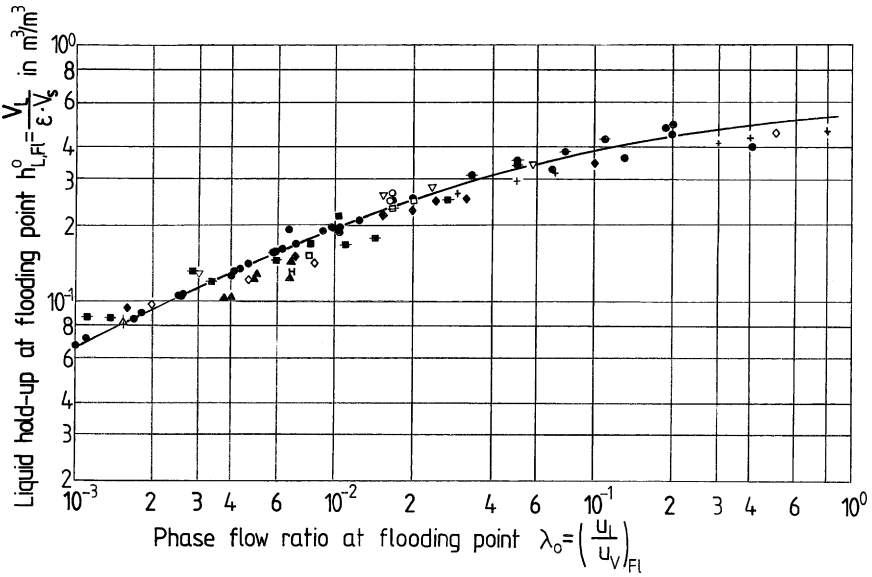

Figure 2-12b. Dependence of the liquid hold-up at the flooding point $h^0_{L,Fl}$ on the phase flow ratio λ_{-0}, valid for various systems and packings made of metal, ceramic and plastic for $Re_L \geq 2$ – experimental data [67–71] for high phase flow ratios at the flooding point λ_{-0} and large column diameters in comparison to calculated values based on Eq. (2-47)

Table Relating to Fig 2-12b Experimental hold-up data at the flooding point $h^0_{L,Fl}$. System: air / water, 1 bar, 293 K

TP	$d \cdot 10^3$ [m]	Packing	Material	a [m^2/m^3]	ε [m^3/m^3]	d_S [m]	H [m]	Literature
▲	50	**Hiflow ring** 6874 m^{-3}	PP	90.7	0.926	1.0	3.70	1991 [66]
◬	58	**Hiflow ring** 5060 m^{-3}	metal (1.4301)	93.0	0.979	1.0	3.15	1991 [66]
H	90	**Hiflow ring** 1415 m^{-3}	PP	61.0	0.954	1.0	3.51	1991 [60]
○	–	**K packing** (25 x 12 x 2 mm)	ceramic	192	0.810	0.2	1.00	[70]
⊠	–	**Mellapak 250 X** φ = 30°	sheet metal	250	0.980	1.0	3.50	1995 [68,69]
⊟	–	**Mellapak 250 Y** φ = 45°	sheet metal	256	0.975	1.0	3.50	1995 [68,69]
▽	–	**Mellapak 500 Y** φ = 45°	sheet metal	500	0.975	1.0	3.50	1995 [68,69]
+	50	**Pall ring** 6846 m^{-3}	PP	112	0.929	1.0	3.43	1991 [66]
●	15	**Raschig ring**	ceramic	300	0.700	0.2	1.00	[71]
△	50	**VSP ring** Gr.2	metal (1.4571)	100	0.98	1.0	3.50 6.00	1991 [67]

For Reynolds numbers $Re_L < 2$ (Chap. 4) in laminar liquid flow, the numerical value is as follows:

$$m = -0.9 + \frac{\lambda_0}{\lambda_0 + 0.5} \tag{2-44}$$

which changes to

$$m \approx -0.88 \pm 12\ \% \tag{2-45}$$

for $h^0_{L,Fl} < 0.20$. The parameter m in Eq. (2-41) for gas/liquid systems is therefore dependent on the liquid flow in the packing as well as on the phase flow ratio at the flooding point λ_0, in the case of higher liquid hold-ups $h^0_{L,Fl} > 0.2$.

Now that the phase flow ratio λ_0 and the exponent m are known, it is possible to solve Eq. (2-40) for $h^0_{L,Fl}$. The general, real solution of the quadratic Eq. (2-40) $h^0_{L,Fl} = f(\lambda_0)$ is as follows:

$$h^0_{L,Fl} = \frac{\sqrt{\lambda_0^2(m+2)^2 + 4\lambda_0(m+1)(1-\lambda_0)} - (m+2)\lambda_0}{2 \cdot (m+1)(1-\lambda_0)} \qquad \left[m^3 m^{-3}\right] \tag{2-46}$$

which, for $\lambda_0 < 0.025$ with $m = -0.8$ and for moderate phase flow ratios $\lambda_0 < 0.025$, acc. to Fig. 2-12a, leads to Eq. (2-47) describing the liquid hold-up $h^0_{L,Fl}$ for $Re_L \geq 2$ at the flooding point.

$$h^0_{L,Fl} = \frac{\sqrt{1.44\lambda_0^2 + 0.8\lambda_0(1-\lambda_0)} - 1.2\lambda_0}{0.4 \cdot (1-\lambda_0)} \qquad \left[m^3 m^{-3}\right] \tag{2-47}$$

This equation is applicable to vacuum rectification and absorption, operated under low and/or moderate liquid loads u_L.

Figures 2-12a and 2-12b show the comparison between the calculated $h^0_{L,Fl}$ values and the experimental data. The evaluation took into account experimental data for randomly filled, stacked and structured packings with void fractions of $0.65 \leq \varepsilon \leq 0.98$ $m^3 m^{-3}$ as well as for packing elements with diameters from $d = 0.015$ to $d = 0.090$ m. The deviation of the experimental values from the curve, which was calculated using Eq. (2-47), is $\delta(h^0_{L,Fl}) \leq \pm 15\%$. Figures 2-12a and 2-12b show that the liquid hold-up $h^0_{L,Fl}$ at the flooding point is dependent on the phase flow ratio λ_0 at the flooding point and can therefore be determined for any type of system, acc. to the single-parameter Eq. (2-47).

The properties and constructive parameters of the test systems are varied in the following ranges:

$$\left.\begin{array}{l}\sigma_L = 26.....72\ mNm^{-1}\\ \eta_L = 0.35.....10\ mPas\\ \rho_V = 0.09.....1.2\ kgm^{-3}\\ \rho_L = 932.....1000\ kgm^{-3}\\ d \cdot 10^3 = 15.....90\ m\\ d_S = 0.15.....1.0\ m\\ H = 0.7.....7.0\ m\\ \lambda_0 \cdot 10^3 = 0.2.....1000\ [-]\end{array}\right\}\ for\ \mathrm{Re}_L \geq 2 \qquad (2\text{-}48)$$

There is little data available for laminar liquid flow, with $Re_L < 2$, for the test system air/water [A] for 12 mm metal Białecki rings, 15 mm Pall rings, 17 mm Nor-Pac rings and 18 mm Hiflow rings made of PP and/or for air/silicone oil [36, 37]. Figure 2-13 shows the comparison between the liquid hold-up $h^0_{L,Fl}$, which was calculated using Eq. (2-46), with the parameter m, based on Eq. (2-44), and the experimental data $(h^0_{L,Fl})_{exp}$. The deviations from the curve, reflecting Eq. (2-49), with $m = -0.88$, acc. to Eq. (2-45), are approx. ±10% in the range of the phase flow ratios $\lambda_0 = (0.2-6)\cdot 10^{-3}$.

$$h^0_{L.Fl} = \frac{\sqrt{1.254 \cdot \lambda_0^2 + 0.48 \cdot \lambda_0 \cdot (1-\lambda_0)} - 1.12\lambda_0}{0.24 \cdot (1-\lambda_0)} \quad \left[m^3 m^{-3}\right] \qquad (2\text{-}49)$$

The applicability of the derived Eqs. (2-47) and (2-49) for determining the gas velocity at the flooding point for low-viscosity and viscous mixtures is shown in Table 2-4, based on the example of 25 mm metal Pall rings.

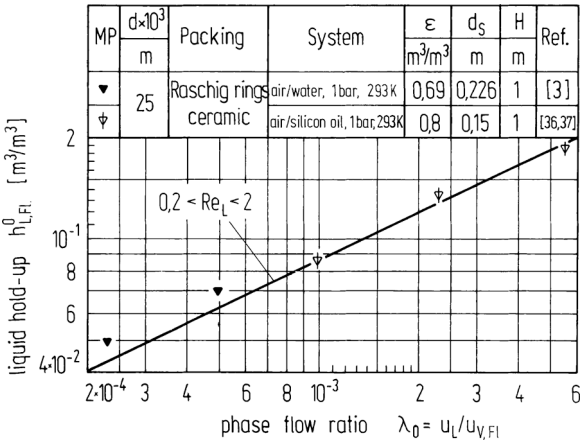

Figure 2-13. Dependence of the liquid hold-up at the flooding point $h^0_{L,Fl}$ on the phase flow ratio λ_0 for $Re_L < 2$ – experimental data in comparison to calculated values based on Eq. (2-49)

Table 2-4. List of experimental data on the flooding point for random 25 mm metal Pall rings, valid for various systems

–	(a) valid for $Re_{L,Fl} \geq 2$, $h^0_{L,Fl}$ calculated acc. to Eq. (2-47), $u_{V,Fl}$ acc. to Eq. (2-69), $C_{Fl,0} = 0.566$					(b) valid for $Re_{L,Fl} \geq 2$, $h^0_{L,Fl}$ calculated acc. to Eq. (2-49), $u_{V,Fl}$, $C_{Fl,0}$ as (a)	
System	ethylbenzene/ styrol $\dot{L}/\dot{V} = 1$ N = 47500 m^{-3}	air/water 293 K N=51500 m^{-3}	air/water 293 K N = 52388 m^{-3}	chlorobenzene/ ethylbenzene $\dot{L}/\dot{V} = 1$ N=53200 m^{-3}	air/glycol 305 K N=51500 m^{-3}	ethyleneglycol/ propylene-glycol N=47500 m^{-3}	air/ engine oil 305 K
p_T [mbar]	133	1000	1000	33 66.7 133	1000	13.3	1000
d_S/H [mm^{-1}]	0.8/2	0.435/ 1.65	0.3/0.8	0.22/1.31 0.22/1.31 0.22/1.31	0.435/1.65	0.5/2	0.435/1.65
ρ_V [kgm^{-3}]	0.482	1.165	1.165	0.212 0.327 0.578	1.135	0.036	1.135
ρ_L [kgm^{-3}]	854.0	998.2	998.2	1026.0 995.0 974.7	1110	1017	850
a [$m^2\ m^{-3}$]	198.7	215.0	218.7	222.1 222.1 222.1	215.0	198.7	215
σ_L [mNm^{-1}]	21.7	72.74	72.74	30.0 28.0 25.6	48.0	30.0	25.6
ε [$m^3\ m^{-3}$]	0.947	0.942	0.941	0.94 0.94 0.94	0.942	0.947	0.942 0.942 0.940 0.940
$\eta_L.10^3$ [$kgm^{-1}\ s^{-1}$]	0.32	1.0	1.0	0.62 0.50 0.41	18.5	4.0	85.5 89.5 91.2 92.6

Table 2-4. (continued)

–	(a) valid for $Re_{L,Fl} \geq 2$, $h^0_{L,Fl}$ calculated acc. to Eq. (2-47), $u_{V,Fl}$ acc. to Eq. (2-69), $C_{Fl,0} = 0.566$					(b) valid for $Re_{L,Fl} \geq 2$, $h^0_{L,Fl}$ calculated acc. to Eq. (2-49), $u_{V,Fl}$, $C_{Fl,0}$ as (a)	
System	ethylbenzene/ styrol $\dot{L}/\dot{V} = 1$ N = 47500 m^{-3}	air/water 293 K N=51500 m^{-3}	air/water 293 K N = 52388 m^{-3}	chlorobenzene/ ethylbenzene $\dot{L}/\dot{V} = 1$ N=53200 m^{-3}	air/glycol 305 K N=51500 m^{-3}	ethyleneglycol/ propylene-glycol N=47500 m^{-3}	air/ engine oil 305 K
$(u_{V,Fl})_{exp}$ $[ms^{-1}]$	3.90	1.550 1.643 1.826	2.51 2.17 2.05 1.91	6.26 5.04 3.705	1.89 1.78 1.72	15.6	1.76 1.57 1.36 1.34
$(u_L.10^3)_{exp}$ $[ms^{-1}]$	2.63	14.92 13.05 10.83	2.78 5.54 8.40 11.10	1.30 1.66 2.20	9.27 11.08 12.90	0.55	5.27 6.95 8.60 10.30
$\lambda_0.10^3$ [-]	0.670	9.63 7.94 5.93	1.11 2.55 4.09 5.81	0.21 0.33 0.60	5.08 6.40 8.11	0.03	3.00 4.43 6.32 7.68
Re_L [-]	27.33	69.23 60.63 50.30	12.70 25.30 38.30 50.65	9.7 14.9 23.5	2.59 3.09 3.60	0.75	0.224 0.300 0.365 0.440
$(u_{V,Fl})_{calc}$ $[ms^{-1}]$	3.68	1.66 1.767 1.907	2.657 2.333 2.083 1.89	6.12 4.71 3.30	2.023 1.90 1.782	16.44	1.56 1.38 1.223 1.09
$\delta(u_{V,Fl})$ [%]	5.6	−8.38 −7.5 −4.4	−5.85 −7.5 −1.6 +0.5	+2.2 +6.6 +10.8	−7.04 −7.9 −3.6	−5.40	+11.4 +12.0 +10.04 +18.6
Literature	Billet [5]	Billet [5]	[A]	[A]	Billet [5]	Billet [5]	Billet [5]

2.2.4.5 Influence of Packing Size on Droplet Velocity u_0

The prediction of the effective individual droplet velocity u_T for packings of any given size, acc. to Eq. (2-24), is only possible, once the correlations for functions $f_2(d_h/d_T)$ and $f_3(\psi)$ have been found. Table 2-5 contains the numerical values of the reduced droplet velocity $\bar{u}_T$ for various types of packing elements. It shows that $\bar{u}_T$ is dependent on the type and size of the packing element and therefore on the packing-specific variables a and ε. Physically, this can be compared to the fall of an individual droplet in a tube near a circular wall. It was referred to as a *wall effect* by Strom and Kinter [62], Reinhart [63] and Clift et al. [65]. Figure 2-14 is a schematic representation of this effect.

If the droplet diameter d_T approximates to the tube diameter d_R, i.e. $d_T \cong d_R$, the ratio of the falling velocity u_T of the droplet to the maximum velocity $u_{T,max}$ tends to zero, see Fig. 2-14. The droplet only reaches its maximum falling velocity $u_{T,max}$ when the diameter ratio d_R/d_T is sufficiently high.

The wall effect in packed columns is analogous to the fall of droplets in tubes, acc. to [62, 63, 65], and can be expressed by the following functions:

$$\frac{u_T}{u_{T,\max}} = \left[1 - \left(\frac{d_T}{d_h}\right)^b\right]^c \qquad \text{b,c} = \text{exponent} \tag{2-50}$$

and/or based on the equation developed by Wallis [65]:

$$\frac{u_T}{u_{T,\max}} = d \cdot \left[\frac{d_T}{d_h}\right]^e \qquad \text{d} = \text{const.}, \quad \text{e} = \text{exponent} \tag{2-51}$$

where the hydraulic diameter of the packing d_h is introduced instead of d_p. For simplification purposes, the wall effect in packed columns is expressed by the correlation in Eq. (2-51), as this requires one less constant to be determined when deriving the final equation for the gas velocity at the flooding point $u_{V,Fl}$.

The proximity of the packing wall also has an influence on the droplet fall in the packing. In the channel model, the tube diameter depends on the channel diameter, acc. to Eq. (2-52), see Chap. 3.

$$d_h = 4 \cdot \frac{\varepsilon}{a} \tag{2-52}$$

When the droplet size is equal to the hydraulic diameter d_h of the packing, acc. to Eq. (2-52), it is not possible for the droplet to fall in the packing, i.e. $u_T \rightarrow 0$. It can therefore be assumed that the reduced droplet velocity $\bar{u}_T$ changes with the diameter ratio d_h/d_T, if d_h becomes larger than the droplet diameter d_T, acc. to Eq. (2-26).

Figure 2-15 leads to the following correlation between the reduced droplet velocity $\bar{u}_T$ and the ratio d_h/d_T and therefore between the effective droplet velocity $u_T$and the quotient (d_h/d_T), see Eq. (2-53):

Table 2-5. List of experimental data of the reduced gas velocity of an individual droplet $\bar{u}_T$ for various types of packings, used for determining the gas or vapour velocity $u_{V,Fl}$ – data relating to Fig. 2-15

No.	TP	Number of TP	Packing	Material	d·10³ [m]	a [m²/m³]	ε [m³/m³]	$\bar{u}_T \cdot 10^2$ [m/s]	d_S [m]	H [m]	Literature
1	□	4	**Pall ring**	metal	15	376.8	0.93	9.63	0.22-0.3	1.4	[A], [5,28]
		5			15	368.4	0.933	10.4	0.15-0.8	2	
2	▣	24			25	215	0.950	11.8	0.22-0.8	2	[A],[5,16,25]
		4			25	217	0.950	12.6	0.3	0.8	[A]
		5			25	292	0.970	12.0	0.15	1.3	[A]
3	■	12			35	150	0.946	12.8	0.3-0.8	1.2-4	[A],[5]
		5			38	149.6	0.952	13.3	0.22-0.3	1.45	[A]
4	▣	8			50	110	0.952	13.5	0.5-1.2	2-5.5	[5]
		4			50	110	0.952	14.1	0.305-0.75	3.85	[16,25,28]
		5			58	112	0.979	15.5	0.45	2	[A]
5	■	4			80	78	0.96	18.0	0.75	3	[28]
6	■	12		plastic (PP,PVDF)	25	239.7	0.88	10.3	0.22-0.5	1.4-2	[A],[23]
7	■	5			35	142	0.922	13.0	0.3-0.45	1.4	[A]
8	■	2			50	110	0.92	12.9	0.75	3	[28]
		2			50	111	0.919	13.2	0.3	1.4	[A]
9	●	8	**Białecki ring**	metal	25	238	0.94	11.3	0.3	1.4	[20]
		7			25	225	0.945	11.3	0.15	1.4	[A]
10	●	7			35	155	0.95	12.8	0.22-0.3	1.45	[A],[20]
11	●	7			53.5	110	0.973	14.8	0.3	1.4	[20]
12	△	9	**VSP ring**	metal	32 (Gr.1)	200.8	0.972	13	0.22-0.45	1.4-2	[A]
13	▲	5			50 (Gr.2)	104.9	0.98	15.6	0.22-0.45	1.4-2	[A]
14	✳	2	**Intalox-saddle**	ceramic	25	255	0.73	8.1	0.3	2	[19]
		5			25	194	0.79	8.35	0.3	0.8	[A]
15	◎	2	**Top-Pak**	metal	45 (Gr.1)	105	0.975	15.0	0.4	2	[27]
16	◎	4			80 (Gr.2)	75	0.98	16.2	0.45	2	[A]
17	+	8	**Dtnpac**	plastic (PP,PVDF)	50	112.7	0.937	15.4	0.3	1.4	[A]
18	◆	4	**NSW ring (Nor-Pac)**		15	309	0.92	12.0	0.30	1.4	[40]
19	◆	6			28	193	0.922	12.8	0.15	1.4	
20	◆	7			50	90.3	0.952	17.2	0.3-0.45	2	
21	▲	3	**Hiflow ring**	metal	28	198.5	0.962	13.4	0.3	1.4	[A]
		4			28	182	0.965	13.7	0.45	2	[A]
22	▲	8			58	100.6	0.976	15.9	0.45	2	[45]
23	△	4		plastic (PP,PVDF)	28	190	0.920	12.3	0.30	1.4	[44]
24	△	5			50	108	0.935	15.1	0.30	1.4	[44]
25	△	3			90	69.5	0.965	18.8	0.45	2	[44]
26	▲	1		ceramic	20	272	0.763	8.3	0.22	1.4	[46]
		4			20	280	0.76	8.8	0.3	1.4	
27	▲	3			35	111.8	0.824	12.2	0.3	1.4	[A]
		5			35	110	0.926	12.1	0.3	1.4	
28	▲	4			50	89.8	0.809	12.5	0.3	1.2	[A]
		4			50	85.6	0.817	13.0	0.3	0.9	
29	+	4	**Hiflow saddle**	plastic	50	82.6	0.94	16.2	0.45	2	[A]
30	✳	3	**Ralu ring**	(PP)	50	112.7	0.938	14.0	0.45	2	[A]
31	○	10	**Mellapak**	sheet metal	-	250	0.96	13.2	0.22-1	1.2-4	[A],[24,26]
32	✳	7	**Ralu Pak**		-	250	0.963	13.45	0.45	2	[48]
33	◇	4	**Montz packing**		B1-100	100	0.987	18.2	0.3	1.4	[A]
34	◇	9			B1-200	200	0.978	14.36	0.3	1.4	[A]
35	◇	12			B1-300	300	0.972	12.44	0.22-0.45	1.4-2	[A]
36	◆	3		PP	C1-200	200	0.96	13.7	0.3	1.4	[A]
37	◆	3		sheet metal	B2-500	500	0.95	10.1	0.22	1.5	[A]

A ≡ Author

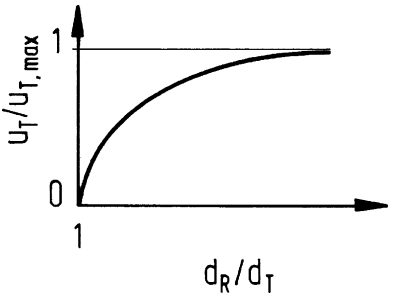

Figure 2-14. Schematic representation showing the influence of the column diameter ratio d_R/d_T on the falling velocity of droplets

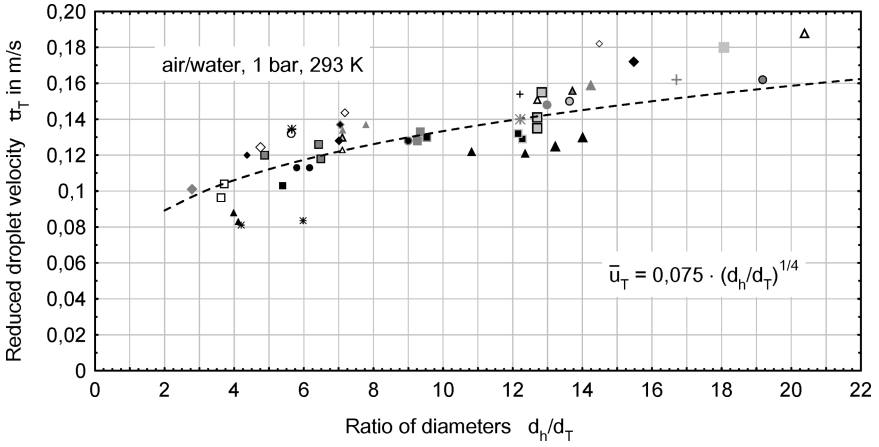

Figure 2-15. Reduced gas velocity of an individual droplet u_T as a function of the diameter ratio d_h/d_T, valid for Pall, Białecki and VSP rings, d = 15–80 mm, and the air/water system under normal conditions

$$\text{for } \bar{u}_T \approx \left[\frac{d_h}{d_T}\right]^{1/4} \quad \rightarrow \quad u_T \approx \left[\frac{d_h}{d_T}\right]^{1/4} \tag{2-53}$$

Hence, $f_2(d_h/d_T)$ in Eq. (2-24) takes the form:

$$f_2\left(\frac{d_h}{d_T}\right) = C_2 \cdot \left(\frac{d_h}{d_T}\right)^{1/4} \quad \text{for } \frac{d_h}{d_T} > 3 \tag{2-54}$$

2.2.4.6
Deriving the Final Equation for Gas Velocity at Flooding Point $u_{V,Fl}$

Stichlmair [53] found that the effective velocity $\bar{u}_0$ of droplets flowing through individual packing elements increases to a value higher than u_0/ε, which is due to the deflection of the fluid between the particles and the vortex shedding. As a result, the effective gas

velocity $\bar{u}_0$ can be expressed as:

$$\bar{u}_0 = \frac{u_0}{f_4(\varepsilon)} \tag{2-55}$$

Assuming that $f_4(\varepsilon) = \varepsilon^q$, the correlation for $\bar{u}_0$ is as shown in Eq. (2-56), and the exponent q must be determined experimentally:

$$\bar{u}_0 = \frac{u_0}{\varepsilon^q} \tag{2-56}$$

Flooding occurs for $h^0_{L,Fl} \to 0$, acc. to the model shown in Fig. 2-6 and Eq. (2-21), when the effective falling velocity u_T of an individual droplet is equated with the effective gas velocity $\bar{u}_0$, which keeps the droplet suspended, acc. to (2-21), i.e.

$$\bar{u}_0 = u_T \Rightarrow \frac{u_0}{\varepsilon^q} = u_T \tag{2-57}$$

Equations (2-57), (2-22), (2-53), (2-54) and (2-56) result in the following equation:

$$u_0 = C_1 \cdot C_2 \left[\frac{d_T . \Delta\rho \cdot g}{\rho_V}\right]^{1/2} \cdot \left[\frac{d_h}{d_T}\right]^{1/4} \cdot \varepsilon^q \cdot f_3(\psi) \tag{2-58}$$

Equations (2-19), (2-32) and (2-58) lead to the following correlation for the gas velocity at the flooding point $u_{V,Fl}$, which also applies to packing elements with similar resistance coefficients ψ_{Fl}, see Table 6-1a:

$$\begin{aligned} &u_{V,Fl} = u_0 \cdot \left(1 - h^0_{L,Fl}\right)^n \quad \Rightarrow \\ &C_{Fl} \cdot \left[\frac{d_T \cdot \Delta\rho \cdot g}{\rho_V}\right]^{1/2} \left[\frac{d_h}{d_T}\right]^{1/4} \cdot \varepsilon^q \cdot \left(1 - h^0_{L,Fl}\right)^{7/2} \end{aligned} \tag{2-59}$$

where $C_{Fl} = C_1 \cdot C_2 \cdot f_3(\psi_{Fl})$.

Using the minimisation procedure, the evaluation of the experimental data listed in Tables 2-6, 2-7, 2-8 and 2-9 for various types of packings leads to the following model:

$$u_{V,Fl} = C_{Fl} \cdot \varepsilon^{6/5} \cdot \left[\frac{d_h}{d_T}\right]^{1/4} \left[\frac{d_T \cdot \Delta\rho \cdot g}{\rho_V}\right]^{1/2} \cdot \left(1 - h^0_{L,Fl}\right)^{7/2} \tag{2-60}$$

where C_{Fl} is a dimensionless constant, which has been calculated as:

$$C_{Fl} \approx 0.50 \tag{2-61}$$

for classic, randomly filled packing elements.

Table 2-6. Data relating to the experimental flooding point values, diagrammed in Fig. 2-17a, in columns with randomly filled metal packing elements. No. of test system acc. to Table 2-2

TP	$d \cdot 10^3$ [m]	Packing	Test system	d_S [m]	H [m]	Literature
PART 1						
●	12	**Białecki rings**	1,6	0.22-0.3	0.8-1.4	[A]
●	25		1,6,10	0.15-0.30	0.7-1.4	[A],[20]
●	35		1,6,10	0.15-0.50	0.7-2.0	[A],[20,39]
○	50		1,6,8	0.15-0.80	1.0-2.5	[A],[20,39]
◇	15	**Pall rings**	1,2,3,6,7	0.30-0.788	1.4-2.0	[A],[5]
◆	25		1,2,6,16	0.15-0.75	1.4-4.0	[A],[5]
◇	30-Glitsch		12	0.22	1.5	[A]
◆	35		1,2,3,6	0.22-0.80	1.4-4.0	[A],[5]
◆	38-VFF		1,6	0.22-0.30	1.46	[A]
◆	50		1,2,3,4,8,11	0.50-1.20	1.4-5.5	[A],[5,7,66]
◆	58		1	0.45-1.00	2-3.5	[A],[67]
◆	80		2	0.80	2.0	[5]
+	35	**Ralu rings**	1	0.75	3.0	[28]
+	50					
▲	15	**Raschig rings**	2	0.5	2.0	[5]
▲	25		2			
△	35		2			
▲	50		2,3			
□	0.3	**Raschig Super rings**		0.288	1.0	[94]
■	0.5			0.288	1.0	[94]
■	0.7			0.28	2.0	[94]
□	1.0		1	0.30-0.40	1.4-3.0	[86, 94]
■	1.5			0.28	2.0	[94]
■	2.0			0.30-0.75	1.4-3.0	[86, 94]
■	3.0			0.44	2.0	[94]
PART 2						
●	0.5A	**Glitsch CMR 304 rings**	1,12	0.22-0.30	1.4-1.54	[A]
●	1A		1,6,12	0.22-0.30	1.4-1.54	
●	1.5A		1,6,12	0.22-0.30	1.4-1.54	
●	1.5A Turbo		6	0.22	1.54	
○	2A		1	0.45	2.0	
●	3A		1	0.45	2.0	
+	30P	**Glitsch rings**	1	0.30	1.4	[A]
■	28	**Hiflow rings**	1,6	0.22-0.60	1.4-2.0	[A]
□	58		11	0.45-1.00	2.0-3.5	[A],[45,60]
+	25	**I-13 rings**	1	0.30	0.7-1.4	[20]
+	40	**IMPT rings**	1	0.45	2	[A]
✳	10/15/20	**Interpack**	6	0.218	1.5	[5]
▲	0.7/1.0/1.5	**Nutter rings**	1	0.3	2.25	[95]
△	2.0/2.5/3.0					
■	size 1	**Mc-Pac**	1,8	0.18-0.32	2.8-3.0	[A],[79,80]
■	size 2		1,6	0.32-0.60	1.5-3.0	
✳	50	**PSL ring**	1,6	0.22-0.3	1.4	[A]
△	25	**Rauschert metal saddle rings (RMSR)**	1	0.8	–	[93]
▲	40					
▲	50					
▲	60					
▲	70					
◆	no.1	**Top-Pak**	1	0.30-0.45	1.45-2.0	[A]
◆	no.2			0.45	2.0	
◆	no.1	**VSP rings**	1,6	0.218-0.45	1.45-2.0	[A],[27,93]
◆	no.2			0.218-1.00	1.45-6.0	[A],[67,93]

Number of test points: 435, mean relative deviation $\overline{\delta}(u_{V,Fl}) = 6{,}15\ \%$

A ≡ Author

Table 2-7. Data relating to the experimental flooding point values, diagrammed in Fig. 2-17b, in columns randomly filled with plastic (PP, PVDF) packing elements. No. of test system acc. to Table 2-2

TP	$d \cdot 10^3$ [m]	Packing	Material	Test system	d_S [m]	H [m]	Literature
PART 1							
+	50	**Białecki rings**	PP	1	0.30	1.4	[20]
+ +	size 1 size 2	**Dtnpac**	PP	1	0.45 0.30	2.0	[A]
◆ ◇ ◆	size 1 size 2 size 3	**Envipac**	PP	1	0.30 0.30-0.45 0.45	1.4 1.4-2.0 2.0	[A]
✱ ✳	no.1 no.2	**Glitsch CMR**	PP	1	0.30-0.45 0.45	1.4-2.0 2.0	[A]
●	45	**Hackette**	PP	1	0.45	2.0	[A]
■	25	**Pall rings**	PVDF	6,7	0.218-0.22	1.4	[A]
■ □ ■ □	25 35 50 90	**Pall rings**	PP	1	0.30 0.30-0.45 0.30-1.00 0.75	1.4 1.4 1.4-3.5 3.0	[A], [44] [A] [A], [44,66] [96]
▲ △	38 50	**Ralu rings**	PP	1	0.75 0.30-0.75	3.0 1.4-3.0	[28] [A], [28]
✱	2"	**Super saddles PP**	PP	1	0.75	3.0	[28]
● ○	no.1 no.2	**Telerette**	PP	1	0.15 0.45	1.3 2.0	[A], [40] [A], [54]
PART 2							
+ +	28 50	**Hiflow rings**	PVDF	1,6	0.218-0.30	1.4	[A],[44]
□ ○ △	15 38 90	**Hiflow rings**	PP	1	0.30 0.8 0.45-1.00	1.4 – 2.0-3.5	[A] [97] [66],[A]
□	50	**Hiflow Super**	PP	1	0.30-0.45	1.4-2.0	[A]
○	50	**Hiflow saddles**	PP	1	0.45	2.0	[A]
■ ●	35 50	**Intalox saddles**	PP	1	0.30 0.45	1.4 2.0	[A]
■ ● ▲	17 22 x 27 28	**Nor-Pac**	PVDF	7 6,7 6	0.218	1.4	[A]
■ ● ▲ ◆ ✱	17 22 x 27 28 38 50	**Nor-Pac**	PP	1 1 1,21b 1 1,8,22	0.30 0.30 0.15-1.40 0.30 0.30-1.40	0.9-1.4 1.4 1.0-2.0 1.4 0.9-2.0	[A] [A] [A], [40] [A] [A], [Fi/Lu]
◆	90	**Raflux rings**	PP	1	0.8	–	[97]
▲	50	**VSP rings**	PP	1	0.45	2.0	[A]

Number of test points: 260, mean relative deviation $\overline{\delta}\left(u_{V,Fl}\right) = 4.10\ \%$

A ≡ Author

This packing group includes: 15 to 80 mm Pall rings made of metal, plastic and ceramic, 25 to 50 mm metal Białecki rings, metal VSP rings (sizes 1 and 2), metal Top-Pak packings (sizes 1 and 2), 10 to 50 mm Intalox saddles made of plastic and ceramic, 8 to 50 mm ceramic Raschig rings, Glitsch rings made of metal and plastic (sizes 0.5–3), I-13 rings and PSL rings.

The flooding point constant C_{Fl}

$$C_{Fl} \approx 0.55 \tag{2-62}$$

Table 2-8. Data relating to the experimental flooding point values, diagrammed in Fig. 2-17c, in columns randomly filled with ceramic packing elements. No. of test system acc. to Table 2-2

TP	$d \cdot 10^3$ [m]	Packing	Test system	d_S [m]	H [m]	Literature
●	20	**Hiflow rings**	1,6	0.218-0.30	1.25-1.4	[A]
◍	38		1,6	0.218-0.45	1.4-2.0	
●	50		1,6	0.218-0.30	0.9-1.4	
○	75		1	0.45	2.0	
▲	25	**Intalox saddles**	1,6	0.220-0.30	1.4	[A]
△	38		1,6,21a	0.220-0.50	1.4-2.0	[A], [29]
▲	50		1,6	0.220-0.75	1.4-3.0	[A], [28]
✱	25	**Pall rings**	3,6,11	0.218-0.50	1.0-1.4	[A],[23]
✳	50		6	0.220		[A],[21]
■	8	**Raschig rings**	8,10,14	0.10	1.0	[A],[5]
■	15		1,6	0.20-0.220	1.0	[A],[3,5,71]
□	19		4	1.2	5.5	[5]
■	25		1,3,6,14	0.220-0.50	1.0-2.0	[A],[5,32]
■	25 Glas		20	0.150	1.6	[36,37]
◆	35		1	0.30	0.7	[20]
◇	50		1,6,8	0.30-0.60	0.7-1.4	[A],[Fi],[20,82]
◆	100		21a	1.20	2.0	[84,85]
+	size 1	**R-Pac**	1	0.316	1.0-3.0	[82,83]
+	size 2		1,6	0.320-0.60		
+	size 2	**SR-Pac**	1,6	0.320-0.60	1.0-3.0	[82,83]

Number of test points: 181, mean relative deviation $\overline{\delta}(u_{V,Fl}) = 5.53\ \%$

A ≡ Author

was increased by approx. 10% in the case of modern, highly perforated packing elements, such as 20—90 mm Hiflow rings made of metal, plastic and ceramic, 17—50 mm Nor-Pac rings, plastic VSP rings (size 2), Ralu rings (sizes $1\frac{1}{2}$ and 2), Tellerette (sizes 1 and 2), Envipac (sizes 1, 2 and 3), Dtnpac (sizes 1 and 2), R-Pac, SR-Pac, Mc-Pac. The same applies to non-perforated Montz packing made of sheet metal and plastic as well as to Impuls packing.

For perforated Mellapak 250 Y packings, Ralu-Pak 250YC with slit perforation, Gem-pak 200AT and stacked 25 mm metal Białecki rings, the numerical value of the flooding point constant C_{Fl} was found to be:

$$C_{Fl} \approx 0.615 \tag{2-63}$$

The different numerical values, which were found for the constant C_{Fl} (Eqs. (2-61) ÷ (2-63)), indicate that the wall effect cannot be sufficiently expressed by function $f_2(d_h/d_T)$ alone. It is not only the wall distance, but also the shape of the packing wall that needs to be taken into account. This is linked to the resistance coefficient ψ_{Fl} in single-phase flow.

In Fig. 2-16, the $C_{Fl,i}$ values of the experimental data, listed in Tables 2-6, 2-7, 2-8, 2-9 and substituted into Eq. (2-60), are plotted against the resistance coefficient ψ_{Fl} for the respective gas velocity at the flooding point $u_{V,Fl}$, acc. to Eq. (3-14) or (3-26):

$$\psi_{Fl} = K_1 \cdot (\mathrm{Re}_V)_{Fl}^{K_2} \tag{3-14}$$

$$\psi_{Fl} = \psi_0 \cdot (1 - \varphi_P) \tag{3-26}$$

Table 2-9. Data relating to the experimental flooding point values, diagrammed in Fig. 2-17d, in column filled with structured or stacked packing elements. No. of test system acc. to Table 2-2

TP	Packing	Type	Material	Test system	d_S [m]	H [m]	Literature
	TUBE COLUMNS (TS)						
●	**Białecki rings**	25	metal	1	0.025	1.5	[A]
●		52.5		8	0.273	1	[A]
+	**Pall rings**	25	metal	1	0.025	1	[76]
	STACKED PACKINGS						
●	**Białecki rings**	25	metal	1,6	0.150-0.218	1.4-1.7	[A]
●		35		6	0.218	1.5	
●		50		1,6	0.151-0.30	1.0-1.7	
○	**Białecki rings**	50	plastic	1	0.30	1.0	[77], [A]
●	**Hiflow rings**	50	ceramic	1	0.45	1.0	[A]
+	**Pall rings**	50		1,8	0.40-0.487	1.0	[A],[21]
✚	**PSL rings**	50	metal	1	0.28	1.4	[A]
	STRUCTURED PACKINGS						
■	**Euroform**		PP	1	0.30	1.4	[40]
■	**Fi-Pak (I-13F)**		metal	6	0.147-0.218	1.4	[A]
■	**FX (VFF) 260**		PP	1	0.45	2	[A]
□	**Gempak A2 T304**		metal	6,12	0.218	1.4	[A],[A1]
■	**Impuls 50**		ceramic	1	0.385-0.40	1.4	[21]
▲	**Mellapak**	250X	sheet metal	1	1.00	3.5	[26,68,69]
▲		250Y		1,6	0.218-1.00	1.4-3.5	[A],[26,68,69]
▲		500Y		1	1.00	3.5	[68,69]
◆	**Montz**	A1	metal	6,7	0.218	1.4	[A]
◆		A3-500		1,6	0.218-0.45	2.0	[A],[A1]
◇		B1-100	sheet metal	1	0.30	1.4	[A]
◇		B1-200		1,6	0.218-0.30	1.4	[A],[47]
◇		B1-300		1,6	0.218-0.30	1.4	[A],[47]
◆		B2-300		6	0.218	1.4	[A],[A1]
◆		B2-500		6	0.218	1.4	[A],[A1]
◆		C2-200		1	0.30	1.4	[A]
◆		S1	metal	6	0.218	1.4	[A]
✳	**NorPac**	Gr.3	PP	1	0.30	1.4	[A]
✳		Kompakt no.1		1	0.30	1.4	[A]
✳		Kompakt no.2		1	0.30	1.4	[A]
△	**Ralu-Pak**	250 YC	sheet metal	1,6	0.218-0.45	1.4-2.0	[A],[48]
△	**Sulzer gauze packing**	BX	metal	2,3,6	0.218-0.50	1.4-2.0	[A],[5]
▲	**Honeycomb packing**		PP	1	0.30	1.4	[A]

Number of test points: 196, mean relative deviation $\overline{\delta}(u_{V,Fl}) = 6.06\ \%$

A ≡ Author

based on Tables 6-1a–6-1c, using the numerical values K_1, K_2 and φ_P determined within the scope of this work. This leads to the following correlation (2-64) for calculating the flooding point constant C_{Fl} for Eq. (2-60):

$$C_{Fl} = \left(C_{Fl,0}\right)_{45°} \cdot \psi_{Fl}^{-1/6} \leq \pm 8\ \% \tag{2-64}$$

where $C_{Fl,0} = 0.566$ for a flow angle of gas stream in the packing channels $\alpha = 45°$ is a *dimensionless constant, independent of the type, size and material of the packing.*

Equation (2-64) applies to any types of randomly filled packing elements and structured packings with type Y flow channels (approx. 45°) for resistance coefficients in the range of $\psi_{Fl} = 0.1-8$. As shown in Fig. 2-16 and Eq. (2-60), the gas velocity at the

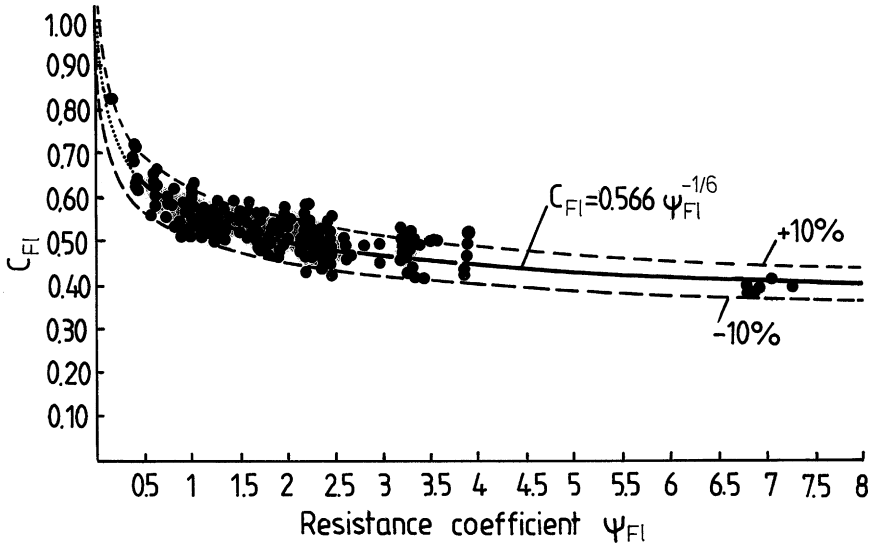

Figure 2-16. Dependency of the constant C_{Fl} on the resistance coefficient at the flooding point ψ_{Fl} plotted on the basis of data in Tables 2-6, 2-7, 2-8 and 2-9

flooding point $u_{V,Fl}$ decreases, as the resistance coefficient ψ_{Fl} increases. The flooding point constant of $C_{Fl} \cong 0.5$ applies to the group of packing elements with a resistance coefficient ψ_{Fl} at the flooding point in the range of 1.8 and 3, see Eq. (2-61). For resistance coefficients in the range of $\psi_{Fl} = 0.9-1.6$, the flooding point constant is assumed to have a mean value of $C_{Fl} \cong 0.55$. The group of perforated packing elements also includes structured packings made of sheet metal, plastic and ceramic (type Y) without wall openings. For practical calculations, the flooding point constant for resistance coefficients ψ_{Fl} in the range of 0.5−0.9 is determined as $C_{Fl} \cong 0.615$. This applies to the group of structured sheet-metal packings (type Y) with slit perforation, e.g. Ralu-Pak 250YC, or perforated packings such as Mellapak 250 Y, Gempak 202 AT, as well as plastic packings 250 Y.

The lowest resistance coefficients ψ_{Fl} are typical of stacked packing elements, honeycomb packings, tube columns as well as for type X packings made of sheet metal and type BX gauze packings with flow channels of 30°. They are in the range of $\psi_{Fl} = 0.1-0.4$.

Metal Raschig rings have been found to have the highest resistance coefficients. A resistance coefficient of approx. $\psi_{Fl} \cong 8.18$ in the turbulent flow range of $Re_V \geq 2100$ results in a flooding point constant of $C_{Fl} \cong 0.4$ for Eq. (2-60).

Influence of the Flow Channel Angle α on the Gas Velocity at the Flooding Point $u_{V,Fl}$

The evaluation of the experimental data shown in Table 2-10 for stacked Hiflow rings, Raschig rings and Pall rings, tube columns with structured Pall rings and Białecki rings,

Table 2-10. Data relating to the experimental flooding point values, diagrammed in Fig. 2-17e, in columns operated at higher pressure. No. of test system acc. to Table 2-2

TP	$d \cdot 10^3$ [m]	Packing	Material	Test system	d_S [m]	H [m]	Literature
▲ △	10 15	**Berl saddle**	ceramic	27 27,28,29	0.086-1.550 0.155	0.8	[75]
+	20	**Interpak**	metal	27	0.155		
✳	20	**Novalox saddle**	ceramic	27	0.155		
■ ■ □	15 35 15	**Pall ring**	metal plastic	27 19 27	0.155 0.50 0.155	2.5	[39]
● ○	15	**Raschig ring**	ceramic metal	27	0.155	0.8	[75]

Number of test points: 177, mean relative deviation $\overline{\delta}\left(u_{V,Fl}\right) = 8.93\ \%$

Hiflow rings, structured Sulzer gauze packings (type BX), as well as type X sheet metal packings and Montz packings X with flow channels of $\alpha = 30°$ resulted in a higher flooding point constant $C_{Fl,0}$, compared to Eq. (2-64), namely:

$$\left(C_{Fl,0}\right)_{30°} = 0.693 \quad \text{for} \quad \alpha = 30° \tag{2-65}$$

A constant numerical value $C_{Fl,0} = 0.566$ for random packings and type Y structured packings with a flow channel angle of $\alpha = 45°$ in relation to the column axis leads to the assumption that gas in a random packing flows through a bundle of parallel flow channels with a diameter of d_h and with a mean angle of approx. $\alpha = 45°$. If the angle of the flow channels α is reduced, the gas velocity at the flooding point increases and reaches its maximum value $C_{Fl,0}$ at $\alpha = 0°$. By substituting the value pairs $(C_{Fl,0})_\alpha$ for $\alpha = 45°$ and $\alpha = 30°$ into correlation (2-64), the following correlation (2-66) can be derived:

$$C_{Fl} = C_{Fl,0} \cdot \cos\alpha \cdot \psi_{Fl}^{-1/6} = 0.80 \cdot \cos\alpha \cdot \psi_{Fl}^{-1/6} \tag{2-66}$$

where:

$C_{Fl,0} = 0.800$ for flow channels with $\alpha = 0°$.
$C_{Fl,0} = 0.693$ for flow channels with $\alpha = 30°$
$C_{Fl,0} = 0.566$ for flow channels with $\alpha = 45°$.

By substituting Eq. (2-65) into Eq. (2-60), it is possible to derive the following Eq. (2-67) for determining the gas velocity at the flooding point $u_{V,Fl}$ in packed columns with any types of column internals.

$$u_{V,Fl} = 0.80 \cdot \cos\alpha \cdot \varepsilon^{6/5} \cdot \psi_{Fl}^{-1/6} \left[\frac{d_T \cdot \Delta\rho \cdot g}{\rho_V}\right]^{1/2} \cdot \left[\frac{d_h}{d_T}\right]^{1/4} \cdot \left(1 - h_{L,Fl}^0\right)^{7/2} \quad \left[ms^{-1}\right] \tag{2-67}$$

The dimensionless flooding point constant $C_{Fl,0} = 0.80$ for Eq. (2-67) applies to various types of packed columns, i.e. for:

(a) randomly filled packed columns
(b) structured packings
(c) stacked packing elements
(d) tube columns stacked with packing elements
(e) empty columns.

The numerical value $C_{Fl,0} = 0.8$ applies to columns in which the angle of the flow channels is assumed to be $\alpha = 0°$. This is the case for tube columns with stacked 25 mm metal Pall rings [76].

It follows from Eq. (2-67) that, as the gas velocity at the flooding point $u_{V,Fl}$ increases, it is possible for increasingly larger droplets to be entrained by the upward gas flow. The gas velocity at the flooding point $u_{V,Fl}$ also increases with the hydraulic diameter d_h and the void fraction ε. In the case of highly perforated packing elements, the gas velocities at the flooding point are higher, due to the lower resistance coefficients ψ_{Fl}. Type X packings with channel angles of $\alpha = 30°$ can always be expected to have higher gas velocities at the flooding point than type Y packings with channel angles of $\alpha = 45°$. In the case of very low liquid loads, e.g. in rectification under vacuum, the liquid hold-up at gas velocities calculated acc. to Eq. (2-67) may be broken down into very small droplets, which leads to the packing being blown empty by the gas.

2.2.4.7
Comparing Experimental Flooding Point Data and SBD Model Acc. to Eq. (2-67)

For the purpose of evaluating the author's own experimental data as well as data taken from literature for columns with $d_S = 0.025-1.4$ m, including data taken by Billet [5] and Bornhütter [66], Sulzer [67–71], Możenski, Kucharski [39] and Krehenwinkel [75] etc., a database was created, which now holds 1,200 experimental items of data for 32 different mixtures from the range of vacuum to normal rectification as well as pressure absorption and/or pressure rectification up to 100 bar, see Table 2-2.

Evaluation of Experimental Flooding Point Data for the Range of Vacuum Rectification and Normal Pressure Range

Figures 2-17a, 2-17b, 2-17c and 2-17d show a comparison between the calculated and experimental gas velocities at the flooding point. More information on the experimental conditions and the test systems can be found in Tables 2-6, 2-7, 2-8 and 2-9.

The gas velocities at the flooding point $(u_{V,Fl})_{calc}$ were determined iteratively, acc. to Eq. (2-67), for the start values $(u_{V,Fl})_{exp}$, $(u_{L,Fl})_{exp}$. Figure 2-17a shows a comparison between the gas velocities $(u_{V,Fl})_{calc}$, calculated using Eq. (2-67), and the experimental values $(u_{V,Fl})_{exp}$ for metal packings. The evaluation was based on approx. 340 experimental values, of which 80−91% were given with a maximum relative error of less than ±8%, using Eq. (2-67). The mean error in the determination of the gas velocity at the flooding point $(u_{V,Fl})_{calc}$ for metal packings was found to be $\bar{\delta}\left(u_{V,Fl}\right) = 4.7\,\%$ during

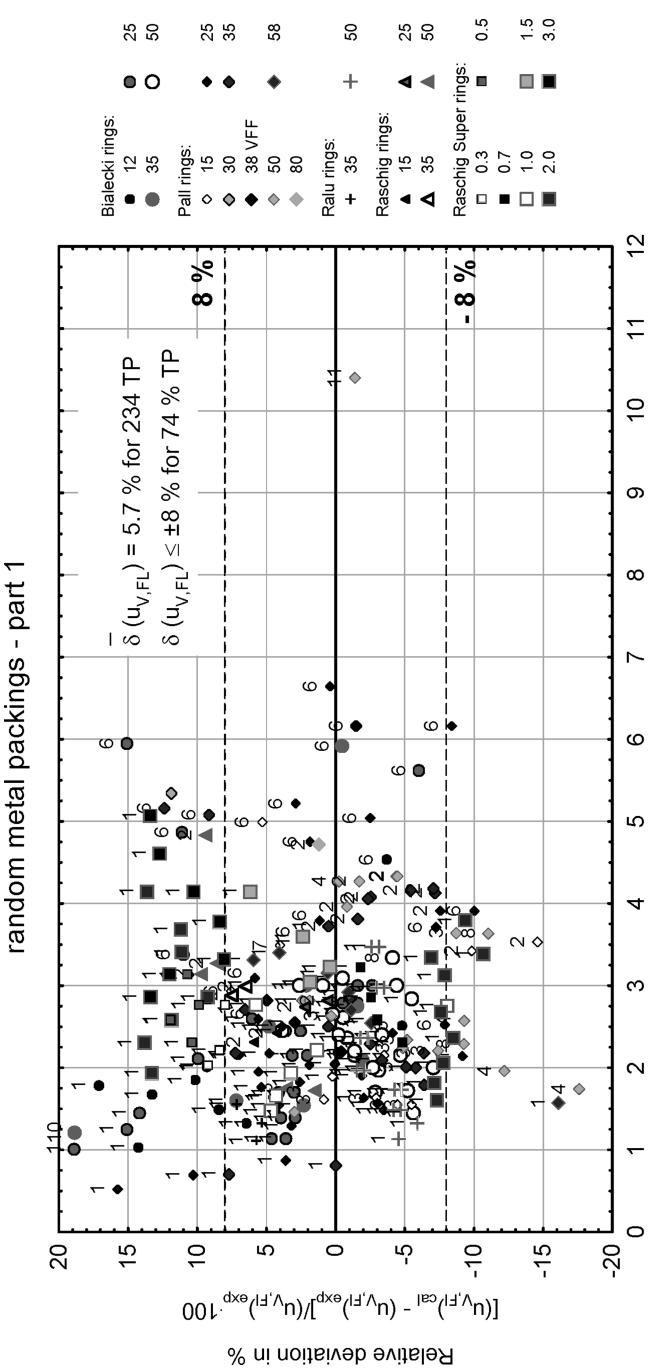

Figure 2-17a. Comparison of experimentally determined gas or vapour velocity at the flooding point $(u_{V,Fl})_{exp}$ and calculated data based on Eq. (2-67), valid for random metal packings of various types, no. of test system as shown in Table 2-2

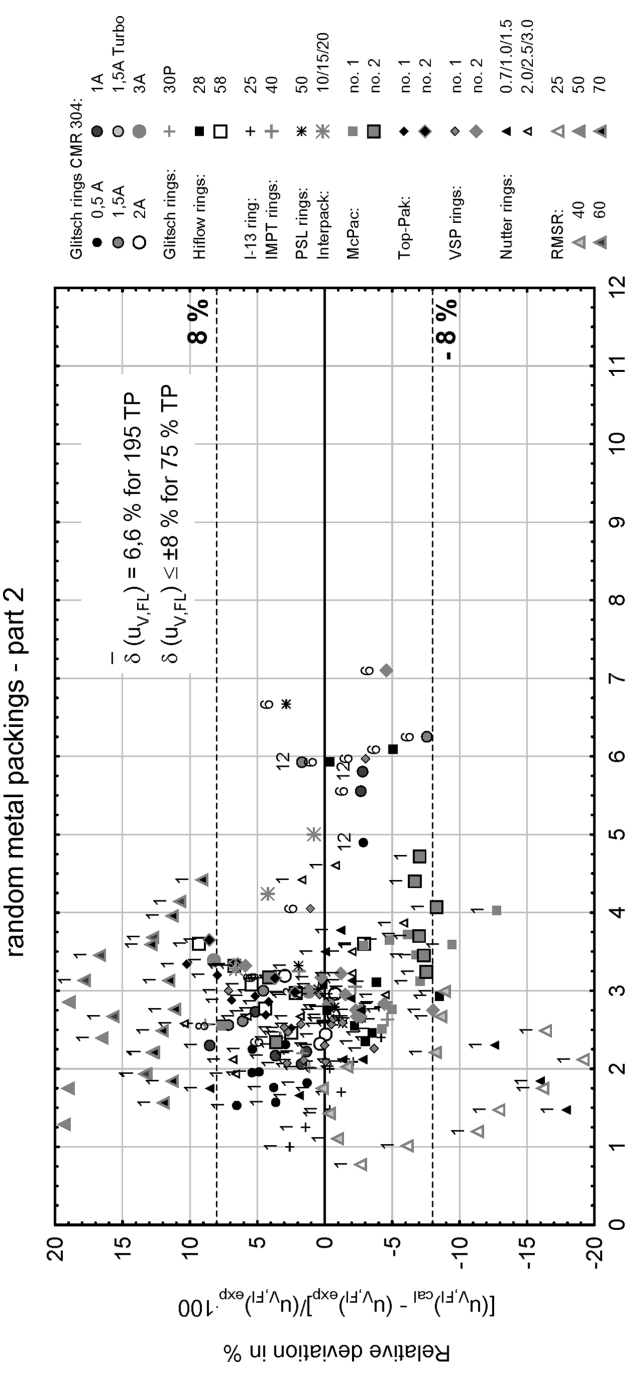

Figure 2-17a. (continued.)

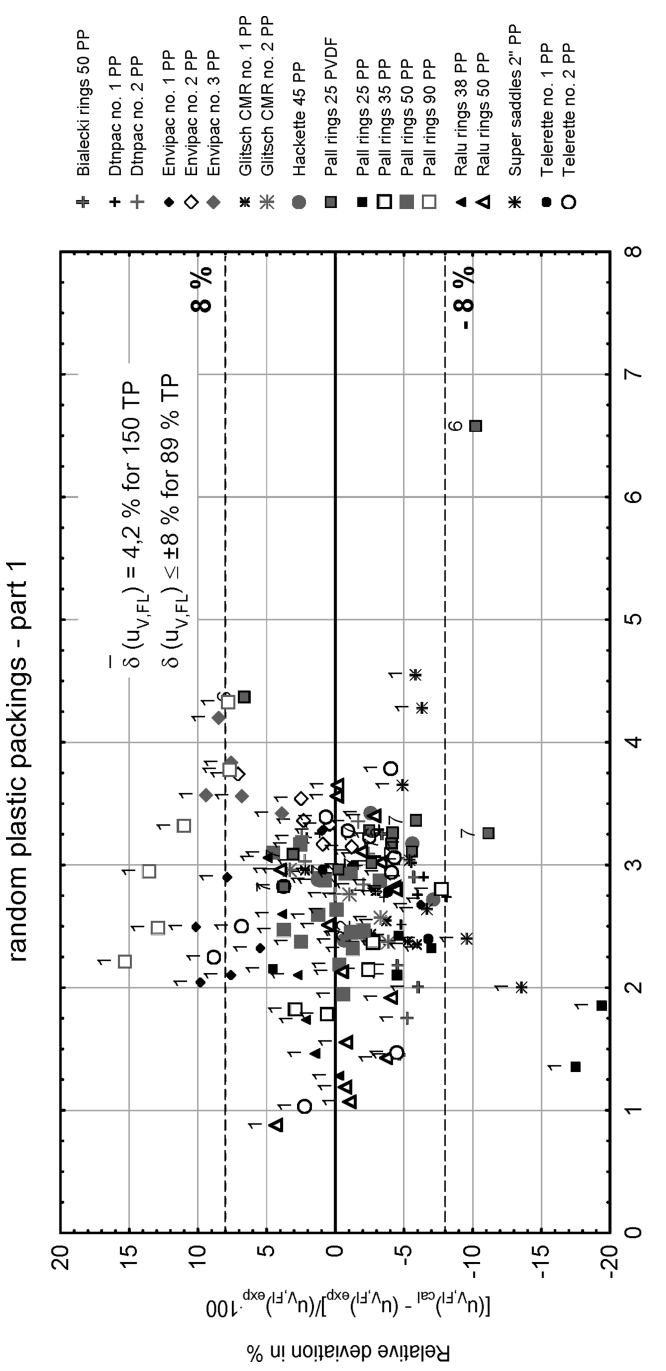

Figure 2-17b. Comparison of experimental determined gas or vapour velocity at the flooding point $(u_{V,FI})_{exp}$ and calculated data based on Eq. (2-67), valid for random plastic packings of various types, no. of test system as shown in Table 2-2

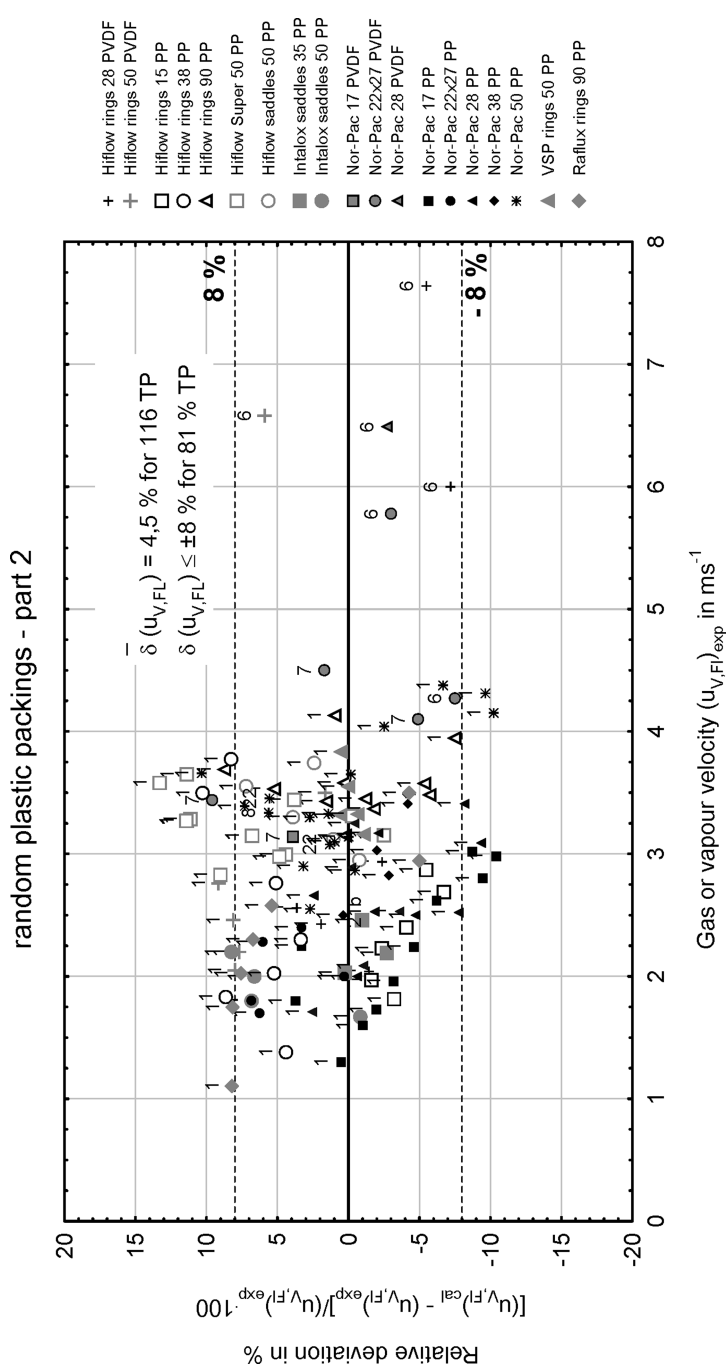

Figure 2-17b. (continued.)

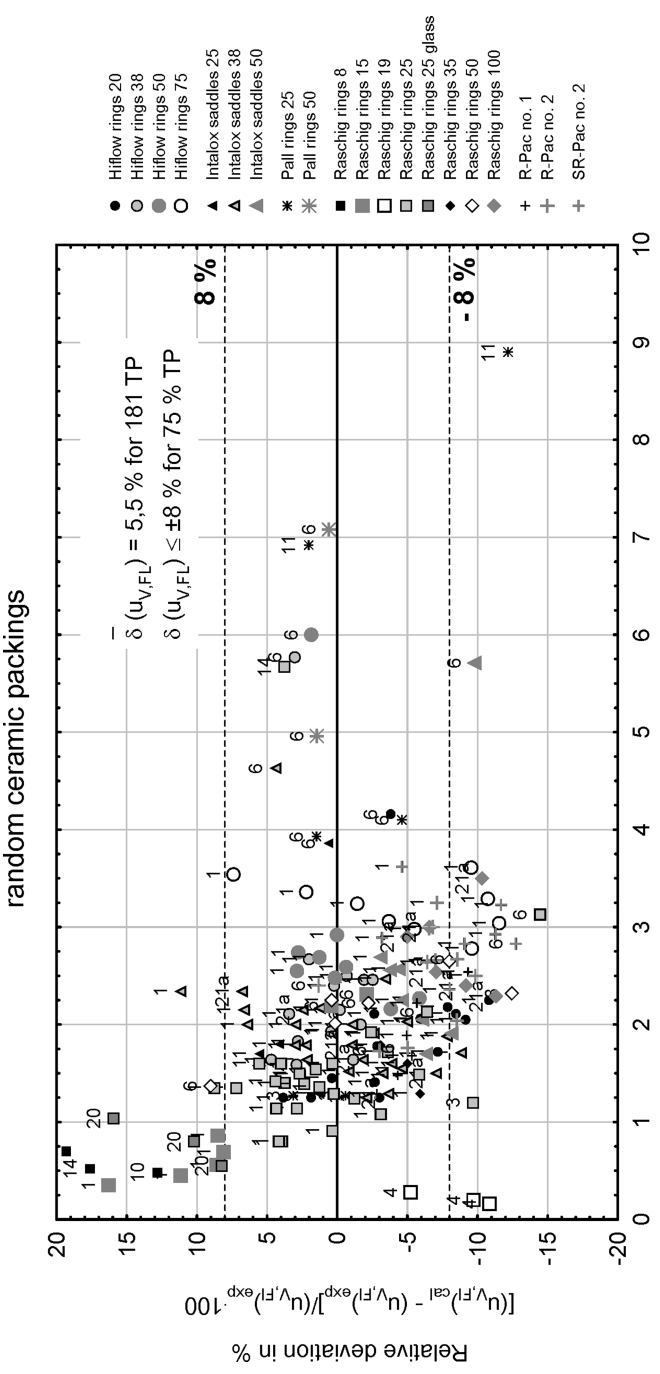

Figure 2-17c. Comparison of experimentally determined gas or vapour velocity at the flooding point $(u_{V,FI})_{exp}$ and calculated data based on Eq. (2-67), valid for random ceramic packings of various types, no. of test system as shown in Table 2-2

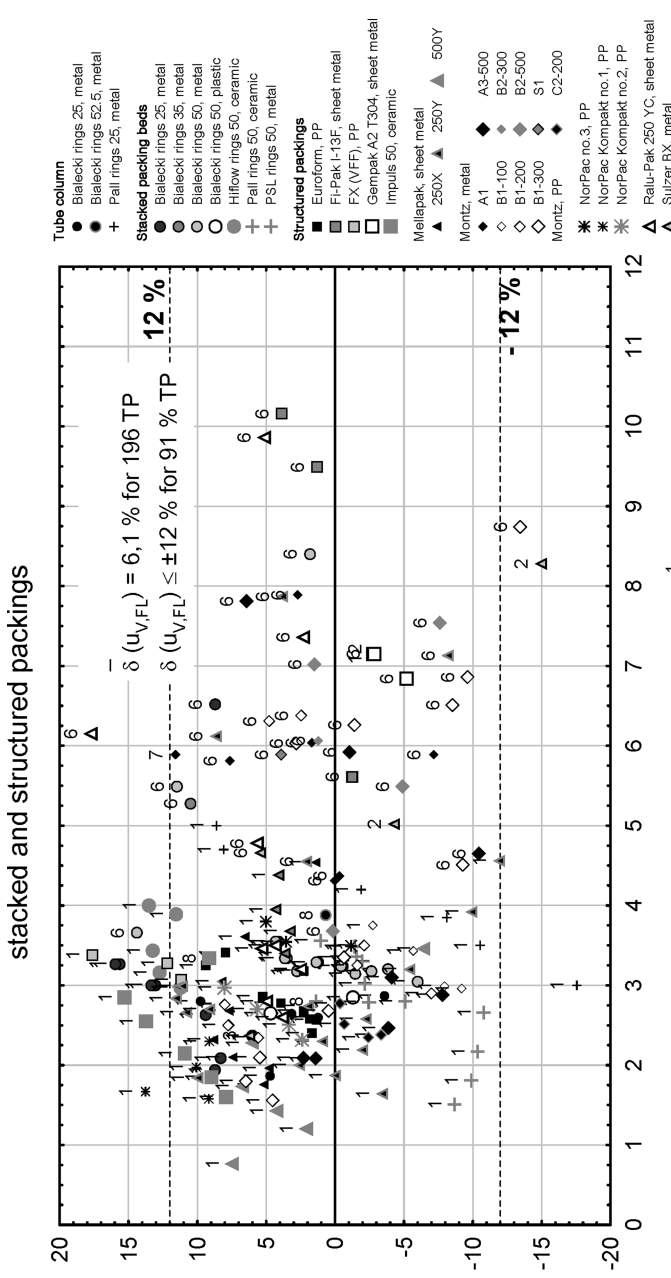

Figure 2-17d. Comparison of experimentally determined gas or vapour velocity at the flooding point $(u_{V,FI})_{exp}$ and calculated data based on Eq. (2-67), valid for structured packings, tube columns and stacked packings, no. of test system as shown in Table 2-2

the evaluation of the experimental data. This applies to experimental data with $d_S/d \geq 6$ within the validity range of this model, i.e. for gas velocities in the air/water system of $u_{V,Fl} > 0.5\ ms^{-1}$ and $B_L < 5.10^{-3}$, see Fig. 2-17a.

Figures 2-17b, 2-17c and 2-17d show a comparison between the experimentally derived gas velocities at the flooding point $(u_{V,Fl})_{exp}$ and the calculated values $(u_{V,Fl})_{calc}$ for plastic packings (Fig. 2-17b), ceramic packings (Fig. 2-17c) as well as for structured packings and stacked packing elements (Fig. 2-17d). 75—91% of all test points for structured packings are spread over a range of ±12%, see Fig. 2-17d.

The mean relative error $\bar{\delta}\left(u_{V,Fl}\right)$ in the determination of the gas velocity at the flooding point $(u_{V,Fl})_{calc}$, acc. to Eq. (2-67), for the experimental data shown in Figs. 2-17a, 2-17b, 2-17c and 2-17d is given as:

$\bar{\delta}\left(u_{V,Fl}\right) = 4.10\,\%$ for random packings made of plastic – 260 test points
$\bar{\delta}\left(u_{V,Fl}\right) = 5.50\,\%$ for random packings made of ceramic – 181 test points
$\bar{\delta}\left(u_{V,Fl}\right) = 6.10\,\%$ for structured packings, stacked packing elements, tube columns of sheet metal, plastic, ceramic – 196 test points

Equation (2-67) also confirms the test points for diameter ratios of $d_S/d \ll 6$, when the experimentally derived resistance coefficients ψ_{Fl} for smaller columns $d_S/d \ll 6$ are substituted into Eq. (2-67). This is the result of the evaluation of data taken during experiments with the system chlorobenzene/ethylbenzene at 33 and 66.7 bar in a distillation column with $d_S = 0.22$ m ($d_S/d \cong 3.8$) for 50 mm ceramic Intalox saddles, Hiflow rings as well as for 50 mm metal Pall rings and Białecki rings. What is remarkable is that, even in the range of lower $u_{V,Fl}$ values of 0.4—1 ms^{-1}, the new model accurately reflects the experimental vapour velocities $u_{V,Fl}$ for 8 and 15 mm Raschig rings. Deviations greater than ±8% were found mostly in some literature data, for which no detailed information on the packing density N and the geometric data a and ε of the respective packings was available.

Evaluation of Experimental Flooding Point Data for the Pressure Range

Due to the high density of the gas phase, a correction factor for the evaluation of the experimental data has been introduced, as recommended by Mersmann [2], which has proved useful for calculating the droplet velocity u_T, acc. to Eq. (2-75), and the gas velocity at the flooding point $u_{V,Fl}$.

If the density of the continuous phase ρ_V is higher than the density of the ambient air ρ_{air}, the gas velocity at the flooding point $u_{V,Fl}$ is calculated using the correlation:

$$u_{V,Fl} = u_{V,Fl,Eq.(2-67)} \cdot \left(\frac{\rho_V}{\rho_{air}}\right)^{0.18} \quad \left[ms^{-1}\right]. \tag{2-68}$$

Equations (2-67) and (2-68) give the following dimension-dependent final Eq. (2-69) for determining the gas velocity at the flooding point in any type of packed column.

$$u_{V,Fl} = 0.80 \cdot \cos\alpha \cdot \varepsilon^{6/5} \cdot \psi_{Fl}^{-1/6} \left[\frac{d_T \cdot \Delta\rho \cdot g}{\rho_V}\right]^{1/2} \cdot \left[\frac{d_h}{d_T}\right]^{1/4} \cdot (1 - h_{L,Fl}^{0})^{7/2} \cdot K_{\rho V} \quad \left[ms^{-1}\right] \tag{2-69}$$

where:

$$K_{\rho V} = 1 \quad \text{for} \quad \rho_V \leq \rho_{air\,(1.165\ kgm^{-3})} \text{ and/or} \tag{2-70}$$

$$K_{\rho V} = \left(\frac{\rho_V}{1.165}\right)^{0.18} \quad \text{for} \quad \rho_V > \rho_{air} \tag{2-71}$$

The exponent n = 0.18 in the above equation was determined by evaluating approx. 180 experimental flooding point values in the range of higher pressures up to 100 bar, taken during the course of this work, see Fig. 2-17e.

Figure 2-17e shows a comparison between the experimental flooding point data $u_{V,Fl,exp}$, taken by Krehenwinkel [75], Możenski et al. [39], and the calculation based on Eqs. (2-69) and (2-71) $u_{V,Fl,calc}$. The experimental data is based on various test systems and an operating pressure of up to 100 bar. The experimentally derived gas velocities at the flooding point $u_{V,Fl}$ are in the range of approx. 0.01 to 0.85 ms^{-1}.

A list of individual symbols and systems used can be found in Table 2-10. The comparison shows excellent concurrence of the experiments with the calculation. 80% of the experimental values deviate within ±15% from the graph. After evaluating approx. 180 experimental data points, the mean relative error in the determination of the gas velocity at the flooding point in pressure systems was found to be approx. 8.93%.

An analysis of the experimental results has led to the significant conclusion that it is indeed possible to determine the fluid dynamics of packed columns in the pressure or vacuum range without performing any experimental work, as the results shown by the above correlations are transferable to any pressure range and any type of packing. This is an important conclusion, in particular for practical applications, as experiments in the pressure and negative pressure range are extremely complicated and costly.

The most important result of this work is the ability of the SBD model to describe the flooding in columns with any internals, any test systems in the vacuum, normal pressure and pressure range up to 100 bar accurately enough for practical applications.

In addition, strong proof has been provided, based on a large amount of experimental data using the test system air/water under ambient conditions, that the results are transferable to any test systems and mixtures with extremely divergent properties. Hence, the experimental effort in designing packed columns can be minimised to just a few experiments, using the test system air/water and/or experiments with single-phase flow, in order to determine the resistance coefficient ψ in relation to the Reynolds number of the gas phase.

2.2.4.8
New Dimensionless Correlation for Gas Velocity at Flooding Point Based on SBD Model

Based on Eqs. (2-72) and (2-73), correlation (2-69) is now expressed with an extended Froude number Fr^*_{Fl} at the flooding point. By introducing the dimensionless, extended Froude number of the gas phase

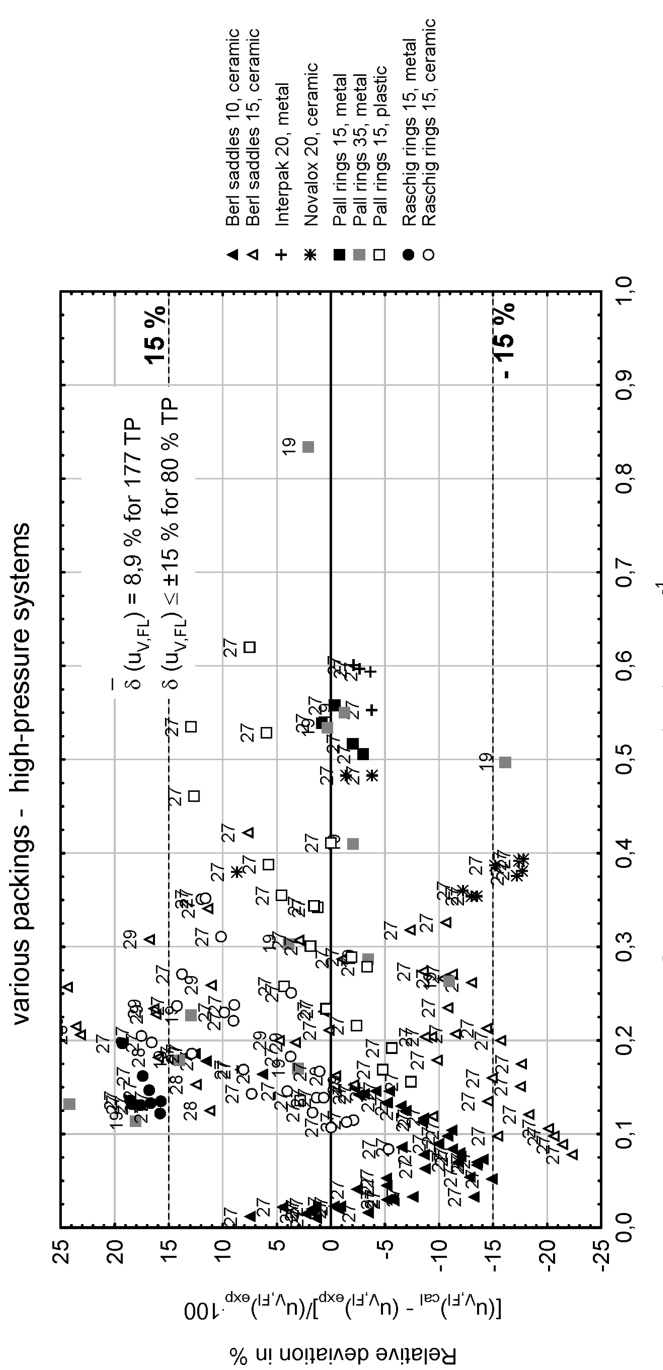

Figure 2-17e. Comparison of experimentally determined gas or vapour velocity at the flooding point $(u_{V,FI})_{exp}$ and calculated data based on Eq. (2-69), valid for random packings in pressure range up to 100 bar, no. of test system as shown in Table 2-2b

$$Fr_{Fl}^{*} = \frac{u_{V,Fl}^{2}}{d_T \cdot g} \cdot \frac{\rho_V}{\Delta\rho} \tag{2-72}$$

it is possible to derive the following flooding point correlation, applicable to any type of column internal, which constitutes the main result of this work:

$$Fr_{Fl}^{*1/2} = 0.8 \cdot \cos\alpha \cdot \psi_{Fl}^{-1/6} \cdot \left[\frac{d_h}{d_T}\right]^{1/4} K_{\rho V} \cdot \varepsilon^{6/5} \cdot \left(1 - h_{L,Fl}^{0}\right)^{7/2} \tag{2-73}$$

Equation (2-73) is now applicable within the following limits:

$$\frac{d_T^2 \cdot \Delta\rho \cdot g}{\sigma} < 9, \;\; \eta_V/\eta_L \to 0 \;\; \text{as well as } \rho_V/\rho_L << 1 \text{ and } d_h/d_T > 3 \tag{2-74}$$

and for $Re_L \leq 600$, $Ar = 6.4 \cdot 10^4 - 10^6$, for any types of packing elements and structured packings with resistance coefficients in the range of $\psi_{Fl} \in (0.1-8.5)$.

2.2.4.9 Evaluation of Experimental Data Using Mersmann's Film Model [3]

For the purpose of plotting the flooding curves presented by Mersmann [3], as shown in Figs. 2-5a, 2-5b, 2-5c and 2-5d, the pressure drop of dry random or structured packings $\Delta p_0/H$ was determined using the correlations (3-8) and (3-14), presented in Chap. 3. The empirical constants for determining the resistance coefficient ψ, acc. to Eq. (3-14) or (3-26), in the range of $Re_V \in (500–15{,}000)$ were taken from Tables 6-1a–6-1c.

The experimental results are presented in Figs. 2-5a, 2-5b, 2-5c and 2-5d. They show strong deviations of up to +50% and more, compared to Mersmann's film model [3], in the case of large packing elements, in particular those with lattice structures, as well as structured packings with low irrigation densities. In the case of larger, dimensionless liquid loads $B_L > 2-3 \cdot 10^{-3}$, the experimental data is spread more closely around Mersmann's [3] flooding point curve, and increasingly so for larger-surface packing elements, i.e. those with large geometric surfaces a and small void fractions ε.

In his work, Mersmann [3] only evaluated data for air/liquid systems at ambient conditions for classic packing elements, such as Raschig rings, spheres and Berl saddles. The evaluation of rectification data carried out during the course of this work, also confirms the applicability of the flooding point diagram, acc. to Fig. 2-5, for determining the vapour velocity $u_{V,Fl}$ at the flooding point for small packing elements $d \leq 0.015$ m, e.g. for randomly filled, metal 10 and 20 mm Interpack, 12 mm metal Białecki rings, 17 mm plastic Nor-Pac, 15 mm Pall rings made of metal and plastic as well as 17 mm plastic Hiflow rings, as long as they are within the model's range of validity.

Mersmann's [3] flooding point diagram describes the flooding in packed columns for small packing elements with $d < 25$ mm sufficiently accurately throughout the entire

operating range B_L. In the case of lattice and structured packings, the model is only applicable in the range of high liquid loads $B_L > 3{-}5{\cdot}10^{-3}$.

2.2.4.10 New Equation for Calculating Individual Droplet Velocity u_T

Equations (2-19), (2-21), (2-56) and (2-67) lead to the following correlation (2-75) for the effective falling velocity of individual droplets in the packing:

$$\begin{aligned} u_T &= \frac{u_{V,Fl}}{\varepsilon^{1.2} \cdot (1 - h^0_{L,Fl})^{3.5}} \cdot 0.566 \\ &= 0.80 \cdot \cos\alpha \cdot \psi_{Fl}^{-1/6} \cdot \left(\frac{d_h}{d_T}\right)^{1/4} \cdot \left(\frac{d_T \Delta\rho \cdot g}{\rho_V}\right)^{1/2} \qquad \left[ms^{-1}\right] \end{aligned} \tag{2-75}$$

The first term in Eq. (2-75) is used to determine the effective droplet velocity u_T, based on the experimental flooding point data, if the values $u_{V,FL}$ and $h^0_{L,Fl}$ as well as the void fraction ε are known. Equation (2-75) therefore constitutes the full form of the correlation based on Eq. (2-24). The second term in Eq. (2-75) is important for various design tasks and constitutes the final equation for the falling velocity of droplets in packed columns.

A similar correlation with d_T, acc. to Eq. (2-26),

$$u_T \approx A_i \cdot \sqrt{\frac{d_T \cdot \Delta\rho \cdot g}{\rho_V}} \tag{2-76}$$

$$u_T \approx A_i \cdot \sqrt{\frac{\sigma_L \cdot \Delta\rho \cdot g}{\rho_V^2}} \tag{2-77}$$

and with $A_i = 1.55$ was found by Mersmann [38] in relation to deformed droplets falling in gases and liquids in columns without internals.

The following correlation (2-78) is applicable to systems with a higher-density gas phase, analogous to Eq. (2-69):

$$u_T = u_{T,\ eqn.(2-75)} \cdot K_{\rho V} = u_{T,\ eqn.(2-75)} \cdot \left(\frac{\rho_V}{\rho_{air}}\right)^{0.18} \tag{2-78}$$

where $K_{\rho V}$ is based on correlation (2-70).

2.2.5 Conclusions Chapter 2.2

1. Based on the evaluation of approx. 1,200 items of experimental flooding point data, the *model of suspended bed of droplets* (SBD model), which is presented in this book, is applicable to any types of randomly filled packing elements, stacked packings, struc-

tured packings and tube columns filled with stacked packing elements, in the range of small, moderate and high phase flow ratios λ_0 in the vacuum and normal pressure range and at high pressures of up to 100 bar.

The latest experiments [66] with random packings have confirmed the droplet formation in packed columns as a result of dripping from the edges and walls of the individual packing elements. This explains why flooding can occur in packed columns at certain phase flow ratios, even in the case of smaller gas velocities, before the packing is filled with films and sprays, as assumed by the film model. Hence, the packed column is flooded earlier than predicted by the film model [3], and the gas velocities at the flooding point, calculated acc. to the film model [3], are much higher for larger lattice packing elements and structured packings than the experimentally derived values, see numerical example 2.1.

The SBD model is based on the assumption that droplet formation occurs at the flooding point and therefore describes the flooding point mechanism accurately, both for higher and smaller gas velocities in pressure absorption and rectification processes, see Fig. 2-17a, 2-17b, 2-17c, 2-17d and 2-17e

The new dimensionless equation for calculating the gas velocity at the flooding point (2-73), based on the *SBD model*, is as follows:

$$Fr_{Fl}^{*1/2} = 0.8 \cdot \cos\alpha \cdot \psi_{Fl}^{-1/6} \cdot \left[\frac{d_h}{d_T}\right]^{1/4} K_{\rho V} \cdot \varepsilon^{6/5} \cdot \left(1 - h_{L,Fl}^{0}\right)^{7/2},$$

with the dimensionless extended Froude number, acc. to Eq. (2-72)

$$Fr_{Fl}^{*} = \frac{u_{V,Fl}^{2}}{d_T \cdot g} \cdot \frac{\rho_V}{\Delta\rho},$$

which in practice can also take a dimension-dependent form acc. to Eq. (2-69)

$$u_{V,Fl} = 0.80 \cdot \cos\alpha \cdot \varepsilon^{6/5} \cdot \psi_{Fl}^{-1/6} \left[\frac{d_T \cdot \Delta\rho \cdot g}{\rho_V}\right]^{1/2} \cdot \left[\frac{d_h}{d_T}\right]^{1/4} \cdot (1 - h_{L,Fl}^{0})^{7/2} \cdot K_{\rho V} \left[ms^{-1}\right]$$

where: $K_{\rho V} = 1$ for $\rho_V \leq \rho_{air\,(1.165\ kgm^{-3})}$ and/or

$$K_{\rho V} = \left(\frac{\rho_V}{1.165}\right)^{0.18} \quad \text{for} \quad \frac{\rho_V}{\rho_{air}} > 1$$

acc. to Eqs. (2-70) and (2-71).

Equation (2-69) applies to any types of random and structured packings made of any material, provided the resistance coefficient ψ_{Fl} at the flooding point for single-phase flow is known. The validity of Eq. (2-69) for internals in the range of $\psi_{Fl} = 0.1-8.2$ has been verified. The calculation of the gas velocity $u_{V,FL}$ at the flooding point, acc. to Eq. (2-67) and/or the extended Eq. (2-69), is performed iteratively. The simplification of Eq. (2-67) leads to Eq. (2-60).

2. Based on the dimensionless Eq. (2-73) and/or (2-69), it is possible to determine the gas and/or vapour velocity with a mean relative error of ∼ 6% for systems used in vacuum and normal pressure rectification as well as in absorption processes, if the physical properties ρ_L, σ_V, η_L, η_V, ε_L, the geometric packing data a and ≤ and the liquid hold-up at the flooding point $h^0_{L,Fl}$ are known. In the case of pressure systems, the gas velocity at the flooding point can be determined with an accuracy of ±15%, see Fig. 2-17e.
3. If the phase flow ratio at the flooding point λ_0 is known, it is possible to determine the liquid hold-up $h^0_{L,Fl}$, acc. to Eq. (2-46)

$$h^0_{L,Fl} = \frac{\sqrt{\lambda_0^2(m+2)^2 + 4\lambda_0(m+1)(1-\lambda_0)} - (m+2)\lambda_0}{2\cdot(m+1)(1-\lambda_0)} \qquad \left[m^3 m^{-3}\right] \quad (2\text{-}46)$$

The parameter m in this equation is calculated using Eq. (2-43) for turbulent liquid flow $Re_L \geq 2$

$$m = -0.82 + \frac{\lambda_0}{\lambda_0 + 0.5} \quad (2\text{-}43)$$

and Eq. (2-44) for laminar liquid flow $Re_L < 2$.

$$m = -0.90 + \frac{\lambda_0}{\lambda_0 + 0.5} \quad (2\text{-}44)$$

In the case of larger packing elements, at moderately negative and normal pressure, the liquid flow is practically turbulent, which means that Eqs. (2-46) and (2-42) are mostly applicable. Hence, it is possible to determine the flooding point without having to ascertain any experimental hold-up data at the flooding point.
4. The evaluation of the experimental flooding point data acc. to Eq. (2-73) and/or (2-69) was based on roughly 1,200 items of experimental data for approx. 200 random and structured packings and tube columns. The columns, internals and operating parameters were varied within the following ranges:

$$\begin{array}{rcccl}
0.1 & \leq & \boldsymbol{\psi_{Fl}} & \leq & 8.5 \quad [-] \\
0.025 & \leq & \mathbf{d_S} & \leq & 1.4 \quad \mathrm{m} \\
0.59 & \leq & \boldsymbol{\varepsilon} & \leq & 0.988 \quad \mathrm{m^3 m^{-3}} \\
0.008 & \leq & \mathbf{d} & \leq & 0.100 \quad \mathrm{m} \\
54 & \leq & \mathbf{a} & \leq & 750 \quad \mathrm{m^2 m^{-3}} \\
0.45 & \leq & \mathbf{H} & \leq & 6.0 \quad \mathrm{m} \\
0.013 & \leq & \mathbf{p_T} & \leq & 100 \quad \mathrm{bar} \\
0 & \leq & \boldsymbol{\lambda_0 \cdot 10^3} & \leq & 1000 \quad [-] \\
0.01 & \leq & \mathbf{u_V} & \leq & 18 \quad \mathrm{ms^{-1}} \\
0.1 & \leq & \mathbf{F_{V,Fl}} & \leq & 5.5 \quad \sqrt{Pa} \\
0 & < & \mathbf{u_L} & \leq & 56\cdot 10^{-3} \quad \mathrm{ms^{-1}} \\
0 & < & \mathbf{Re_L} & \leq & 600 \quad [-]
\end{array} \quad (2\text{-}79)$$

Table 2-2 contains a list of 32 mixtures with widely different physical properties, which were used for evaluating the experimental flooding point data.

5. Based on the *SBD model*, the gas and/or vapour velocity at the flooding point can be determined in the following way: Firstly, the phase flow ratio at the flooding point λ_0 is calculated as a start value, acc. to Eq. (2-1), for $V_{V,Fl} = V_V$. Subsequently, the liquid hold-up at the flooding point $h^0_{L,Fl}$ is calculated in the first iteration, acc. to Eq. (2-46). Now Eq. (2-69) is used to determine the gas and/or vapour velocity at the flooding point $u_{V,Fl}$, based on the physical properties of the system ρ_V, ρ_L, σ_L, η_V, η_L, the geometric data a and ε of the respective packing elements and the mean resistance coefficient, acc. to Table 6-1a–6-1c.

   Finally, it must be ascertained whether or not the assumption $Re_L \geq 2$ is applicable. If Re_L is below 2, the new calculation of the hold-up at the flooding point is performed, based on Eq. (2-42), followed by the calculation of the gas velocity at the flooding point. Only a few iterations are necessary to determine a sufficiently accurate value for $u_{V,Fl}$ and thus for the variables λ_0 and $h^0_{L,Fl}$.

   Further to the correlations presented above, there are a number of calculation examples at the end of this chapter, which illustrate how the model can be used to determine the vapour velocity at the flooding point for 50 mm randomly filled Pall rings for the system ethyl benzene/styrene under vacuum, and the gas velocity at the flooding point under pressure for 25 mm randomly filled Białecki rings for the air/water system, for structured gauze packing BX as well as for 15 mm Pall rings made of plastic.

6. The *film gas thrust shear force model,* developed by Mersmann (1965) [3], for determining the gas velocity at the flooding point is most suitable for applications using classic and/or large-surface packing elements with $a \geq 300\ m^2m^{-3}$ throughout the entire operating range. This is reflected by the shading in the flooding point diagram developed by Mersmann [3], see Fig. 2-18. The *film gas thrust shear force model*, on

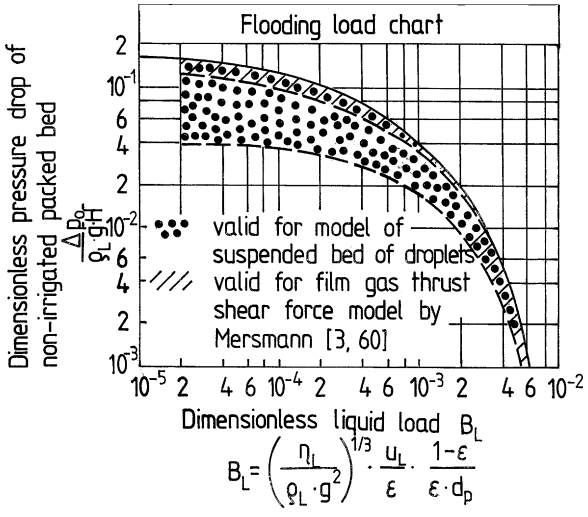

Figure 2-18. Flooding line depending on the dimensionless liquid load with ranges of validity of the SBD model, based on the results of this work, and the film gas thrust shear force model, developed by Mersmann [3, 60, 91]

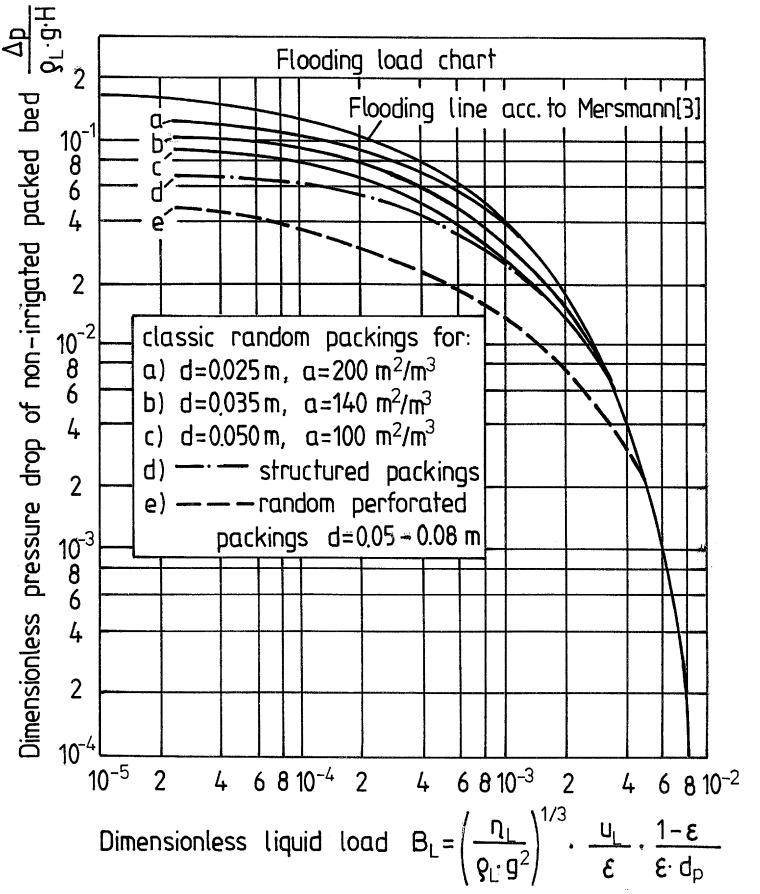

Figure 2-19. Flooding line for various packings. Compilation of results from Figs. 2-5a–d

the other hand, only applies to perforated packing elements, if the dimensionless liquid loads are high, $B_L \geq 5 \cdot 10^{-3}$, as shown by Figs. 2-5a, 2-5b, 2-5c and 2-5d as well as Fig. 2-19. These operating conditions mostly occur in the case of extremely high liquid loads, in pressure absorption and pressure rectification.

A further modification of Mersmann's diagram, based on the model presented in the first German edition of this book [90, 91], can be found in Bornhütter's work (1991) [66, 87] and by Grabbert, Bonitz (1998) [92].

Farther capacity diagrams for different packings are shown in Annex to this chapter, Figs. 2-22, 2-23, 2-24, 2-25, 2-26, 2-27, 2-28, 2-29, 2-30, 2-31, 2-32, 2-33, 2-34, 2-35, 2-36, 2-37 and 2-38.

2.3 Determining Column Diameter

If the gas capacity factor $F_{V,Fl}$ at the flooding point is determined in relation to a given packing element, it is possible to ascertain the operating point marked by the gas capacity factor F_V. The following applies:

$F_{V,U} < F_V < F_{V,Fl}$. Depending on the separation process, the gas capacity factor F_V is set at approx. 10–80% of the value at the flooding point. This leads to the following correlation for the column diameter d_s:

$$d_S = \sqrt{\frac{4 \cdot A_S}{\pi}} = \sqrt{\frac{4}{\pi}} \cdot \sqrt{\frac{V}{\sqrt{\rho_V} \cdot F_V}} \qquad [m] \qquad (2\text{-}80)$$

where V is the gas capacity in kgs^{-1}.

2.4 Lower Loading Line

Vacuum distillation columns are mostly operated at very low liquid loads u_L, in particular in the rectifying section. For this reason, it is important to ascertain the lower loading line $u_{L,U}$, Fig. 2-20, as well as the flooding point. Kirschbaum [19] and Schmidt [7, 32] have looked at methods to determine the lower loading line.

The lower loading line is largely dependent on the physical properties of the mixture to be separated as well as on the material and geometric dimensions of the packing

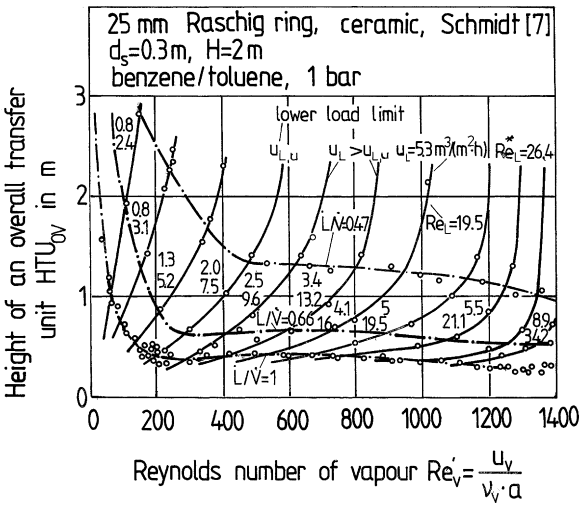

Figure 2-20. Height of an overall transfer unit for various L/V ratios as a function of the Reynolds number of vapour Re_V and liquid $Re*_L$ acc. to Schmidt [32]. As shown in this diagram, the lower loading line is below the flooding line

elements, whereas interfacial instabilities do not appear to have an effect on the lower loading line.

Schmidt [32] has presented various equivalent correlations for determining the lower loading line $u_{L,U}$. The simplest equation, which is also the clearest and easiest one to apply, is as follows:

$$u_{L,U} = 7.7 \cdot 10^{-6} \cdot \frac{C_L^{2/9}}{(1 - T_L)^{1/2}} \cdot \left[\frac{g}{a}\right]^{1/2} \quad \left[ms^{-1}\right], \tag{2-81}$$

The relative error of this equation is ±20%, which has been verified for vacuum conditions up to 20 mbar and for liquid/vapour ratios of L/V = 0.5−1.25.

The liquid number is given as:

$$C_L = \frac{\rho_L \cdot \sigma_L^3}{\eta_L^4 \cdot g} \tag{2-82}$$

and the shear stress number is:

$$T_L \cong 0.9 \cdot \left[\frac{u_V}{u_{V,Fl}}\right]^{2.8} = 0.9 \cdot \left[\frac{F_V}{F_{V,Fl}}\right]^{2.8} \tag{2-83}$$

Equation (2-81) was derived by Schmidt [7, 32], based on his own experimental results and those found in literature, using the systems ethanol/water, dichloroethane/toluene and benzene/toluene under normal pressure and vacuum of up to 20 mbar. It is applicable to 25−50 mm ceramic Raschig rings and metal Pall rings.

Schmidt [7, 32] noticed the dewetting phenomenon, which causes the separation efficiency below the loading line $u_{L,U}$ to drop. The phenomenon is amplified by a decrease in the specific liquid load u_L. Equation (2-81) shows that, in the case of mixtures with a decreasing liquid number C_L, the lower loading line $u_{L,U}$ shifts towards the lower values of the specific liquid load u_L, which has a positive effect on the elasticity of the column. The operating range of packed columns using such systems is therefore larger, Fig. 2-21.

In the case of mixtures with low viscosity η_L and high surface tension σ_L, such as aqueous mixtures, the specific liquid load at the flooding point $u_{L,Fl}$ can fall below the lower loading line $u_{L,U}$, i.e. $u_{L,Fl} < u_{L,U}$, as shown in Fig. 2-21 [7, 32]. These operating conditions lead to the downward liquid flow being impounded and entrained by the gas (vapour), without sufficiently wetting the packing surface.

2.4.1 Conclusions Section 2.4

Based on Schmidt's [32] correlation (2-81) for calculating the lower loading line $u_{L,U}$ and the knowledge of the loading line of the type of packing used, it is easy to determine by calculation whether the specific liquid load u_L, selected for the separation task of the column, is above the lower loading line $u_{L,U}$, $u_{L,U} < u_L < u_{L,Fl}$.

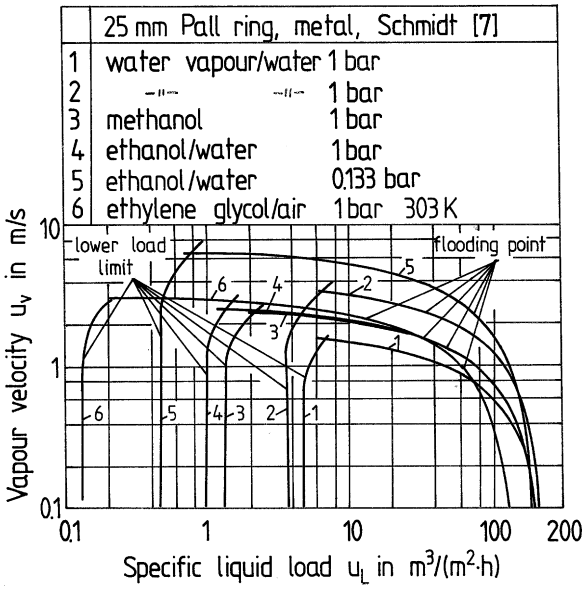

Figure 2-21. Lower loading line $u_{L,U}$ and flooding line for 25 mm Pall ring column acc. to Schmidt [32]. This diagram highlights the overlapping of both limit lines and shows the operating range of the packed column for a given system

List of Numerical Examples – Chapter 2 "Flooding Point"

2.1 Determining the vapour capacity factor $F_{V,Fl}$ at the flooding point, acc. to Eq. (2-67) and the column diameter d_S for metal, randomly filled 50 mm Pall rings for the separation of the mixture ethyl benzene/styrene under vacuum.

2.2 Determining the vapour capacity factor $F_{V,Fl}$, acc. to Eq. (2-67), for metal, randomly filled 25 mm Białecki rings for the air/water test system at ambient conditions.

2.3 Determining the vapour capacity factor $F_{V,Fl}$, acc. to Eq. (2-67), for Sulzer gauze packing BX for the separation of the mixture ethyl benzene/styrene at a top pressure of 66.7 mbar.

2.4 Determining the vapour capacity factor $F_{V,Fl}$ at the flooding point, acc. to eqns (2-69) and (2-71), and the column diameter d_S for randomly filled 15 mm plastic Pall rings for the separation of the mixture methanol/nitrogen (N_2) at 30 bar.

2.5 Determining the vapour capacity factor $F_{V,Fl}$ at the flooding point, acc. to Eq. (2-69), and the relative column load $F_V/F_{V,Fl}$ in an existing column of a demethaniser being upgraded to a structured Mellapak 350Y sheet metal packing at an operating pressure of 32 bar.

Numerical Example 2.1 – Sections 2.2.4 and 2.3

A column filled with metal 50 mm Pall rings is used to separate 1,000 kg of the mixture ethyl benzene/styrol with $x_F = 0.5895$ mol mol^{-1} per hour, at a top pressure of

$p_T = 66.7$ mbar. The aim is to achieve a top product with a mole fraction of higher-volatility ethyl benzene of $x_D = 0.9618$ mol mol^{-1} and a bottom product with a mole fraction of $x_W = 0.0018$ mol mol^{-1} x_W. What column diameter is required, if the column is operated at 46.3% of the flood load and the reflux ratio is $r = 6.28$?

The vapour capacity factor $F_{V,Fl}$ at the flooding point is determined using the method described in Sect. 2.2.4 as well as Eq. (2-67). The following variables are given, with the physical properties applicable for a top pressure of $p_T = 66.7$ mbar.

– vapour density	ρ_V
– liquid density	$\rho_L = 835.2$ kgm^{-3}
– surface tension	$\sigma_L = 25.1$ mNm^{-1}
– viscosity of the liquid	$\eta_L = 0.437 \cdot 10^{-3}$ kgm^{-1} s^{-1}
– viscosity of the vapour mixture	$\eta_V = 7.14 \cdot 10^{-6}$ kgm^{-1} s^{-1}
– molar mass of the distillate product	$M_D = 106.1$ kg kmol^{-1}
– molar mass of the feed	$M_F = 105.34$ kg kmol^{-1}
– relative vapour capacity	$F_V/F_{V,Fl} = 0.463$

Solution

A. Calculating the flows and flow rates at the column top according to the task definition

1. *Feed rate:*

$$\begin{aligned} F &= 1000 \ kgh^{-1} \\ \dot{F} &= F/M_F \\ &= 1000/105.34 = 9.493 \ kmolh^{-1} \end{aligned}$$

2. *Distillate rate:*

$$\begin{aligned} \dot{D} &= \dot{F} \cdot \frac{x_F - x_W}{x_D - x_W} \\ &= 9.493 \cdot \frac{05895 - 0.0018}{0.9618 - 0.0018} = 5.812 \ kmolh^{-1} \end{aligned}$$

3. *Vapour rate at column top:*

$$\begin{aligned} \dot{V} &= (r+1) \cdot \dot{D} \\ &= (6.28 + 1) \cdot 5.812 = 42.3 \ kmolh^{-1} \end{aligned}$$

with a molar mass of $M_D = 106.1$ kg kmol^{-1}:

$$\begin{aligned} V &= \dot{V} \cdot M_D \\ &= 42.3 \cdot 106.1 = 4488.9 \ kgh^{-1} \end{aligned}$$

4. *Liquid rate L at column top:*

$$\begin{aligned} L &= r \cdot \dot{D} \cdot M_D \\ &= 6.28 \cdot 5.812 \cdot 106.1 = 3872.2 \ kgh^{-1} \end{aligned}$$

B. Determining the vapour capacity factor $F_{V,Fl}$

1. The phase flow ratio at the flooding point λ_0 is given as:

$$\lambda_0 = \frac{\dot{V}_L}{\dot{V}_V} = \frac{L \cdot \rho_V}{\rho_L \cdot V} = \\ = \frac{3872.2 \cdot 0.257}{835.2 \cdot 4488.9} = 2.654 \cdot 10^{-4}$$

2. The liquid hold-up $h^0_{L,Fl}$ at the flooding point is determined, acc. to Eq. (2-47), using a start value of $\lambda_0 = 2.654 \cdot 10^{-4}$. As a result, $h^0_{L,Fl}$ is given as:

$$h^0_{L,FL} = \frac{\sqrt{1.44 \cdot \lambda_0^2 + 0.8 \cdot \lambda_0 \cdot (1 - \lambda_0)} - 1.2 \cdot \lambda_0}{0.4 \cdot (1 - \lambda_0)}$$

$$= \frac{\sqrt{1.44 \cdot \left(2.654 \cdot 10^{-4}\right)^2 + 0.8 \cdot 2.654 \cdot 10^{-4} \cdot \left(1 - 2.654 \cdot 10^{-4}\right)} - 1.2 \cdot 2.654 \cdot 10^{-4}}{0.4 \cdot (1 - 2.654 \cdot 10^{-4})}$$

$$= 3.565 \cdot 10^{-2} m^3 m^{-3}$$

3. The vapour velocity at the flooding point for 50 mm metal Pall rings is determined acc. to Eq. (2-67). The following values apply for the geometric data a and ε as well as the constants K_1, K_2 for $Re_V > 2100$ in relation to Eq. (3-14), acc. to Table 6-1a: $N_0 = 6100\ Nm^{-3} \Rightarrow a_0 = 110\ m^2\ m^{-3}$, $\varepsilon_0 = 0.952\ m^3\ m^{-3}$, $K_1 = 3.23$, $K_2 = -0.0343$ for Eq. (3-15) to calculate the resistance coefficient.
The application of Eq. (2-67) also requires the following parameters:

   – the hydraulic diameter

$$d_h = 4 \cdot \varepsilon / a = 4 \cdot 0.952 / 110 = 0.0346\ \text{m}$$

   – the droplet diameter

$$d_T = \sqrt{\sigma / \Delta\rho \cdot g} = \\ = \sqrt{0.0251 / \left((835.2 - 0.257) \cdot 9.81\right)} = 1.75 \cdot 10^{-3} m$$

4. Firstly, Eq. (2-67) for $\alpha = 45^o$ is used to estimate the gas velocity at the flooding point $u_{V,Fl}$ for $\psi_{Fl} \cong 2.42$ with $Re_V \geq 2100$ and $h_{L,Fl} = 0.0365\ m^3\ m^{-3}$.

$$u_{V,Fl} = 0.566 \cdot \psi_{Fl}^{-1/6} \left[\frac{d_h}{d_T}\right]^{1/4} \cdot \varepsilon^{6/5} \cdot \left[\frac{d_T \Delta\rho \cdot g}{\rho_V}\right]^{1/2} \cdot \left[1 - h^0_{L,Fl}\right]^{3.5}$$

$$= 6.43\ ms^{-1}$$

As a result, the vapour velocity u_V with $F_V/F_{V,Fl} = 0.463$ is given as:

$$\begin{aligned} u_V &= 0.463 \cdot u_{V,Fl} \\ &= 0.463 \cdot 6.43 = 2.98\ ms^{-1} \end{aligned}$$

the column cross section A_S is:

$$A_S = \frac{V_w}{3600 \cdot \rho_V \cdot u_V} = \frac{4488{,}9}{3600 \cdot 0{,}257 \cdot 2{,}98} = 1{,}628\ \mathrm{m}^2$$

and, finally, the column diameter d_S is given as:

$$d_S = \sqrt{\frac{4 \cdot A_S}{\pi}} = 1.44m; \text{ based on the assumption that } d_S = 1.45\mathrm{m}$$

5. Based on the specific liquid load u_L

$$\begin{aligned} u_L &= \frac{L}{3600 \cdot \rho_L \cdot A_S} = \frac{3872.2}{3600 \cdot 835.2 \cdot 1.65} \\ &= 7.8 \cdot 10^{-4}\ ms^{-1} \end{aligned}$$

the Reynolds number Re_L is calculated as:

$$\mathrm{Re}_L = \frac{u_L}{\nu_L \cdot a} = \frac{u_L \cdot \rho_L}{\eta_L \cdot a} =$$

$$= \frac{7.8 \cdot 10^{-4} \cdot 835.2}{0.437 \cdot 10^{-3} \cdot 110} = 13.55 > 2$$

As a result, the use of Eq. (2-47) for calculating the liquid hold-up $h^0_{L,Fl}$ at the flooding point is justified.

6. Based on a specific liquid load of $u_L = 7.8\ 10^{-4}\ \mathrm{ms}^{-1}$, the vapour velocity at the flooding point $u_{V,Fl}$ is calculated as $u_{V,Fl} = 6.69\ \mathrm{ms}^{-1}$, acc. to Eq. (2-67), using iterative calculation. The phase flow ratio at the flooding point λ_0 is given as $1.1 \cdot 10^{-4}$ for $\psi_{Fl} = 2.34$ and for $h^0_{L,Fl} = 2.38\ 10^{-2}\ \mathrm{m}^3\ \mathrm{m}^{-3}$.
The calculated value for $u_{V,Fl}$ is only 4.1% higher than the velocity of $6.43\ \mathrm{ms}^{-1}$ obtained by approximate calculation (point 4).
The vapour capacity factor at the flooding point $F_{V,Fl}$ is now given as:

$$F_{V,Fl} = u_{V,Fl} \cdot \sqrt{\rho_V} = 3.39\ \ ms^{-1}\sqrt{\mathrm{kgm}^{-3}}\ \left[\sqrt{\mathrm{Pa}}\right]$$

The following numerical value was found by Billet [5], Chap. 2, for the vapour capacity factor $F_{V,Fl}$ with $\dot{L}/\dot{V} = 1$ for the same system and a marginally different phase flow ratio, compared to the one specified in the task definition:

$$F_{V,Fl} = 3.3\ \ ms^{-1}\sqrt{kgm^{-3}}\quad \left[\sqrt{Pa}\right]$$

Relative error $\delta(F_{V,Fl})$:

$$\delta(F_{V,Fl}) = \frac{(F_{V,Fl})_{calc} - (F_{V,Fl})_{\exp}}{(F_{V,Fl})_{\exp}} \cdot 100$$

$$= \frac{3.39 - 3.3}{3.3} \cdot 100 = 2.73\%$$

Further calculations were performed, based on other methods, to determine the flood load factor $F_{V,Fl}$, acc. to this task definition. The results were as follows:

1. Eckert's method [9]:	$F_{V,Fl} = 5.0$	$Pa^{0.5}$	$\delta(F_{V,Fl}) = 51.5\%$
2. Mersmann's method [3]:	$F_{V,Fl} = 4.98$	$Pa^{0.5}$	$\delta(F_{V,Fl}) = 50.9\%$
3. Billet's method [5]:	$F_{V,Fl} = 3.55$	$Pa^{0.5}$	$\delta(F_{V,Fl}) = 7.6\%$
4. Equation (2-67):	$F_{V,Fl} = 3.39$	$Pa^{0.5}$	$\delta(F_{V,Fl}) = 2.73\%$
5. Exp. value:	$F_{V,Fl} = 3.3$	$Pa^{0.5}$	acc. to Billet [5] for $\left(\dot{L}/\dot{V}\right) = 1$.

Numerical Example 2.2 – Chapter 2

The aim is to determine the gas velocity at the flooding point $u_{V,Fl}$ in a column randomly filled with 25 mm metal Białecki rings with a diameter of $d_S = 0.15$ m. The column is operated at a gas velocity of $u_V = 1\ ms^{-1}$ and a specific liquid load of $u_L = 0.0111\ ms^{-1}$, using the test system air/water at 1 bar and 293 K. The technical data of the Białecki rings is as follows:

$N = 55000\ m^{-3}$
$\Rightarrow a = 238\ m^2\ m^{-3}$, $\varepsilon = 0.94\ m^3 m^{-3}$.

The physical properties are valid for 1 bar and 293 K:

$\eta_V = 18.2 \cdot 10^{-6}\ m^2\ s^{-1}$	$\rho_L = 998.2\ kgm^{-3}$
$\eta_L = 10^{-3}$ Pas	$\rho_L = 1.17\ kgm^{-3}$
$\sigma_L = 72.4 \cdot 10^{-3} Nm^{-1}$	$g = 9.80665\ ms^{-2}$

Solution

1. The following parameters are required for calculating the gas velocity at the flooding point $u_{V,Fl}$, acc. to Eq. (2-67):

   1.1 K_3, K_4 coefficients for determining the resistance coefficient for the dry packing at the flooding point for $Re_V > 2100$.
   Based on Eq. (3-16) and Table 6-1a, the numerical values for the model constants K_3, K_4, [20] for $Re_V \geq 2100$ are as follows:

   $K_3 = 4.13$, $K_4 = -0.0522$.

   The start value is assumed to be a mean value of $\psi_{Fl,m} \cong 2.60$, acc. to Table 6-1a.

1.2 Hydraulic diameter d_h:

$$d_h = 4 \cdot \frac{\varepsilon}{a} = 4 \cdot \frac{0.942}{238} = 1.583 \cdot 10^{-2} m$$

1.3 Droplet diameter:

$$d_T = \sqrt{\frac{\sigma_L}{(\rho_L - \rho_V) \cdot g}} = \sqrt{\frac{0.0724}{(988.2 - 1.17) \cdot 9.80665}}$$

$$= 2.72 \cdot 10^{-3} m$$

2. The Reynolds number Re_L is given as:

$$Re_L = \frac{u_L}{\nu_L \cdot a} = \frac{u_L \cdot \rho_L}{\eta_L \cdot a} =$$

$$= \frac{11.1 \cdot 10^{-3} \cdot 998.2}{10^{-3} \cdot 238} = 46.55 > 2$$

The liquid hold-up $h^0_{L,Fl}$ is determined using correlation (2-47). The start value for the phase flow ratio at the flooding point λ_0 is assumed to be:

$$\lambda_0 = \frac{u_L}{u_V} = 11.1 \cdot 10^{-3} \quad where \quad u_V = 1\ ms^{-1}$$

This leads to a value of $h^0_{L,Fl} = 0.2056\ m^3\ m^{-3}$, acc. to Eq. (2-47). Based on the first iteration, the gas velocity at the flooding point $(u_{V,Fl})_1$ is given as the numerical value of $(u_{V,Fl})_1 = 1.7132\ ms^{-1}$. Subsequently, a new phase flow ratio of $\lambda_0 = 11.1 \cdot 10^{-3} / 1.713 = 6.46 \cdot 10^{-3}$ is created, for which the $(u_{V,Fl})_2$ value is now calculated iteratively. If the difference between the value $(u_{V,Fl})_{i+1}$, based on iteration *i+1*, and the value $(u_{V,Fl})_I$, based on iteration *I*, is less than 0.01 ms^{-1}, the iteration is finished.

The iterative calculation leads to the following numerical value for $u_{V,Fl}$:

$$u_{V,Fl} = 1.776\ ms^{-1},$$

which is practically identical to the value $u_{V,Fl} = 1.75\ ms^{-1}$ for $u_L = 11.1 \cdot 10^{-3}\ ms^{-1}$, shown in Figs. 2-2a and 2-2b, which was experimentally derived. The relative error is therefore:

$$\delta\left(u_{V,Fl}\right) = \frac{1.75 - 1.776}{1.75} \cdot 100\% = -1.49\ \%$$

The column is operated at approx.

$$\frac{F_V}{F_{V,Fl}} = \frac{u_V}{u_{V,Fl}} = \frac{1}{1.776} = 0.563$$

i.e. at a flood load of 56.3%. The phase flow ratio at the flooding point

$$\lambda_0 = \frac{u_L}{u_{V,Fl}} = \frac{11.1 \cdot 10^{-3}}{1.776} = 6.25 \cdot 10^{-3}$$

now gives the following liquid hold-up at the flooding point:

$$h^0_{L,Fl} = 15.3 \cdot 10^{-2}\,\mathrm{m^3 m^{-3}}.$$

Based on Table 2-3, the experimentally derived $h^0_{L,Fl}$ value is 16.2%.
This gives a relative error of:

$$\delta\left(h^0_{L,Fl}\right) = \frac{15.3 - 16.2}{16.2} \cdot 100\% = -5.55\%$$

for $Re_{V,Fl} = 2553.7$, hence:

$$\psi_{Fl} = 4.13 \cdot 2553.7^{-0.0522} = 2.745$$

Example 2.3 – Chapter 2

The aim is to determine the gas velocity at the flooding point for the Sulzer gauze packing BX, using the system ethyl benzene/styrene at 66.7 mbar. The column diameter is $d_S = 0.5$ m, the reflux rate at the column top is L = 1491 kg/h, as shown in Fig. 6-33 [5]; $\dot{L}/\dot{V} = 1$. The angle of the flow channels for BX packings is $\alpha = 30°$. The gas velocity at the flooding point, which was experimentally derived by Billet [5], is $u_{V,Fl} = 7.50\ \mathrm{ms^{-1}}$.

Solution

Based on a mean value of $\psi_m \in (2100–10{,}000)$ $\psi_m = 0.374$ and the geometric data a and ε, shown in Table 6-1c, the numerical values for Eq. (2-67) are as follows:

$$d_h = 4 \cdot \frac{\varepsilon}{a} = 4 \cdot \frac{0.95}{500} = 0.0076\ \mathrm{m}$$

$$d_T = 1.75 \cdot 10^{-3}\ \mathrm{m}$$

$$u_L = \frac{1491}{0.52 \cdot \frac{\pi}{4} \cdot 835.2 \cdot 3600} = 2.52 \cdot 10^{-3}\ \mathrm{ms^{-1}}$$

$$\lambda_0 = \frac{L}{V} \cdot \frac{\rho_V}{\rho_L} = 1 \cdot \frac{0.257}{835.2} = 3.08 \cdot 10^{-4}$$

For $\lambda_0 = 3.08{\cdot}10^{-4}$, m is calculated using Eq. (2-43):

$$m = -0.82 + \frac{\lambda_0}{\lambda_0 + 0.5} = -0.82 + \frac{3.08 \cdot 10^{-4}}{3.08 \cdot 10^{-4} + 0.5} \cong -0.82$$

and the liquid hold-up at the flooding point, acc. to Eq. (2-47), is given as:

$$h^0_{L,Fl} = 3.834 \cdot 10^{-2}\ m^3 m^{-3}$$

After the first iteration, the gas velocity at the flooding point, acc. to Eq. (2-66), is calculated as:

$$u_{V,Fl} = 0.8 \cdot \cos 30° \cdot 0.374^{-1/6} \cdot \left[\frac{7.6 \cdot 10^{-3} m}{1.75 \cdot 10^{-3} m}\right]^{0.25} \cdot 0.95^{1.2} \cdot$$

$$\cdot \left[\frac{1.75 \cdot 10^{-3} \cdot 835 \cdot 9.81}{0.257}\right]^{1/2} \cdot (1 - 0.03834)^{3.5} =$$

$$= 7.222\ ms^{-1}$$

In the second iteration, the numerical values for λ_0 and Re_V are calculated as:

$$\lambda_0 = \left(\frac{u_L}{u_V}\right)_{Fl} = \frac{2.52 \cdot 10^{-3}}{7.677} = 3.28 \cdot 10^{-3} \quad \Rightarrow \quad h^0_{L,Fl} = 4 \cdot 10^{-2}\ m^3 m^{-3}$$

and

$$\mathrm{Re}_V = \frac{u_V \cdot d_P}{(1 - \varepsilon) \cdot \nu_V} = \frac{6 \cdot u_V}{a \cdot \nu_V} = \frac{6 \cdot 7.220 \cdot 0.257}{500 \cdot 7.14 \cdot 10^{-6}} = 3116.8$$

Based on Eq. (3-14) and Table 6-1c, the resistance coefficient of the dry packing ψ is calculated as:

$$\psi = 1.21 \cdot 3116.8^{-0.14} = 0.3823$$

The gas velocity at the flooding point $u_{V,Fl}$, acc. to Eq. (2-67) is given as:

$$u_{V,Fl} = 0.8 \cdot \cos 30° \cdot 0.3823^{-1/6} \cdot \left[\frac{7.61}{1.75}\right]^{0.25}$$

$$\cdot 0.95^{1.2} \cdot \left[\frac{1.75 \cdot 10^{-3} \cdot 835 \cdot 9.81}{0.257}\right]^{1/2} \cdot (1 - 0.039)^{3.5}$$

$$= 7.18\ ms^{-1}$$

At 0.58%, this value only differs marginally from the numerical value given by the first iteration, which means that the value for the gas velocity at the flooding point can be assumed to be:

$$u_{V,Fl} \cong 7.18 \text{ ms}^{-1}$$

The relative error in the determination of the gas velocity at the flooding point $u_{V,Fl,exp}$ is therefore:

$$\delta\left(u_{V,Fl}\right) = \frac{7.18 - 7.50}{7.50} \cdot 100\% = -6.18\ \%$$

Numerical Example 2.4 – Chapter 2

A column with a diameter of $d_S = 0.155$ m is filled with 15 mm plastic Pall rings for the separation of the mixture methanol/nitrogen at 30 bar and 251 K. What is the column load, assuming a liquid flow of 464 kgh^{-1} and a gas flow of 472 kgh^{-1}? The physical properties and technical data of the packing are as follows:

Physical properties:

gas density:	$\rho_L = 41.06\ \text{kgm}^{-3}$
liquid density:	$\rho_L = 831.0\ \text{kgm}^{-3}$
surface tension:	$\sigma_L = 24.17{\cdot}10^{-3}\text{Nm}^{-1}$
viscosity:	
– liquid	$\eta_L = 122{\cdot}10^{-5}$ Pas
– gas phase	$\eta v = 16.2{\cdot}10^{-6}$ Pas

Technical packing data:

(acc. to Krehenwinkel, Chapter 2 [75])	15 mm Pall ring – PP
column diameter:	$d_S = 0.155$ m
packing density:	$N = 247600\ \text{m}^{-3}$
specific weight:	$G = 130\ \text{kgm}^{-3}$
geometric surface of packing elements:	$a = 375\ \text{m}^2\ \text{m}^{-3}$
void fraction:	$\varepsilon = 0.846\ \text{m}^3\ \text{m}^{-3}$

Loads:

gas phase:	$V = 472\ \text{kgh}^{-1}$
liquid phase:	$L = 464\ \text{kgh}^{-1}$
specific column loads:	$u_V = 0.169\ \text{ms}^{-1}$
	$u_L = 29.6\ \text{m}^3\ \text{m}^{-2}\ \text{h}^{-1}$
	$= 8.22{\cdot}10^{-3}\ \text{ms}^{-1}$

Solution

The gas velocity at the flooding point $u_{V,Fl}$ is determined for higher gas densities as $\rho_V = 1.2\ kg/m^3$, based on Eq. (2-69).

The phase flow ratio at the flooding point $\lambda_{0,1}$

$$\lambda_{0,1} = \frac{u_L}{u_V} = \frac{8.22 \cdot 10^{-3}}{0.169} = 4.864 \cdot 10^{-2}$$

based on Eq. (2-46), and for m= −0.7313, acc. to Eq. (2-43), is given as:

$$h^0_{L,Fl} = 33.19 \cdot 10^{-2}\ m^3\ m^{-3}$$

The application of Eq. (2-69) requires the following variables:

– the hydraulic diameter of the packing d_h:

$$d_h = 4 \cdot \frac{\varepsilon}{a} = 4 \cdot \frac{0.846}{375} = 9.024 \cdot 10^{-3} m$$

– the droplet diameter d_T, based on the Eq. (2-26):

$$d_T = \sqrt{\frac{\sigma}{(\rho_L - \rho_V)}} = \sqrt{\frac{0.0242}{(831 - 41.06) \cdot 9.81}} = 1.77 \cdot 10^{-3}\ m$$

– the numerical value of the Reynolds number of the gas phase Re_V, which is calculated using Eq. (3-10):

$$Re_V = \frac{u_V \cdot d_p}{(1 - \varepsilon) \cdot \nu_V} \cdot K$$

with a constant particle diameter d_p

$$d_p = 6 \cdot \frac{1 - \varepsilon}{a} = 2.464 \cdot 10^{-3} m$$

and the wall factor K

$$K = \left(1 + \frac{4}{d_S \cdot a}\right)^{-1} = 0.936$$

as well as the kinetic viscosity of the gas phase

$$\nu_V = \frac{\eta_V}{\rho_V} = \frac{16.2 \cdot 10^{-6}}{41.06} = 3.945 \cdot 10^{-7} \quad m^2 s^{-1}$$

and for

$$u_V = 0.169\,\mathrm{ms}^{-1}$$

which gives:

$$\mathrm{Re}_V = \frac{0.169 \cdot 2.464 \cdot 10^{-3}}{(1 - 0.846) \cdot 3.945 \cdot 10^{-7}} \cdot 0.936 = 6415.6 \geq 2100$$

Based on Table 6-1a, the numerical values K_3 and K_4, used for determining the resistance coefficient ψ in the turbulent flow range $\mathrm{Re}_V > 2100$, are given as:

$$K_3 = 3.23 \quad K_4 = -0.0343$$

Hence:

$$\psi = 3.23 \cdot 6415.6^{-0.0343} = 2.391$$

Based on Table 6-1a, the packing form factor φ_P, used for determining the resistance coefficient ψ acc. to Eq. (3-27) leads to the same value:

$$\psi = \frac{522.4}{\mathrm{Re}_V} + 2.306 = \frac{522.4}{6415.6} + 2.306 = 2.387 \approx 2.39$$

Based on Eq. (2-71) for $\rho_V >> \rho_{V,air}$, the following applies:

$$K_{\rho V} = \left(\frac{\rho_V}{1.165}\right)^{0.18} = 1.90$$

Equation (2-69) now leads to the following result:

$$u_{V,Fl} = 1.90 \cdot 0.566 \cdot 2.391^{-1/6} \left[\frac{9.024 \cdot 10^{-3}}{1.77 \cdot 10^{-3}}\right]^{1/4} \cdot$$

$$\cdot 0.846^{1.2} \cdot \left[\frac{1.77 \cdot 10^{-3} \cdot (831.0 - 41.06) \cdot 9.81}{41.06}\right]^{1/2} \cdot [1 - 0.3319]^{7/2} =$$

$$= 0.161\ ms^{-1}$$

Note

The column floods, as the experimental gas velocity u_V in the column $u_V = 0.169\ \mathrm{ms}^{-1}$, acc. to [75], is approximately equal to the gas velocity at the flooding point $u_{V,Fl} = 0.161\ \mathrm{ms}^{-1}$, based on Eq. (2-69), with a relative deviation of: $\delta(F_{V,Fl}) = 4.72\%$.

Numerical Example 2.5 – Chapter 2

The trays of a demethaniser, operated at approx. 32 bar, are upgraded to Mellapak 350Y. The aim is to determine the maximum loading capacity of the upgraded packed column in the rectifying section with a diameter of $d_S = 1.2$ m and in the stripping section with $d_S = 2.282$ m [72]. The operating data is taken from the article by Ghelfi, Kreis, Alvarez and Hunkeler [72].

Solution

1.

Table 2-11. Physical properties and operating data of the upgraded column

Column diameter $\mathbf{d_S}$ [m]	$\mathbf{d_S = 1.2}$	$\mathbf{d_S = 2.282}$
Top pressure **p** [bar]	30.8	28.7
Temperature $\mathbf{t_V = t_L}$ [°C]	19.8	−2.7
Gas density $\boldsymbol{\rho_V}$ [kgm^{-3}]	51.46	63.10
Liquid density $\boldsymbol{\rho_L}$ [kgm^{-3}]	394.6	392.2
Surface tension $\boldsymbol{\sigma_L}$ [mNm^{-1}]	2.5	1.8
Gas viscosity $\boldsymbol{\eta_V}$ [Pas]	$8.9 \cdot 10^{-6}$	$9.0 \cdot 10^{-6}$
Liquid viscosity $\boldsymbol{\eta_L}$ [Pas]	$0.083 \cdot 10^{-3}$	$0.078 \cdot 10^{-3}$
Mass stream of gas **V** [kgh^{-1}]	12438	42930.7
Mass stream of liquid **L** [kgh^{-1}]	16.060	93731.9
Specific liquid load $\mathbf{u_L}$ [ms^{-1}]	$10 \cdot 10^{-3}$	$16.21 \cdot 10^{-3}$
Gas velocity $\mathbf{u_V}$ [ms^{-1}]	0.0534	0.0462

2. The technical data of the Mellapak 350Y, acc. to Table 6-1c, is as follows:

   $a = 350$ m^2 m^{-3}
   $\varepsilon = 0.965$ m^3 m^{-3}
   $K_1 = 5.756$, $K_2 = -0.321$, $K_3 = 1.3662$, $K_4 = -0.133$
   $C_{Fl,0} = 0.566$

   The predicted maximum loading capacity of the Mellapak 350Y is calculated iteratively, acc. to Eq. (2-69), in the first iteration for:

$$\lambda_{0,I} \leq \left(\frac{u_L}{u_{V,Fl}} \right) = \frac{L \cdot \rho_V}{\rho_L \cdot V}$$

   The following applies to the rectifying section with $d_S = 1.2$ m:

$$\lambda_{0,I} = \frac{16.060 \cdot 51.46}{12438 \cdot 394.6} = 0.1684$$

and with $d_S = 2.282$ m:

$$\lambda_{0,I} = \frac{93731.9 \cdot 63.10}{42930.7 \cdot 392.2} = 0.3513$$

Now the liquid hold-up $h^0_{L,Fl}$ at the flooding point is determined using Eq. (2-46) with the parameter m, based on Eq. (2-43):

$$m = -0.82 + \frac{\lambda_{0,I}}{\lambda_{0,I} + 0.5} = -0.82 + \frac{0.1684}{0.1684 + 0.5} = -0.568 \qquad (d_S = 1.2\ m)$$

and

$$m = -0.82 + \frac{0.3513}{0.3513 + 0.5} = -0.4073 \qquad (d_S = 2.282\ m)$$

Equation (2-46) now leads to the following result, valid for $d_S = 1.2$ m and $\lambda_0 = 0.1684$:

$$h^0_{L,Fl} = \frac{\sqrt{0.1684^2 \cdot (-0.568 + 2)^2 + (4 \cdot 0.1684 \cdot (-0.568 + 1) \cdot (1 - 0.1684))}}{2 \cdot (-0.568 + 1) \cdot (1 - 0.1684)} -$$

$$- \frac{(-0.568 + 2) \cdot 0.1684}{2 \cdot (0.568 + 1) \cdot (1 - 0.1684)} = 0.427\ m^3 m^{-3}$$

and valid for $d_S = 2.282$ m and $\lambda_{0,I} = -0.4073$:

$$h^0_{L,Fl} = 0.47\ \mathrm{m^3\ m^{-3}}$$

3. The gas velocity at the flooding point $u_{V,Fl}$ is calculated, using Eq. (2-69) for:

$$d_h = 4 \cdot \frac{\varepsilon}{a} = 4 \cdot \frac{0.965}{350} = 0.01103\ m$$

$$d_T = \sqrt{\frac{\sigma_L}{\Delta\rho \cdot g}} = \sqrt{\frac{0.0025}{(394.6 - 51.46) \cdot 9.81}} = 8.62 \cdot 10^{-4}\ m \qquad (d_S = 1.2\ m)$$

and/or

$$d_T = 7.47 \cdot 10^{-4}\ m \quad (d_S = 2.282\ m)$$

The resistance coefficient ψ, for the dry column $d_S = 1.2$ m and $u_V = 4 \cdot V/(\pi \cdot d_S{}^2 \cdot \rho_V) = 0.0594\ \mathrm{ms^{-1}}$, is given as:

$$\mathrm{Re}_V = \frac{u_V \cdot d_p}{(1 - \varepsilon) \cdot \nu_V} = \frac{6 \cdot u_V}{a \cdot \nu_V} = \frac{6 \cdot 0.0594 \cdot 51.46}{350 \cdot 8.9 \cdot 10^{-6}} = 5887.2$$

$$\Rightarrow \psi = K_3 \cdot \mathrm{Re}_V^{K_4} = 0.4306$$

and based on $d_S = 1.2$ m and $u_V = 0.0462$ ms^{-1}:

$$\mathrm{Re}_V = 5556.6 \qquad \text{and} \qquad \psi = 0.343$$

Now the gas velocity at the flooding point $u_{V,Fl}$ can be calculated, using Eq. (2-69), for a column diameter of $d_S = 1.2$ m:

$$u_{V,Fl} = 0.566 \cdot 0.4306^{-1/6} \cdot 0.97^{1.2} \cdot \left(\frac{11.03 \cdot 10 - 3}{0.862 \cdot 10 - 3}\right)^{1/4} \cdot$$

$$\cdot \left(\frac{8.62 \cdot 10 - 4 \cdot (394.6 - 5.46) \cdot 9.81}{51.46}\right)^{1/2} \cdot$$

$$\cdot \left(\frac{51.46}{1.17}\right)^{0.18} \cdot (1 - 0.43)^{3.5} = 0.0809 \text{ ms}^{-1}$$

The flood gas load factor is therefore given as:

$$F_{V,Fl,I} = u_{V,Fl,I} \cdot \sqrt{\rho_V} = 0.5805 \sqrt{\text{Pa}}$$

Following the creation of new phase flow ratios at the flooding point $\lambda_{0,II}$ and $\lambda_{0,III}$, further iterations lead to the final result, for a column diameter of $d_S = 1.2$ m:

$$u_{V,Fl} = 0.096\ ms^{-1} \qquad \text{and} \qquad F_{V,Fl} = 0.69\ \sqrt{Pa}$$

and on $d_S = 2.282$ m:

$$u_{V,Fl} = 0.056\ ms^{-1} \qquad \text{and} \qquad F_{V,Fl} = 0.44\ \sqrt{Pa}$$

The column load in the rectifying section is as follows, for a column diameter of $d_S = 1.2$ m:

$$\frac{F_V}{F_{V,Fl}} = \frac{u_V}{u_{V,Fl}} = \frac{0.0594}{0.096} \cdot 100 = 61.9\%$$

and in the stripping section, for a column diameter of $d_S = 2.282$ m:

$$\frac{F_V}{F_{V,Fl}} = \frac{u_V}{u_{V,Fl}} = \frac{0.0462}{0.056} \cdot 100 = 82.5\%$$

According to information found in literature, the maximum column load [72] is given as:

$$\frac{F_V}{F_{V,Fl}} = 58\% \qquad \text{for} \quad d_S = 1.2\ m$$

and

$$\frac{F_V}{F_{V,Fl}} = 72\% \qquad \text{for} \quad d_S = 2.282\ m$$

This leads to the following flood gas load factors $F_{V,Fl}$:

$$F_{V,Fl} = 0.735\ \sqrt{Pa} \qquad \text{for} \quad d_S = 1.2\ m$$

and

$$F_{V,Fl} = 0.509\ \sqrt{Pa} \qquad \text{for} \quad d_S = 2.282\ m$$

The relative deviations $\delta(F_{V,Fl})$ are therefore:

$$\delta(F_{V,Fl}) = -6.12\% \qquad \text{for} \quad d_S = 1.2\ m$$

and

$$\delta(F_{V,Fl}) = -13.5\% \qquad \text{for} \quad d_S = 2.282\ m$$

Note

The load values of the Mellapak pressure column, which were calculated using the SBD model, are safe and only marginally different from the values found in literature, given the extreme physical properties of the separated system and the operating conditions under high pressure.

Annex Chapter 2

Flood Load Diagrams for Various Random and Structured Packings

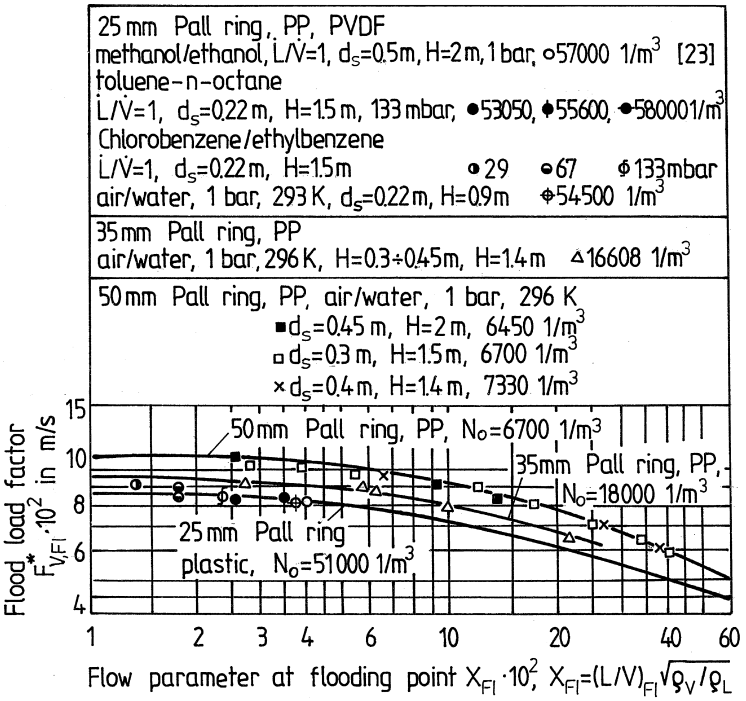

Figure 2-22. Capacity diagram $F^*_{V,Fl} = f(X_{Fl})$ for random 25—50 mm Pall rings made of plastic

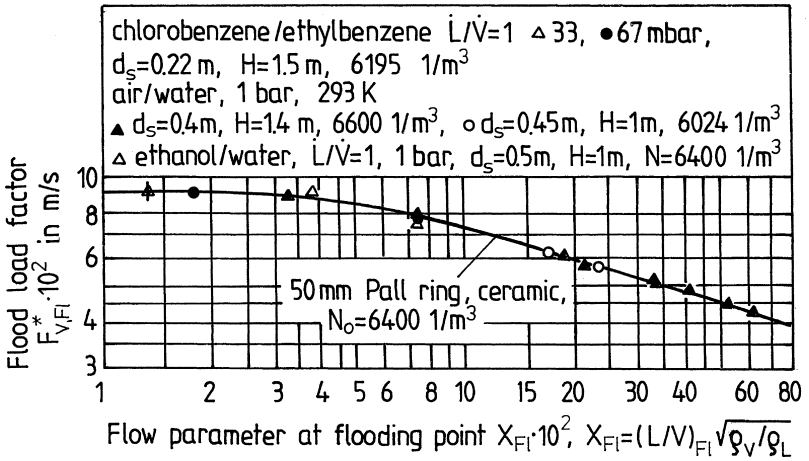

Figure 2-23. Capacity diagram $F^*_{V,Fl} = f(X_{Fl})$ for random 50 mm Pall rings made of ceramic

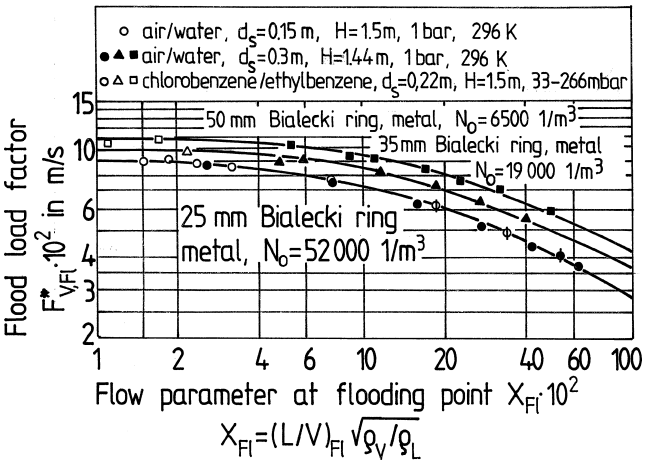

Figure 2-24. Capacity diagram $F^*_{V,Fl} = f(X_{Fl})$ for random 25−50 mm metal Pall rings

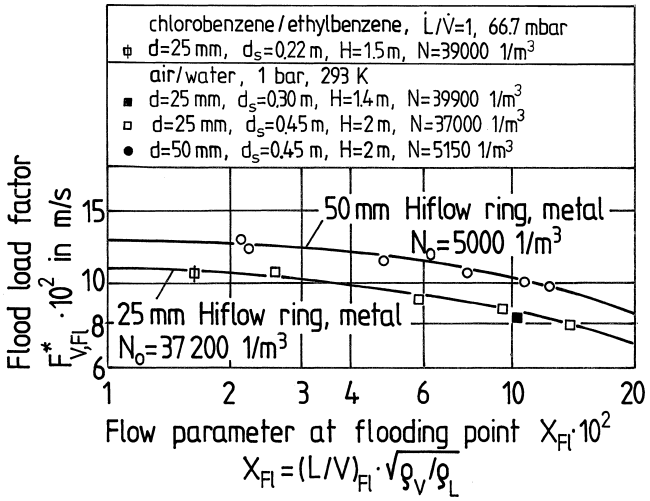

Figure 2-25. Capacity diagram $F^*_{V,Fl} = f(X_{Fl})$ for random 25−50 mm metal Hiflow rings

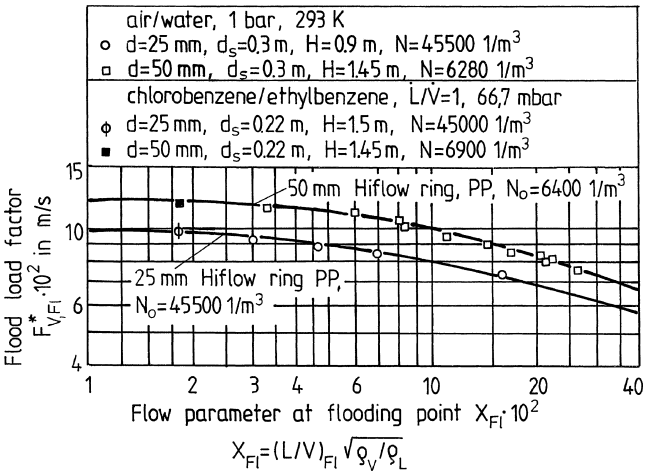

Figure 2-26. Capacity diagram $F^*_{V,Fl} = f(X_{Fl})$ for random 25–50 mm Hiflow rings made of plastic

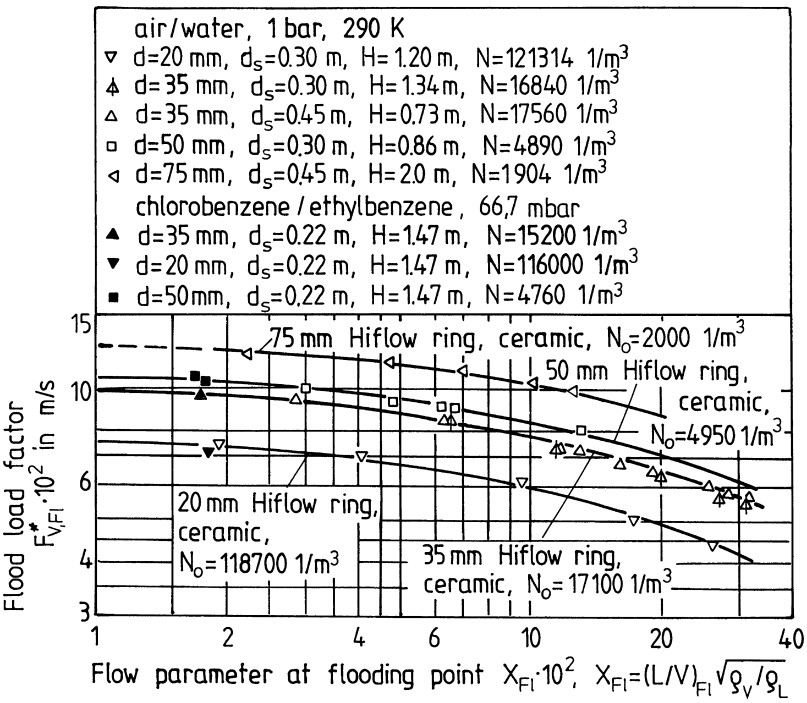

Figure 2-27. Capacity diagram $F^*_{V,Fl} = f(X_{Fl})$ for random 25–75 mm Hiflow rings made of ceramic

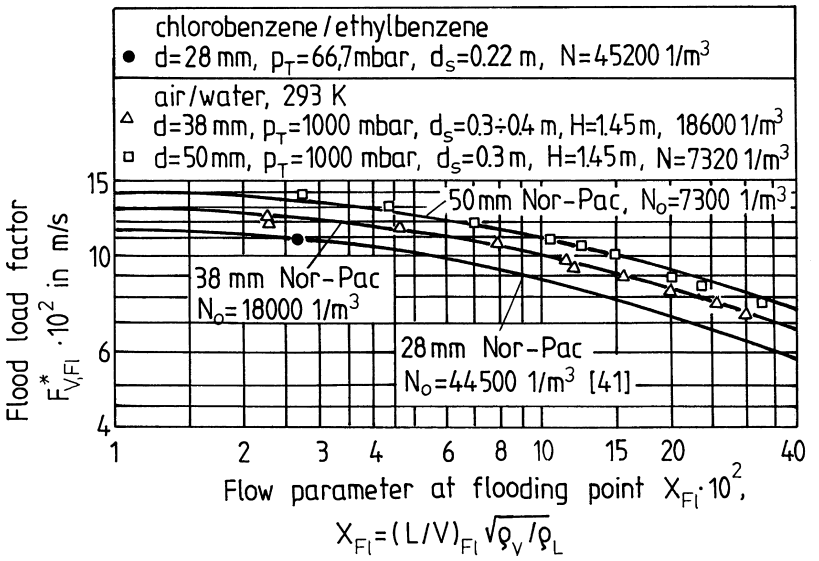

Figure 2-28. Capacity diagram $F^*_{V,Fl} = f(X_{Fl})$ for random 28−50 mm Nor-Pac packing made of plastic

Figure 2-29. Capacity diagram $F^*_{V,Fl} = f(X_{Fl})$ for random metal VSP rings, sizes 1 and 2

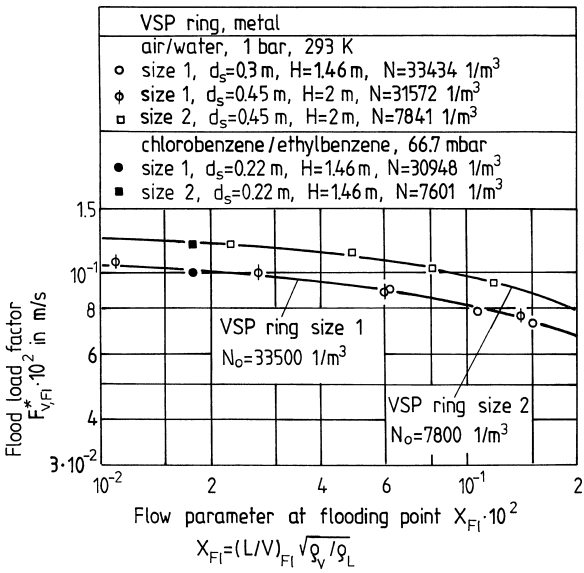

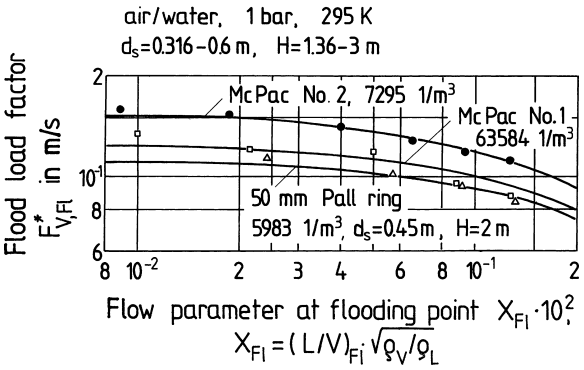

Figure 2-30. Capacity diagram $F^*_{V,Fl} = f(X_{Fl})$ for random Mc-Pac, sizes 1 and 2, and 50 mm Pall rings made of metal

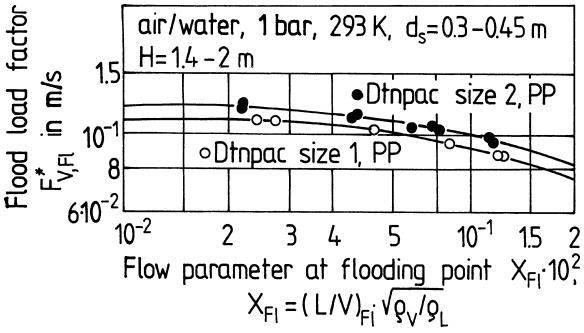

Figure 2-31. Capacity diagram $F^*_{V,Fl} = f(X_{Fl})$ for random Dtnpac, sizes 1 and 2, made of plastic

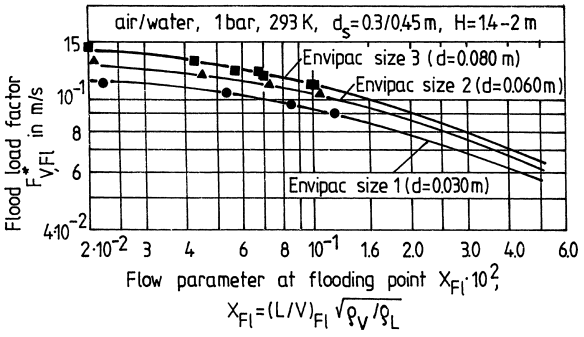

Figure 2-32. Capacity diagram $F^*_{V,Fl} = f(X_{Fl})$ for random Envipac, sizes 1–3, made of plastic

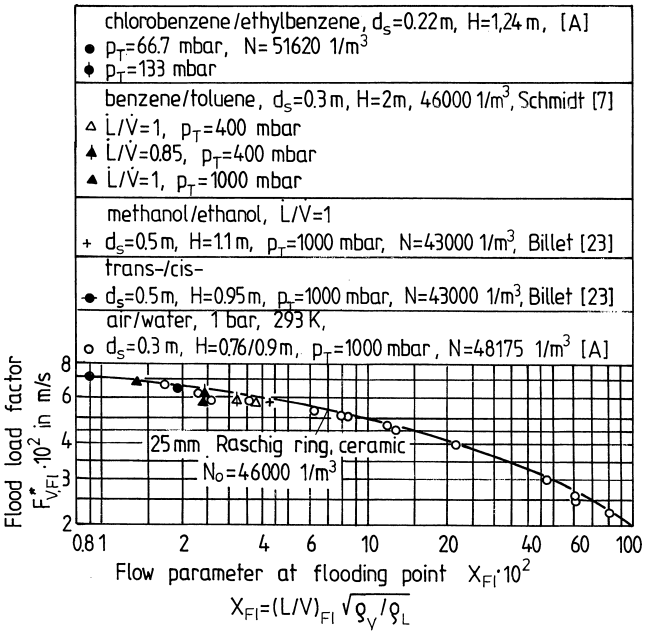

Figure 2-33. Capacity diagram $F^*_{V,Fl} = f(X_{Fl})$ for random 25 mm Raschig rings made of ceramic

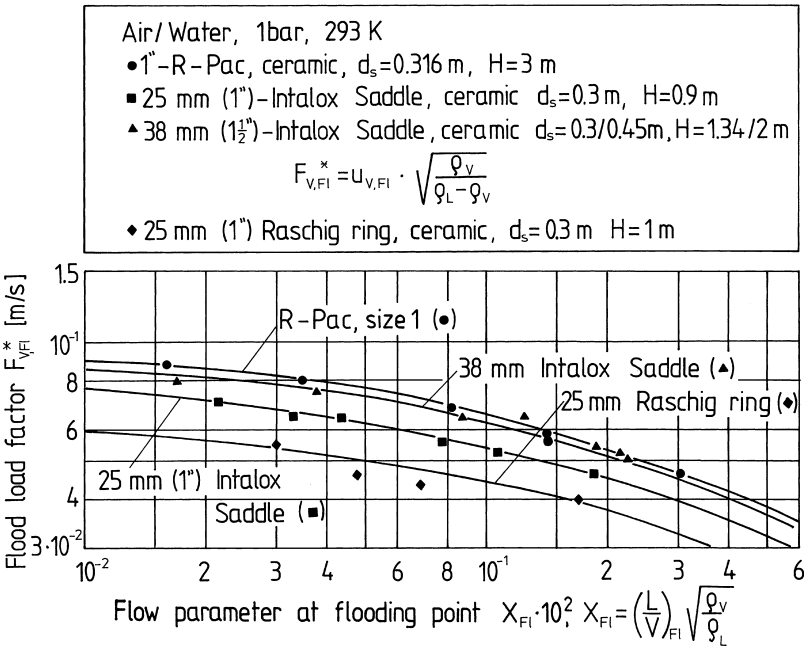

Figure 2-34. Capacity diagram $F^*_{V,Fl} = f(X_{Fl})$ for random R-Pac size 1, 25—38 mm Intalox saddles and 25 mm Raschig rings, made of ceramic

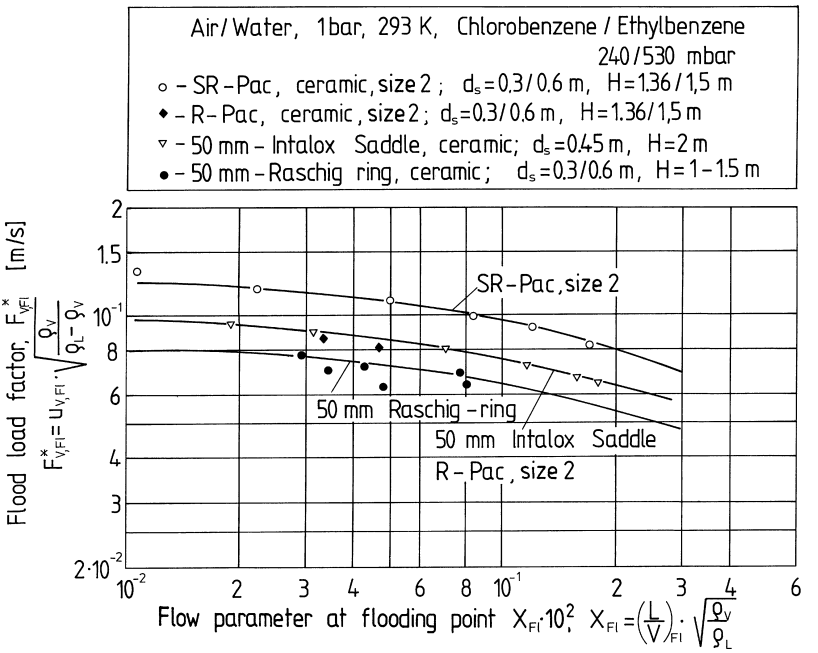

Figure 2-35. Capacity diagram $F^*_{V,Fl} = f(X_{Fl})$ for random R-Pac size 2, SR-Pac, 50 mm Intalox saddles and 50 mm Raschig rings, made of ceramic

Figure 2-36. Capacity diagram $F^*_{V,Fl} = f(X_{Fl})$ for stacked 25 and 50 mm metal Białecki rings

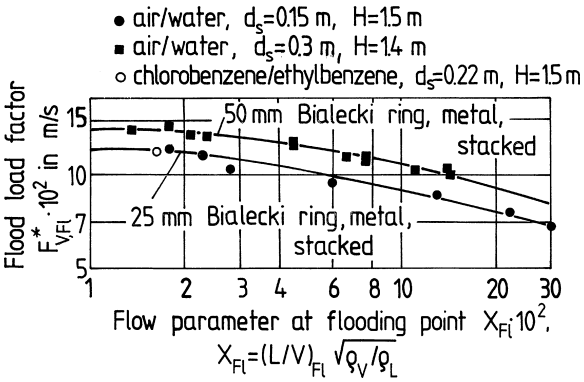

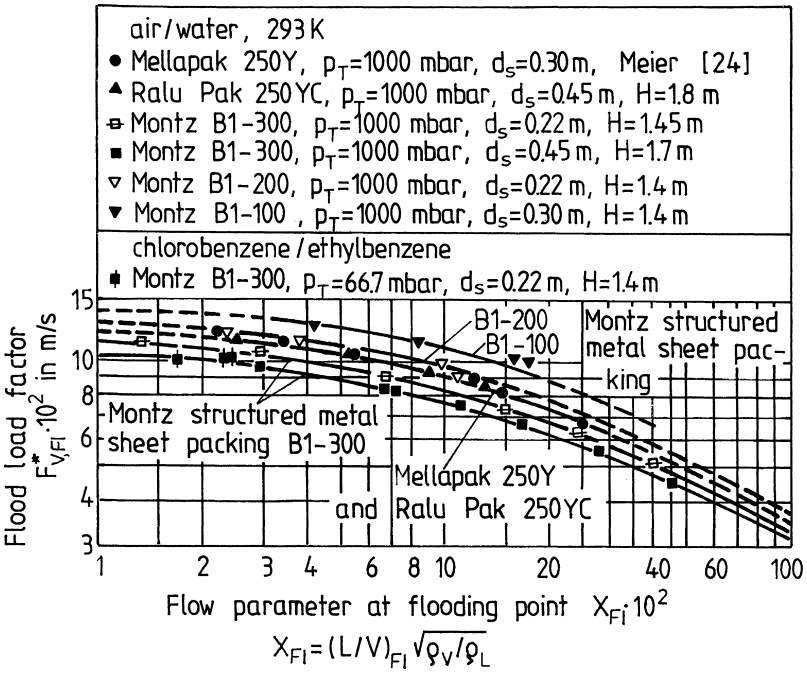

Figure 2-37. Capacity diagram $F^*_{V,Fl} = f(X_{Fl})$ for various structured packingss

Figure 2-38. Capacity diagram $F^*_{V,Fl} = f(X_{Fl})$ for GEA-H2 plastic structured packings

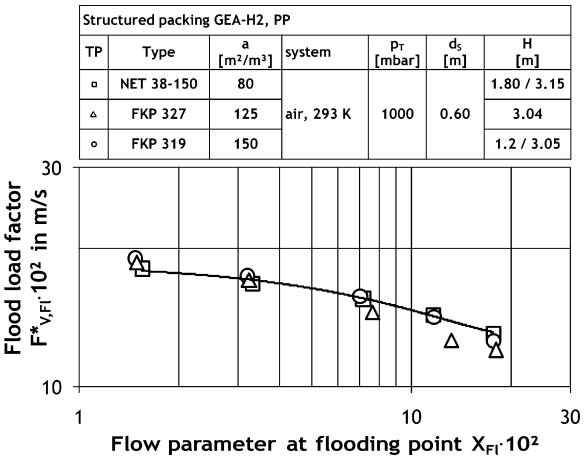

References Chapter 2

1. Walker WH, Levis WK, Mc Adams WH, Gilliland ER. Principles of Chemical Engineering 3rd ed., Mc Graw-Hill, New York (1937)
2. Mersmann A. Thermische Verfahrenstechnik. Springer, Berlin/Heidelberg (1980)
3. Mersmann A. Zur Berechnung des Flutpunktes in Füllkörperschüttungen. Chem.-Ing.-Techn., vol. 37 (1965) no. 3, p. 218/226
4. Sherwood TK, Shipley GH, Holloway FA. Flooding Velocities in Packed Column. Ing. Eng. Chem., vol. 30 (1938) no. 7, p. 765/769
5. Billet R. Recent Investigations of Metal Pall Rings. Chem. Eng. Prog., vol. 63 (1967) no. 9, p. 53/65
6. Lobo WE, Friend L, Hashmall F, Zenz F. Trans AICHE-J, vol. 41 (1945), p. 693
7. Schmidt R. Zweiphasenstrom und Stoffaustausch in Schüttungsdichten. VDI-Verlag, Düsseldorf (1972), VDI-Forschungsheft 550
8. Bolles WL, Fair JR. Performance and design of packed distillation columns. 3rd Int. Symp. on Destillation, London, April (1979). EFCE Publications Series No. 3, vol. 2, p. 3.3./35–89
9. Eckert JS. Selecting the proper distillation column packing. Chem. Eng. Progr., vol. 66 (1970) no. 3, p. 39 resp.. Chem. Eng. Progr., vol. 59 (1963) no. 5, p. 76
10. Schumacher R. Gasbelastung und Druckverlust von berieselten Füllkörperschüttungen. "vt"-Verfahrenstechnik, vol. 10 (1976) no. 11, p. 727/732
11. Weiß S, Schmidt E, Hoppe K. Obere Belastungsgrenze und Druckverlust bei der Destillation in Füllkörperkolonnen. Chem.Techn., Leipzig, vol. 27 (1975) no. 7, p. 394/396
12. Reichelt W. Strömung in Füllkörperapparaten bei Gegenstrom einer flüssigen und einer gasförmigen Phase. Verlag Chemie, Weinheim (1974)
13. Lapidus L, Elgin JC. Mechanics of vertical-moving fluidized systems. AIChE-J., vol. 1 (1957), p. 63/68
14. Richardson JF, Zaki WN. Trans. Inst. Chem. Eng., vol. 32 (1954), p. 35/53
15. Hu S, Kinter RC. The fall of single drops through water. AICHE J. (1955) no. 1, p. 42
16. Eckert JS, Walter LF. What affects packed bed distillation. Hydrocarbon Processing, vol. 43 (1964) no. 2, p. 107/114
17. Maćkowiak J, Billet R. New method of packed column design for liquid-liquid. Processes with Random and Stacked Packings. Ger. Chem. Eng., vol. 9 (1986) no. 1, p. 48/64 resp., Chem.-Ing.-Tech., vol. 57 (1985) no. 1, p. 56/57
18. Billet R, Maćkowiak J, Pajk M. Hydraulic and mass transfer in filled tube columns. Chem. Eng. Processing, vol. 2 (1985), no. 1
19. Kirschbaum E. Destillier- und Rektifiziertechnik. Springer, Berlin/Heidelberg/New York (1969)
20. Maćkowiak J. Einfluss der Form eines Füllkörpers auf die Hydraulik und den Stoffübergang bei der Absorption. Dissertation TU-Wrocław (Polen) (1975)
21. Billet R, Maćkowiak J, Ługowski Z, Filip S. Development and performance of impulse packing for gas/liquid-systems. Fette, Seifen, Anstrichmittel, vol. 85 (1983) no. 10, p. 383/391
22. Wiggert U. Druckverlust und Flüssigkeitsinhalt in berieselten Schüttungen. Report – Max Plack Institut (1959) no. 92, p. 243
23. Billet R. Stand, Entwicklung und Aussichten der Destillation und Rektifikation im Vergleich zu anderen Trennmethoden. Chemie-Technik, vol. 2 (1974), p. 355/361
24. Meier W, Hunkeler R, Stöcker WD. Performance of a new regular tower packing 'Mellapak'. 3rd Int. Symp. on Distillation, London, April (1979). vol. 2, p. 3.3/1–17 resp.. Chem.-Ing.-Tech., vol. 51 (1979) no. 2, p. 119/122
25. Eckert JS, Foote EH, Walter LF. What affects packing performance. Chem. Eng. Process, vol. 62 (1966) no. 1, p. 59/67
26. Informationsmaterial der Firma Sulzer/Winterthur. Trennkolonnen für Destillation und Absorption Packungen, Kolonnen, Anlagen. d./22.13.06.20-V.85-20
27. Informationsmaterial der Firma VFF, Ransbach/Baumbach., Westerwald (1986)
28. Informationsmaterial der Firma Raschig, Raschig GmbH. Ludwigshafen/Rhein no. 6 (1985) and VPR-5903/86
29. Bańczyk L, Grobelny A, Jarzynowski M. Porównawcze badania ceramiczynch siodełek. Intalox i pierścieni Raschiga (orig. Polish). Inż. Chem. i Procesowa vol. 4 (1983) no. 1, p. 3/14. as well as Inż. Chem. i Procesowa, vol. 4 (1983) no. 2, p. 267/279
30. Yilmaz T. Flüssigkeitsseitiger Stoffübergang in berieselten Füllkörperschüttungen. Chem.-Ing.-Techn., vol. 45 (1973) no. 5, p. 253/259

31. Strigle RR, Porter JKE. Metal Intalox – A new distillation packing. 3rd Int. Symp. on Distillation, London (1979)
32. Schmidt R. The lower capacity limits of packed column. I. Chem. E. Symp. Series No. 56, EFCE Publications. Series No. 3, vol. 2, p. 3.1/1–3.1/13
33. Mersmann A, Beyer von Morgenstern L, Deixler A. Deformation, Stabilität und Geschwindigkeit fluider Partikel. Chem.-Ing.-Tech., vol. 55 (1983) no. 11, p. 865/867
34. Mersmann A, Deixler A. Packungskolonnen. Chem.-Ing.-Tech., vol. 56 (1986) no. 1, p. 19/31
35. Gieseler M. Durchströmungsverhalten von Packungen und Schüttungen aus Koksen unterschiedlicher Größe und Gestalt in Gegenwart einer Flüssigkeit hoher Viskosität. Dissertation TU Clausthal (1972)
36. Blaß E, Kurtz R. Der Einfluss grenzflächenenergetischer Größen auf den Zweiphasen-Gegenstrom durch Raschigring-Füllkörpersäulen; Teil 1: Flüssigkeitsinhalt. "vt"-verfahrenstechnik, vol. 10 (1976) no. 11, p. 721/724
37. Blaß E, Kurtz R. Der Einfluss grenzflächenenergetischer Größen auf den Zweiphasen-Gegenstrom durch Raschigring-Füllkörpersäulen; Teil 2: Druckverlust und Flutpunkt. "vt"-verfahrenstechnik, vol. 11 (1977) no. 1, p. 44/48
38. Mersmann A. Zum Flutpunkt in Flüssig-Flüssig-Gegenstromkolonnen. Chem.-Ing.-Tech., vol. 52 (1980) no. 12, p. 933/942
39. Możeński C, Kucharski E. Hydraulika wypełnień pod zwiększonym ciśnieniem (orig. Polish). Inż. Chem. i Procesowa, vol. 3 (1986) no. 3, p. 373/384
40. Billet R, Maćkowiak J. Neuartige Füllkörper aus Kunststoffen für thermische Stofftrennverfahren. Chemie-Technik, vol. 9 (1980) no. 5, p. 219/226
41. Billet R, Maćkowiak J. Wirksamkeit von Kunststoff-Füllkörper bei der Absorption,. Desorption und Vakuumrektifikation. "vt"-verfahrenstechnik, vol. 15 (1982) no. 2, p. 67/74
42. Billet R, Maćkowiak J. Neues Verfahren zur Auslegung von Füllkörperkolonnen für die Rektifikation. „vt"-verfahrenstechnik, vol. 17 (1983) no. 4, p. 203/211
43. Billet R, Maćkowiak J. How to Use the Absorption Data for Design and Scale-up of Packed Columns. Fette, Seifen, Anstrichmittel, vol. 86 (1984) no. 9, p. 349/358
44. Billet R, Maćkowiak J. Hiflow-Ring ein Hochleistungsfüllkörper für Gas-Flüssig-Systeme. Teil 1: Ausführung in Kunststoff. Chemie-Technik, vol. 13 (1984) no. 12, p. 37/46
45. Billet R, Maćkowiak J. Hiflow-Ring ein Hochleistungsfüllkörper für Gas-Flüssig-Systeme. Teil 2: Ausführung in Metall. Chemie-Technik, vol. 14 (1985) no. 4, p. 91/99
46. Billet R, Maćkowiak J. Hiflow-Ring ein Hochleistungsfüllkörper für Gas-Flüssig-Systeme. Teil 3: Ausführung in Keramik. Chemie-Technik, vol. 14 (1985) no. 5, p. 195/206
47. Billet R, Maćkowiak J. Application of Modern Packings in Thermal Separation Processes. Chem.Eng. Technol. vol. 11 (1988), p. 213/227
48. Billet R, Maćkowiak J. Hochwirksame metallische Packung für Gas- und Dampf-Flüssig-Systeme. Chem.-Ing.-Tech., vol. 57 (1985) no. 11, p. 976/978
49. Vogt M. Modifizierte Darstellung der Flutgrenze in Füllkörperschüttungen. Chem.-Ing.-Tech., vol. 57 (1985) no. 4, p. 332/333
50. Kafarow WW. Osnovy massopjeredatschi, (orig. Russian). Verlag für chemische Literatur, Moskau (1972), p. 391
51. Kleinhückenkotten H. Untersuchung zur Auslegung von Füllkörperkolonnen mit geschütteter Füllung. „vt"-verfahrenstechnik, vol. 2 (1975) no. 6, p. 275/279
52. Won-Hi Hong, Brauer H. Stoffaustausch zwischen Gas und Flüssigkeit in Blasensäulen. VDI-Forschungsheft no. 624 (1984), VDI-Verlag Düsseldorf
53. Stichlmair J. Berechnung des Druckverlustes bei der Durchströmung ruhender Feststoffschüttungen.. Vortrag auf der Internen Sitzung des Fachausschusses "Thermische Zerlegung von Gas- und Flüssigkeitsgemischen" der GVD-VDI-Gesellschaft Verfahrenstechnik und Chemieanlagen in Bochum (1983)
54. Informationsmaterial der Firma Ceilcote. Tellerette-Manual, Ceilcote Company, 140 Sheldon Road/Berea, Ohio 44017
55. Stichlmair J. Grundlagen der Dimensionierung des Gas/Flüssigkeits-Kontaktapparates, BODENKOLONNE. Verlag Chemie (Reprotext), Weinheim, New York (1978)
56. Billet R, Maćkowiak J. 'Hydraulisches Verhalten und Stoffübertragung einer neuartigen Kolonnenpackung für Gas-Flüssig-Systeme'. Chemie-Technik, vol. 11 (1982), p. 1107–1114
57. Levich VG. Physicochemical hydrodynamics. Prentice-Hall, Ing. Englewood Cliffs, New York (1962)

58. Covelli B, Mülli R. Mitschleppen von Flüssigkeitstropfen über einer Sprudelschicht. Chem.-Ing.-Tech., vol. 51 (1981) no. 11, p. 877/879
59. Soo SL. Fluid dynamics of multiphase systems. BlaisdeU Publishing Company (1967), Waltham, M
60. Mersmann A. persönliche Mitteilung (1987)
61. Zenz FA. Petroleum Refiner, vol. 36 (1957) no. 8, p. 147/155
62. Strom JR., Kinter RC. Wall effect for the fall of single drops. AIChE-J., vol. 4 (1958), p. 153/156
63. Reinhart A. Das Verhalten fallender Tropfen. Dissertation no. 3412, Eidgenössische TH in Zürich (1964)
64. Kovalenko VS. For calculation of falling velocity of droplets (orig. Russian). Meor. Osnovy khim. tekhnol., Moscow, vol. 12 (1978) no. 3, p. 464/466
65. Clift R, Grace JR, Weber ME. Bubbles, Drops and Particles. Acad. Press, New York, San Francisco, London (1978)
66. Bornhütter H. Stoffaustausch von Füllkörperschüttungen unter Berücksichtigung der Flüssigkeitsströmungsform. Dissertation, TU München (1991)
67. Plüs RC, Ender Ch. A new high-efficiency packing „Mellaring-VSP". Presentation at Achema 1991 – Frankfurt a.M. on 9.6.1991. Conference volume published by Dechema
68. Süess A, Spiegel L. Hold-up of Mellapak structured packings. Sulzer Bros AG (Schweiz) Ltd., Separation Column, Winterthur
69. Spiegel L, Meier L. Structured packings – Capacity and pressure drop at very high liquids loads. Chemical plants + Processing, vol. 1 (1995) and. Chemical Eng. Technology – Wiley VCM-Verlag (1995)
70. Gierczycki A. Hydraulika aparatów wypełnionych z wybranym wypełnieniem (orig. Polish). Inż. Chem. i. Procesowa vol. 4 (1995) no. 4, p. 507–518
71. Viricny V, Stanek V. An experimental Set-up to Messure Flow Transierts in Counter-Current Packed Bed Column,. Chem. Biochem. Eng. vol. 10 (1996), no. 2, p. 55–61
72. Ghelfi L, Kreis H, Alvarez JA, Hunkeler H. Structured Packing in Pressure Columns. Poster-Int. Conference and Exibition on Destillation and Absorption. Birmingham, England, 7-9 September (1992) (c) 1994 by Sulzer Chemtech Ltd., Wintertur
73. Piche S, Larachi F, Grandjean B. Floading Capacity in Packed Towers,. Database, Correlations and Analysis,. Ind. Eng. Chem. Res. 2 vol. 40 (2001), p. 476–487
74. Kuźniewska-Lach I. Bestimmung der Flutpunktgeschwindigkeit in Füllkörperkolonnen. Inż. Chem. i Procesowa (orig. Polish) vol. 17 (1996) no.2, p. 267–277
75. Krehenwinkel H. Experimentelle Untersuchungen der Fluiddynamik und der Stoffübertragung in Füllkörperkolonnen bei Drücken bis 100 bar. Dissertation, TU Berlin, (Dezember 1986)
76. Maćkowiak J, Suder S. The new tube column with Pall-Rings for countercurrent and cucurrent processes. Vortrag Vesprem (Ungarn) 1979 and. Chem.-Ing.-Techn., vol. 50 (1978) no. 7, p. 550–551
77. Maćkowiak J, Suder S. Hydraulika i wymiana masy w kolumnie wypełnionej układanymi pierścieniami Białeckiego (orig. Polish). Inż. Chem. i. Procesowa vol. 8 (1977) no. 3, p. 651–664
78. Maćkowiak J. Hydraulische Untersuchungen von geordneten 50 mm keramischen Raschigringen. Internal study –TU-Wrocław-1975
79. Maćkowiak J. Mc-Pac – ein neuer metallischer Füllkörper für Gas-Flüssigkeitssysteme. Chem.-Ing.-Techn. vol. 73, no. 1+2 (2001) p. 74–79
80. Maćkowiak J. „Mc-Pac – Nowe metalowe wypełnienie dla układów gaz-ciecz". Inż. Chemiczna i Procesowa, vol. 21 (2000) p. 679–689
81. Bylica J, Jaroszyński M. Badania porównawcze hydrauliki wypełnień usypowych i konstrukcyjnych (orig. Polish). Inż. Chem. i Procesowa, (1995) no. 3, p. 421–439
82. Maćkowiak J, Ługowski Z. Geringe Apparatevolumina und Betriebskosten mit neuen keramischen Füllkörpern – R-Pac und SR-Pac. Verfahrenstechnik, vol. 29 (1995), no. 6, p. 19–22
83. Maćkowiak J, Szust J. Hydraulika i wymiana masy w kolumnach wypełnionych ceramicznymi pierścieniami R-Pac i SR-Pac w układach gaz/ciecz (orig. Polish). Inż. Chem. i Procesowa, vol. 18 (1997), no. 4, p. 675–691
84. Bańczyk L, Woźniak A, Szymkowiak E. Hydraulika kolumny wypełnionej ceramicznymi pierścieniami Białeckiego (orig. Polish). Inż. Chem. i Procesowa, vol. 7 (1977), no. 1, p. 261–274
85. Bańczyk L, Woźniak A, Jarzynowski M, Grobelny A. Hydraulika kolumny wypełnionej ceramicznymi pierścieniami IChN oraz Raschiga (orig. Polish). Inż. Chem. i Procesowa, vol. 9 (1979), no. 1, p. 15–28

86. Produktinformationen – Firma Raschig-Ludwigshafen-vt (1996). Raschig- Super Ring no.1 u.2, Metall und Kunststoff
87. Bornhüter K, Mersmann A. Druckverlust und Flutpunkt in Füllkörperschüttungen. CIT-Chem.-Ing.-Tech. vol. 64 (1992) no.3, p. 305/305
88. Kister MZ. Destillation design. McGraw-Hill, Inc., New York (1992)
89. Billet R. Packed towers. VCH-Weinheim, New York (1995)
90. Maćkowiak J. Determinition of flooding gasvelocity and liquid hold-up at flooding in packed columns for gas/liquid-systems. Chem. Eng. Tech. 13 (1991) p. 184–196
91. Maćkowiak J, Mersmann A. Zur maximalen Belastbarkeit von Kolonnen mit modernen Füllkörpern und Packungen für Gas/Flüssigkeitssysteme. Chem.-Ing.-Tech. vol. 63 (1991) no.5, p. 503–506
92. Grabbert G, Bonitz R. Fluiddynamik bei der Zweiphasenströmung durch Füllkörper- und Packungskolonnen. TU Bergakademie Freiberg, Freiberger Forschungshefte, A 842 (1998)
93. Linek V, Moucha T, Rejl F. Hydraulic and mass transfer characteristics of packings for absorption and distillation columns. Rauschert-metall-sattel-rings. Trans IChemE, Vol 79, Part A, October 2001
94. Schultes M. Raschig Super-Ring. A new Fourth Generation Packing Offers New Advantages. Trans IChemE, Vol 81, Part A, January 2003
95. Metal Random Packing – Superior random packings combined with innovative mass transfer technology. Technical Information by Sulzer Chemtech Ltd., 22.64.06.40 – IV.06 – 50, Switzerland
96. Pall-ring, Technical Information by Raschig, 2008
97. Technical Information by rvt PE GmbH

http://www.springer.com/978-3-540-88780-5

Fluid Dynamics of Packed Columns
Principles of the Fluid Dynamic Design of Columns for Gas/Liquid and Liquid/Liquid Systems
Mackowiak, J.
2010, XXI, 355 p. 147 illus., Hardcover
ISBN: 978-3-540-88780-5